Mathematical modelling of neoadjuvant antiangiogenic therapy and prediction of post-surgical metastatic relapse in breast cancer patients

Chiara Nicolò

université de BORDEAUX

Inria

THÈSE

présentée pour obtenir le grade de

DOCTEUR DE L'UNIVERSITÉ DE BORDEAUX

Ecole doctorale de mathématiques et d'informatique

Specialité :

Mathématiques appliquée et calcul scientifique

Chiara Nicolò

Mathematical modelling of neoadjuvant antiangiogenic therapy and prediction of post-surgical metastatic relapse in breast cancer patients

sous la direction de : Sébastien Benzekry et Olivier Saut

Jury :

Dominique Barbolosi	Pr, Aix Marseille University	Rapporteur (Président)
Sébastien Benzekry	CR, HDR, Inria MONC	Directeur de thèse
John Ebos	Assistant Professor, Roswell Park Cancer Institute	Invité
Marc Lavielle	DR, Inria XPOP	Rapporteur
Christophe Meille	PhD, PharmD, Novartis Pharma	Examinateur
Xavier Muracciole	MD, CHU La Timone	Examinateur
Mélanie Prague	CR, Inria SISTM	Invitée
Olivier Saut	DR, Inria MONC	Directeur de thèse

Abstract

For patients diagnosed with early-stage cancer, treatment decisions depend on the evaluation of the risk of metastatic relapse. Current prognostic tools are based on purely statistical approaches that relate predictor variables to the outcome, without integrating any available knowledge of the underlying biological processes. The purpose of this thesis is to develop predictive models of the metastatic process using an established mechanistic modelling approach and the statistical mixed-effects modelling framework. In the first part, we extend the mathematical metastatic model to describe primary tumour and metastatic dynamics in response to neoadjuvant sunitinib in clinically relevant mouse models of spontaneous metastatic breast and kidney cancers. The calibrated model is then used to test possible hypothesis for the differential effects of sunitinib on primary tumour and metastases, and machine learning algorithms are applied to assess the predictive power of biomarkers on the model parameters.

In the second part of this thesis, we develop a mechanistic model for the prediction of the time to metastatic relapse and validate it on a clinical dataset of breast cancer patients. This model offers personalised predictions of the invisible metastatic burden at the time of diagnosis, as well as forward simulations of metastatic growth, and it could be used as a personalised prediction tool to assist in the routine management of breast cancer patients.

Key words: mixed-effects modelling, mechanistic modelling, breast cancer, metastatic relapse, survival analysis, machine learning.

Résumé

Le cancer est la deuxième cause de décès dans le monde, avec 9.6 millions de décès en 2018 [1]. Bien que, dans la plupart des cas, la tumeur primaire ne mette pas en danger la vie du patient, les métastases endommagent souvent les organes vitaux, et dans 90% des cas, elles sont la cause finale des décès dus au cancer. [2]. En effet, malgré les progrès dans le diagnostic et le traitement de cette pathologie, la maladie métastatique représente toujours une maladie terminale, non curable avec les moyens thérapeutiques actuels [3].

Les approches de modélisation mathématique sont de plus en plus utilisées dans la recherche sur le cancer afin d'améliorer la compréhension des observations expérimentales [4–6]. Elles peuvent aussi être utilisées pour guider les essais cliniques en permettant d'explorer *in silico* un grand nombre de scénarios possibles [6–8]. Les modèles mathématiques fournissent également des prédictions quantitatives qui peuvent être utilisées pour vérifier différentes théories en évaluant la correspondance des simulations de modèles avec les observations expérimentales [9]. Plusieurs modèles mathématiques ont été proposés pour décrire l'impact de diverses thérapies sur la croissance tumorale [7, 10–12]. D'autre part, en raison de la complexité du processus métastatique, il y a relativement peu de modèles mathématiques qui intègrent la dynamique des métastases [13–17]. Le modèle métastatique proposé par Iwata *et al.* [14] réduit la complexité de la formation des métastases à deux composantes principales: la croissance tumorale et la dissémination des métastases. Ce modèle a pu décrire avec précision les données d'un patient atteint d'un carcinome hépatocellulaire métastatique [14] et a été ultérieurement validé sur des données expérimentales provenant de modèles murins du cancer non traités, ainsi que sur

données cliniques de probabilités de rechutes métastatiques [9, 18, 19]. Parallèlement à ces approches mécanistes, des modèles biologiquement agnostiques basés principalement sur la régression de Cox ont été développés pour prédire le risque de rechute métastatique, en particulier pour guider la décision sur le traitement adjuvant (post-chirurgical) du cancer du sein [20–22]. Rares sont les efforts qui utilisent des algorithmes d'apprentissage automatique [23].

Cette thèse contient deux projets : la modélisation de la thérapie antiangiogénique pré-opératoire sur des données pré-cliniques et le développement d'un modèle prédictif pour le temps de rechute métastatique sur des données cliniques de patientes atteintes de cancer du sein. Les sections suivantes décrivent les motivations et résument les résultats de chacun de ces travaux.

Modélisation mathématique de la thérapie antiangiogénique pré-opératoire

Malgré l'action clinique prouvée des inhibiteurs antiangiogéniques [24], des études expérimentales récentes ont suggéré que ces médicaments peuvent avoir des effets différentiels sur la tumeur primaire et sur les métastases [25–27]. Dans une étude de Ebos *et al.* [26] utilisant des modèles murins de cancer du sein et de mélanome, le sunitinib a considérablement inhibé la croissance des tumeurs primaires implantées orthotopiquement. Toutefois, l'administration du sunitinib a augmenté la masse métastatique totale dans divers essais de métastases, y compris après l'injection intraveineuse de cellules tumorales et après l'ablation chirurgicale de tumeurs primaires implantées orthotopiquement. En outre, un certain nombre d'études précliniques et cliniques suggèrent que l'arrêt du traitement antiangiogénique peut entraîner une revascularisation rapide et un rebond de la croissance tumorale [28]. Ces rebonds ont été observés pendant les pauses thérapeutiques avec le sunitinib chez les patients atteints d'un carcinome cellulaire rénal métastatique [29, 30], et avec le bevacizumab chez les patients atteints d'un cancer colorectal [31].

À ce jour, la majorité des modèles mathématiques en oncologie se focalisent sur les

effets du traitement seulement sur la tumeur primaire. Cette étude étend un modèle mécaniste du processus métastatique [19] pour décrire la croissance de la tumeur primaire et de la masse métastatique totale en réponse au traitement néoadjuvant avec le sunitinib dans des modèles murins orthochirurgicaux des cancers du sein et du rein. Le modèle a été développé en utilisant un grand jeu de données comprenant des mesures longitudinales de la taille de la tumeur primaire et de la masse métastatique chez 230 souris au total (132 souris pour le modèle du cancer du sein et 98 souris pour le modèle du cancer du rein), ainsi que les données de survie et biomarqueurs pré-chirurgicaux (cellules tumorales circulantes, cellules myéloïdes suppressives, marqueurs de prolifération et de cellules endothéliales). Pour tester des hypothèses sur les effets différentiels du sunitinib sur la tumeur primaire et les métastases, des simulations du modèle ont été effectuées avec les paramètres estimés dans une étude précédente sur des groupes de contrôle [19]. Les simulations obtenues supposant que le sunitinib inhibe la croissance de chaque métastase ne sont pas capables de représenter les données expérimentales. En revanche, les simulations obtenues supposant que le médicament inhibe seulement la croissance de la tumeur primaire réussissent à bien reproduire les données expérimentales. Cela a été observé dans tous les groupes traités du modèle du cancer du sein, suggérant ainsi un effet limité du traitement sur la croissance des métastases. Pour prendre en compte les différentes traitements, un modèle cinétique-pharmacodynamique (K-PD) a été développé à partir de ces résultats de simulation. Ce modèle a été calibré simultanément sur les données des animaux des groupes traitées et de contrôle en utilisant l'algorithme SAEM [32] et a été en mesure de bien décrire les données tant au niveau de la population qu'au niveau individuel. Confirmant les résultats précédents [19], la variabilité inter-animale était principalement caractérisée par le paramètre du modèle exprimant le potentiel métastatique de la tumeur, μ, qui s'est également révélé significatif dans l'analyse de survie. L'effet des covariables sur ce paramètre du modèle a été évalué utilisant des techniques de régression par apprentissage automatique (réseaux de neurones artificiels, machines à support de vecteur, forêts aléatoires) [33]. Cependant, les biomarqueurs inclus dans tous les algorithmes testés n'ont démontré qu'une valeur prédictive limitée sur le paramètre

mathématique.

Un modèle K-PD pour le traitement néoadjuvant avec sunitinib a également été développé pour le modèle animal du cancer rénal. Dans ce cas, un modèle mathématique avec différents taux de croissance pour la tumeur primaire avant et après le traitement offrait une meilleure description des données, ce qui suggère un effet de rebond après le traitement. Après avoir été calibré, le modèle K-PD a été utilisé pour étudier l'effet de l'arrêt du traitement sur la tumeur primaire et la masse métastatique. Cette analyse a montré que le rebond de la croissance de la tumeur primaire causé par l'arrêt du traitement peut augmenter le masse métastatique par rapport aux animaux du groupe de contrôle, suggérant que le sunitinib doit être administré de façon prolongée pour obtenir un bénéfice thérapeutique.

Développement d'un modèle prédictif pour le temps de la rechute métastatique

Le cancer du sein est le cancer le plus fréquent et la deuxième cause de décès par cancer chez les femmes [34]. Dans la majorité des cas, la maladie est diagnostiquée aux premiers stades, lorsque toutes les lésions détectables sont confinées au sein ou aux ganglions lymphatiques voisins et peuvent être enlevées par intervention chirurgicale [35]. Cependant, après la chirurgie environ 20-30% des patients ont une rechute avec métastases distantes [36], suggérant que des micrométastases cliniquement invisible pourraient déjà être présents au moment de la chirurgie.

La connaissance précise du risque de rechute métastatique est d'importance cruciale afin de personnaliser le traitement adjuvant et d'éviter l'utilisation de thérapies toxiques et coûteuses lorsqu'elles ne sont pas nécessaires. Les outils existants pour la prédiction du risque métastatique sont basés sur des modèles purement statistiques, tels que les modèles de risques proportionnels de Cox [21, 22] et, à de rares occasions, des algorithmes d'apprentissage automatique [37, 38]. Bien que des modèles mathématiques aient été développés pour décrire la dynamique métastatique, aucun d'entre eux n'a à ce jour été

utilisé comme outil prédictif. Cela pourrait être dû à la rareté des données recueillies dans les études cliniques, qui sont souvent limitées aux données de type time-to-event et n'incluent pas des mesures longitudinales de la taille de la tumeur.

Le but de cette étude est d'étendre le modèle mécaniste proposé par Iwata *et al.* [14] pour prédire le temps de la rechute métastatique chez les patients atteints d'un cancer du sein au stade précoce. Le modèle mécaniste a été développé et validé utilisant un jeu de données cliniques contenant les temps de rechute et les caractéristiques clinico-pathologiques de femmes diagnostiquées d'un cancer du sein précoce et opérées à l'Institut Bergonié de Bordeaux entre 1989 et 1993. Les patientes inclus dans cette analyse n'ont reçu aucun traitement en plus de la chirurgie et de la radiothérapie localisée de la tumeur primaire, ce qui a permis d'évaluer l'histoire naturelle de la maladie. Les paramètres du modèle ont été estimés avec une approche à effets mixtes, utilisant l'algorithme SAEM [39]. L'algorithme random survival forest (RSF) [40] a été utilisé pour sélectionner un premier ensemble de covariables prédictives de la rechute métastatique. Ces covariables ont ensuite été considérées pour expliquer la variabilité des paramètres du modèle mécaniste utilisant une méthode de backward sélection. Avec un c-index de (0.63-0.70), le modèle mécaniste était comparable pour performance prédictive à l'algorithme RSF (c-index 0.67-0.71), à un modèle de régression de Cox (c-index 0.67-0.72) ainsi que à des algorithmes de classification pour la prédiction de la survie à 5 ans. Le modèle proposé représente une première tentative de modèle mécaniste dans le contexte de l'analyse de survie pour la prédiction de la rechute métastatique. Il permet d'estimer individuellement l'importance des métastases cliniquement invisibles et le temp de rechute à partir des données cliniques et histologiques disponibles au moment du diagnostic, et pourrait donc être utilisé comme un outil de prédiction personnalisé pour mieux évaluer le risque de rechute.

Mots clés : modélisation à effets mixtes, modélisation mécaniste, cancer du sein, rechute métastatique, analyse de survie, apprentissage statistique.

Remerciements

Je voudrais tout d'abord remercier mon directeur de thèse, Sébastien Benzekry, pour son aide et intérêt à l'avancée de mon travail pendant ces trois années de doctorat. Je souhaite aussi remercier Olivier Saut, qui a co-encadré cette thèse. Je leur suis également reconnaissant pour m'avoir donné l'opportunité de participer à plusieurs conférences, ainsi que d'avoir relu et apporté des corrections à mon manuscrit.

Je remercie Marc Lavielle et Dominique Barbolosi pour avoir accepté de rapporter ma thèse. Merci aussi à John Ebos, Christophe Meille, Xavier Muraciolle et Mélanie Prague pour leur participation au jury. En particulier, je tiens à remercier John Ebos pour avoir fourni les données expérimentales sur lesquelles j'ai travaillé, et Mélanie Prague pour les discussions très utiles qui ont contribué au développement du modele pour la rechute métastatique. Merci également à Gaetan MacGrogan et Carine Bellera pour leur collaboration et pour avoir fourni les données cliniques.

Je voudrais aussi remercier touts les doctorants et post-docs des équipes MONC et MEMPHIS que j'ai eu le plaisir de connaître et avec qui j'ai partagé des bons moments ensemble : Cédrick, Erwan, Manon, Agathe, Maria, Marie, Antoine, Giuliano, Guillaume, Sébastien, Cristina, Floriane, Cécile, Christèle, Costanza, Cynthia, Sergio, Charles, Pedro, Olivier, Romain, Florian, Gwladys, Emanuela, Andrea, Alice, Federico, Stefano.

Enfin je tiens à remercier toute ma famille en Italie pour le soutien moral et encouragement constant pendant ces années.

Bordeaux, Septembre 2019

Contents

Chapter 1

Introduction

Cancer is the second leading cause of death worldwide, being responsible for 9.6 million deaths in 2018, according to the World Health Organisation [1]. Although the majority of primary tumours do not compromise the survival of cancer patients, metastasis – the spread of a tumour throughout the body – often impairs the functioning of vital organs and in the 90% of cases is the ultimate cause of death from cancer [2]. Indeed, despite the progresses made in the diagnosis and treatment of cancer, metastatic disease still represents a terminal illness, not curable with the current therapeutic means [3].

Mathematical modelling approaches are increasingly used in cancer research to complement experimental investigations [4–6]. They may have utility in providing rationales and computational tools to guide the design of clinical trials by allowing *in silico* exploration of a large number of possible scenarios, impossible to all test by empirical means [6–8]. Mathematical models also provide quantitative predictions that can be used to verify different theories by assessing the agreement of model simulations with the experimental observations [9]. Several mathematical models that describe the impact of various cancer therapies on tumour growth have been proposed [7, 10–12]. However, owing to the complexity of the metastatic process, mathematical models that also describe metastatic dynamics are relatively few [13–17]. The metastatic model proposed by Iwata and colleagues [14] reduces the complexity of metastasis formation to the main components of tumour growth and metastatic dissemination. It was shown to accurately describe CT

scans data from a patient with metastatic hepatocellular carcinoma [14] and was further validated against experimental data from untreated non-surgical and surgical metastatic models of cancer, as well as clinical data of metastatic relapse probabilities [9, 18, 19]. In parallel to these mechanistic approaches, biologically agnostic models mostly based on Cox regression have been developed for prediction of the risk of metastatic relapse, in particular to guide decision on adjuvant (post-surgical) therapy for breast cancer [20–22]. Rare efforts exist that make use of machine learning algorithms [23].

The first part of this work extends the mechanistic approach introduced by Iwata *et al.* to investigate the differential efficacies and the effects of different treatment schedules of neoadjuvant sunitinib on primary and metastatic tumour growth, using primary tumour and metastatic data from mouse models of spontaneous metastatic breast and kidney cancers. This is the first modelling work utilising metastatic data from clinically relevant mouse models to describe the impact of antiangiogenic therapy on metastatic disease progression. Furthermore, it is the first to combine machine learning algorithms to mechanistic modelling of metastasis.

The second part of this thesis focuses on the development of a mechanistic model to predict the time to metastatic relapse. The model is built and validated on a clinical dataset of breast cancer patients, using the random survival forest algorithm to preselect the most predictive covariates. This study represents the first attempt of mechanistic modelling in the context of survival analysis. Moreover, unlike current predictive models of metastatic relapse, the developed mechanistic model, not only estimates the likelihood of relapse, but also provides personalised predictions of the state of metastasis at the time of diagnosis and of the future growth of metastases.

This chapter starts with a description of the biology of metastasis (Section 1.1). Section 1.2 outlines the main strategies currently employed for the treatment of cancer, focusing on antiangiogenic therapy, which is the one that we focus on in Chapters 3 and 4 of this thesis. Section 1.4 presents a short review of quantitative modelling approaches in oncology and their contributions to the improvement of treatment strategies. The chapter concludes with the objectives of this work (Section 1.5) and the outline of the

thesis (Section 1.6).

1.1 The metastatic process[1]

The spread of cancer cells from the primary tumour and the subsequent formation of metastatic colonies at distant sites involves a series of steps commonly referred to as the invasion-metastatic cascade (Figure 1.1). These steps comprise local invasion of primary tumour cells into nearby tissues and vessels; intravasation and transport of these cells via the circulatory system; arrest and extravasation in distant organs to form micrometastatic tumours; and colonisation of the new sites, namely the development of micrometastatic tumours into clinically detectable metastatic lesions.

1.1.1 Local invasion

The dissemination of cancer cells requires the acquisition of mutations enabling cells of the primary tumour to leave the primary site and travel to distant organs. One important process conferring the abilities of motility and invasiveness is the cell-biological program termed epithelial-mesenchymal transition (EMT). During the EMT, cancer cells assume traits similar to those of cells of mesenchymal origin, leading to a reduced expression of adhesion molecules, such as E-cadherin, whose role is to keep cells joined to each other in epithelial tissues. Invading cells also acquire the ability to release various proteases which disintegrate the extracellular matrix, allowing their passage to the stromal compartment.

1.1.2 Intravasation and transport in circulation

Cancer cells that reach the stromal compartment may intravasate into blood and lymphatic vessels. Transport of cancer cells via the bloodstream is called hematogenous spread, while transport via the lymph is called lymphatic transport. Primary tumour cells can enter either the vasculature of the normal surrounding tissues or the neovascula-

[1] Based on [41, Chap. 14]

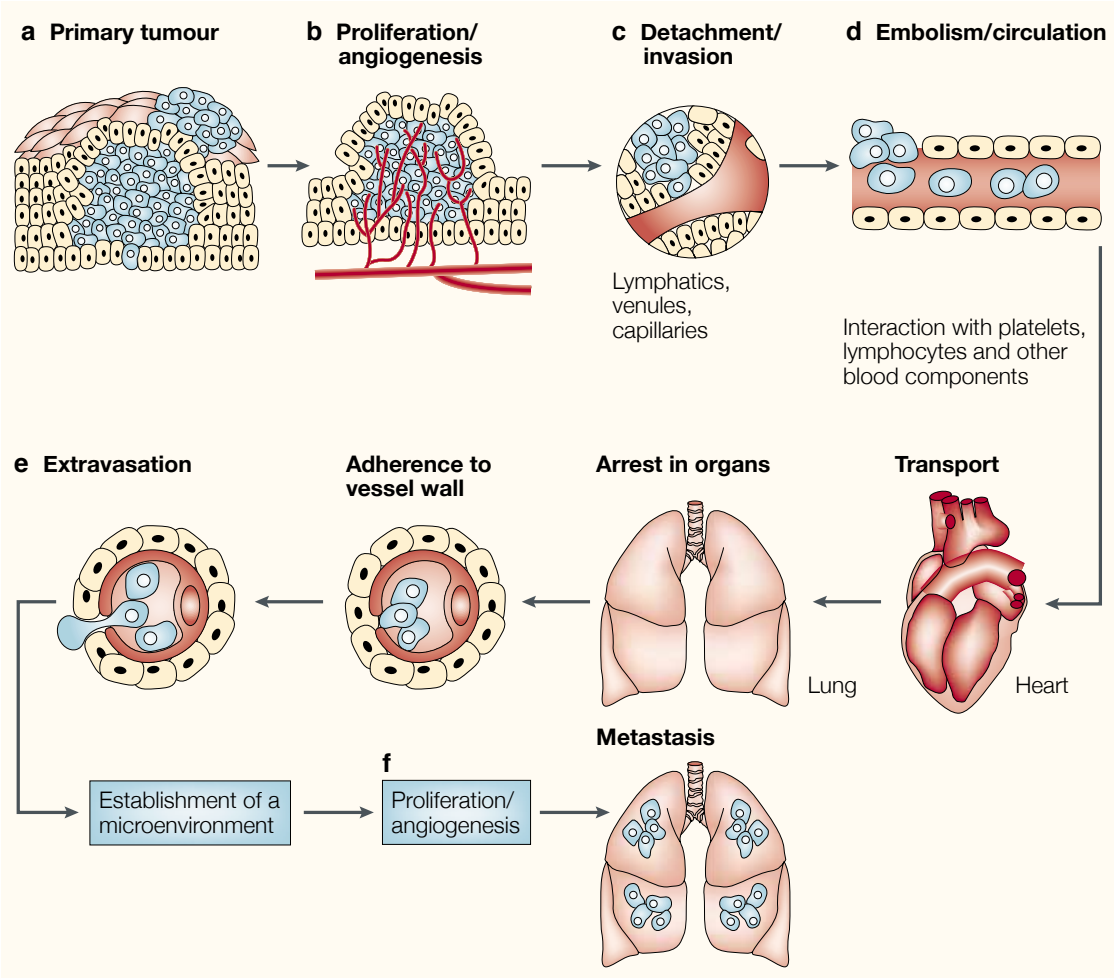

Figure 1.1 – The invasion-metastatic cascade. (Image from [42]).

ture that has been developed by the activation of tumour angiogenesis[2]. Cancer cells that have intravasated remain for short time in circulation. They are usually arrested in the first capillary bed encountered (often within the lung), because of their low deformability and larger size compared to the internal diameters of microvessels.

Hematogenous spread is thought to be the main route of metastatic dissemination. The role of lymphatic vessels in the metastatic process is less clear. In breast, colorectal, cervical and oral carcinomas, some tumour cells do enter lymphatic vessels and accu-

[2]Angiogenesis is the formation of new blood vessels from the preexisting vasculature. It occurs physiologically in reproduction, development and wound healing. Pathological angiogenesis is required for a tumour to obtain blood supply and grow beyond a microscopic size [43].

mulate in nearby lymph nodes. Cells within these nodes, however, rarely move to other sites. Nevertheless, their presence represents an important clinical parameter, because it is indicative of the metastatic aggressiveness of the tumour. Patients with a small number of positive lymph nodes are diagnosed with localised disease and may not progress to the metastatic stage. In contrast, patients found with a large number of positive lymph nodes at diagnosis may already have developed distant metastases.

1.1.3 Extravasation

The process of extravasation involves complex steps requiring the interaction between cancer cells and the walls of capillaries in which they are trapped. In a similar way to the mechanism of local invasion, cancer cells may release proteins, such as angiopoietin, that make endothelial cells retract from one another, leaving holes in the capillary walls through which they can extravasate. The extravasation process may require different mechanisms depending on the target site. For instance, the capillaries in the bone marrow and in the liver are fenestrated and allow a passive entry of circulating tumour cells. In contrast, dissemination of cancer cells in the brain requires the activation of a tissue-specific program in order to overcome the blood-brain barrier.

1.1.4 Metastatic colonisation

The colonisation of a new site is considered the most difficult step of the entire metastatic process, because tumour cells have to adapt to a foreign environment which might be very different from the primary site. Once extravasated, cancer cells can persist for a long time in an inactive state of dormancy either as single cells or small micrometastatic tumours. Moreover, only a very small number of these micrometastases will awaken from this state of dormancy and eventually grow into clinically detectable lesions. For instance, about 30% of breast cancer patients are found with thousands of disseminated tumour cells in the bone marrow[3]. However, only half of these women will eventually

[3] A technique to identify micrometastases in the bone marrow consists in using antibodies reactive with cytokeratins. Cytokeratin-positive cells are cells of epithelial origins, suggesting the presence of cancer cells in otherwise fully mesenchymal tissues [44].

develop a metastatic disease [44].

Cancer cells from a given type of tumour have the propensity to metastasise in specific organs. Usually, the frequency at which metastases occur in a given organ is determined by two factors: the connection of the primary tumour site to this organ through the circulatory system and the suitability of cancer cells to the microenvironment of the new site. Breast carcinomas seed metastases preferentially in the brain, liver, bones and lungs. In prostate tumours, metastases are often found in the bones, while colon carcinomas tend to disseminate cancer cells in the liver.

1.2 Overview of anticancer treatments[4]

Depending on the characteristics and the clinical stage of a cancer, the aim of anticancer treatments may be either to achieve a complete cure, or prolong survival and improve symptoms. The main treatment modalities are surgery, radiotherapy, chemotherapy and targeted therapies.

1.2.1 Surgery

Surgery is usually the first option for the majority of solid tumours diagnosed at the initial localised stages. It may be preceded by cytotoxic chemotherapy or local radiation in order to shrink the tumour so that to facilitate surgery and spare tissue for tumours located in critical organs (neoadjuvant treatment). The excised tissue is then examined in the laboratory to evaluate the risk of metastasis and decide whether/what type of additional post-surgical treatment is needed.

1.2.2 Radiation

Radiotherapy utilises high doses of radiations that kill cancer cells by damaging their DNA. It is usually combined with surgery or chemotherapy but can also be administered alone in cancers displaying high sensitivity to radiations. There are two main adminis-

[4]Based on the National Cancer Institute (NCI) website (https://www.cancer.gov)

tration modalities, external beam and internal radiation therapy. In the latter case, the source of radiations is positioned inside the body, near the tumour (brachytherapy).

1.2.3 Chemotherapy

Chemotherapy utilises drugs that kill cancer cells by interfering with mechanisms involved in cell division. It is used for the treatment of many types of cancers. However, because it kills preferentially cells in the dividing phase, chemotherapy is usually more effective on rapidly growing tumours. Because chemotherapy is given systemically, it also damages normal cells, in particular those of tissues with rapid turnover, such as the haematopoietic tissue, which causes important, possibly life-threatening, toxicities.

Chemotherapeutic drugs are classified according to their mechanisms of action. Alkylating agents are substances able to form covalent bounds with the DNA bases, disrupting the process of DNA replication. Besides having cytotoxic effects, alkilating agents are also potent mutagens and can favour the development of secondary malignancies [41]. Antimetabolites are substances that interfere with the normal functioning of metabolites produced inside cells. Some of these drugs are chemical analogs of normal metabolites and operate by substituting them in the DNA strands [41]. Other antimetabolites work by destabilising microtubule assembly. For instance, paclitaxel and docetaxel induce cell apoptosis by blocking the disintegration of microtubules at the end of mitosis [41].

Chemotherapeutic agents are often administered in combination. In order to maximise efficacy while maintaining tolerable levels of toxicity, multi-drug protocols usually include drugs with different modes of action and dose-limiting toxicities [41].

1.2.4 Targeted therapy

These drugs are designed to target specific molecular pathways that are critical in the development of cancer [45]. Targeted therapies are either monoclonal antibodies or small molecules. Monoclonal antibodies are proteins produced in laboratory, usually by injecting mice with the target protein. They are used for targets that are outside cells or on the outer cell surface. Small molecules are usually developed for targets that are inside cells

because these drugs can enter cells relatively easily. Tyrosine kinase inhibitors (TKI) are examples of such drugs. These small molecules block the transmission of intracellular signals by targeting receptor tyrosine kinases (RTKs) [45].

Targeted therapies approved for the treatment of cancer include hormone therapies, signal transduction inhibitors and immunotherapies. Angiogenesis inhibitors are also targeted therapies. Because they are the focus of this thesis, they will be described in a separate section.

Hormone therapies

Hormone therapies are used for cancer whose growth depends on hormones, such as some types of breast and prostate cancers. Hormone therapies can either block the production of hormones or inhibit their action at the receptor level on cells. Tamoxifen is an example of hormone therapy used for breast cancers expressing the oestrogen receptor (ER). This drug prevent the growth of ER-positive cells by binding to ER receptors.

Signal transduction inhibitors

Unlike normal cells that proliferate under control of exogenous stimulatory signals, cancer cells are able to produce growth signals by their own. Signal transduction inhibitors interfere with this improper signalling. The monoclonal antibody trastuzumab, used in breast cancer, is an example of such drugs. Its binding to the epidermal growth factor receptor 2 (HER-2) inhibits the function of this receptor, slowing the growth of breast cancers that overexpress HER-2.

Immunotherapies

The immune system is able to recognise and eliminate many types of tumours in their initial stages. However, through new mutations, cancer cells acquire the ability to circumvent immune recognition and/or destruction [46]. Immunotherapies aim at improving the immune response against cancer cells. Types of immunotherapy used to treat cancer include adoptive cell transfer and drugs targeting immune checkpoints.

- **Adoptive cell transfer therapy**, such as Chimeric Antigen Receptor (CAR)-T cells therapy, consists in extracting T-cells from the tumour of the patient. Those T-cells that are able to recognise and kill cancer cells are then expended in laboratory and reintroduced in the patient.

- **Immune checkpoints inhibitors** are drugs that target mechanisms that keep immune cells in an inactive state (immune checkpoints). These mechanisms, which in normal conditions are critical for the maintenance of self-tolerance, are exploited by cancer cells to escape immunesurveillance [47]. The cytotoxic T-lymphocyte associated antigen 4 (CTLA4) and the programmed cell death protein 1 (PD1) are the main targets of current checkpoints inhibitors. Immune checkpoint inhibitors are approved for the treatment of several cancers, including melanoma, non-small cell lung cancer, bladder cancer, head and neck cancers, liver cancer, renal cell carcinoma and stomach cancer. However only a limited number of patients respond to these therapies. Some patients do not benefit at all from these drugs and experience rapid disease progression at the first clinical evaluation, a phenomenon known as hyperprogression [48]. In addition, infiltrated lymphocytes can make the tumour appear larger under radiological evaluation, suggesting disease progression when the tumour is indeed responding to therapy. The identification of biomarkers to predict response of patients to these drugs is one of the main objectives of current research.

1.3 Antiangiogenic therapy

Growth of a tumour beyond few millimetres in size requires blood supply, which largely depends on the ability of tumour to release chemical signals that stimulate the development of new blood vessels from the pre-existing vasculature [49]. The concept of inhibiting tumour growth by blocking angiogenesis was introduced in the 1970's by J. Folkman [50]. Since then research in tumour angiogenesis has progressed, leading to the identification of the main molecules implicated in tumour angiogenesis, namely the vas-

cular endothelial growth factor (VEGF) and its tyrosine kinase receptor VEGFR-2 [51]. VEGF is secreted by tumour cells and binds to VEGFR-2 on endothelial cells, stimulating their proliferation and migration. In addition to VEGF, other signalling pathways contributes to angiogenesis. However, most drugs developed to inhibit angiogenesis target the VEGF pathway because it is activated in many types of human tumours as a consequence of hypoxic conditions. Drugs targeting the VEGF pathway include VEGF-neutralizing antibodies (e.g. bevacizumab) and small molecules tyrosine kinase inhibitors (TKIs) that block the kinase activity of VEGF receptors (e.g. sorafenib and sunitinib).

The first phase III trials demonstrating the efficacy of an angiogenesis inhibitor was in metastatic colorectal cancer (mCRC), where adding bevacizumab to a fluorouracil-based combination chemotherapy improved survival compared to the chemotherapy-alone arm [52]. Tyrosine kinase inhibitors (TKIs) have demonstrated single-agent activity in a number of metastatic cancers, including renal cell carcinoma (sunitinib [53, 54] and sorafenib [55, 56]) and a number of highly angiogenic tumours, such as hepatocellular carcinoma (sorafenib [57]), and pancreatic neuroendocrine tumours (sunitinib [58]). In renal cell carcinoma, sensitivity to VEGF inhibitors relates to the inactivation of the von Hippel Lindau (VHL) gene which causes increased expression of hypoxia-inducible factor 1 (HIF1A) and thus VEGF [24]. However, the reasons why certain cancer types respond to anti-angiogenic agents whereas others do not, are not fully understood. Examples of cancers where antiangiogenic therapies have repeatedly failed to improve survival in the metastatic setting include breast, melanoma, pancreatic and prostate cancers [59].

Several phase II and III trials have been carried out to evaluate VEGF pathway inhibitors in the neoadjuvant (pre-surgical) and adjuvant (post-surgical) settings. The rationale for the administration of antiangiogenic agents in these perioperative settings is to prevent local relapse and the growth of distant micrometastatic tumours. Moreover, neoadjuvant therapy is used to reduce tumour size, in order to turn an unresectable tumour into one that can be resected or improve surgical outcomes for resectable tumours [28]. Use of sunitinib in the adjuvant setting was recently approved to treat patients with renal cell carcinoma at high risk of recurrence based on the results of a randomised

trial where adjuvant sunitinib significantly improved disease-free survival [60]. However, several phase III trials with VEGF pathway inhibitors failed in the adjuvant setting, including trials with bevacizumab in colorectal [61] and breast cancers [62], and with sorafenib in hepatocellular carcinoma [63], suggesting that even when anti-angiogenic therapy is effective for a cancer in the advanced stage, the same may not be true in earlier stages. According to [24], one possible explantation of these differential efficacies is that the biology of micrometastases might not involve VEGF.

Antiangiogenic drugs were developed with the hope of circumventing resistance by targeting the more genetically stable endothelial cells of the tumour vasculature [64]. This hope, however, was not confirmed in practice, and both intrinsic and acquired resistance were found to be a limitation also of this new treatment modality. One possible mechanism of resistance is that the increased level of hypoxia caused by antiangiogenic therapy activate alternative signalling pathways that drive tumour vascularisation [24]. Other mechanisms that have been proposed are selection of tumour cell populations that can survive despite limited vascular supply, the heterogeneity of the tumour vasculature, with more mature vessels less dependent on VEGF, and the infiltration of bone-marrow-derived cell populations able to induce angiogenesis in a VEGF-independent manner [24]. Another reported resistance mechanism is vessel co-option, in which tumours rather than inducing angiogenesis, exploit the pre-existing vasculature from the surrounding normal tissue. Vessel co-option has been observed in many human tumours located in well vascularised organs, such as the lungs, liver and brain [65–67].

1.4 Quantitative mathematical modelling in oncology

1.4.1 Tumour growth

The analysis of tumour growth patterns has perhaps been the first application of mathematical modelling in oncology [68]. Classical tumour growth models provide a mathematical description of the macroscopic growth patterns without seeking deep-level explanation of the biological processes driving tumour growth [69]. These models are generally

defined by an ordinary differential equation (ODE) of the form

$$\frac{dV}{dt} = f(V)V, \quad V(t=0) = V_0, \tag{1.1}$$

where $V(t)$ is the tumour volume at time t, which is assumed to be proportional to the total number of cells in the tumour. The function $f(V)$ is the specific growth rate and can be interpreted as the fraction of volume that doubles in size during dt [10].

Exponential model

Assuming a constant $f(V)$ for all V, equation (1.1) yields the exponential growth model,

$$\frac{dV}{dt} = \alpha V, \quad V(t=0) = V_0. \tag{1.2}$$

The exponential model implies that the tumour doubling time is constant over time ($DT = \frac{\log 2}{\alpha}$). Exponential growth seems appropriate for describing tumour growth at the initial stages [68] and experimental tumours [70, 71]. However, most human tumours do not grow exponentially, showing a growth pattern characterised by decelerating growth (i.e. increased doubling time) as the tumour size increases [72, 73]. To describe decelerating growth patterns a variety of sigmoidal models have been introduced [73]. Examples of these models are the Gompertz and logistic growth models. However, unlike the Gompertz model, the logistic model has often been found unable to describe experimental tumour growth data satisfactorily [69, 74].

Gompertz model

One of the most used models for describing tumour growth is the Gompertz model, defined by

$$\frac{dV}{dt} = \alpha_0 e^{-\beta t} V, \quad V(t=0) = V_0. \tag{1.3}$$

Parameter α_0 is the specific growth rate at size V_0 and β represents the exponential decay of the specific growth rate. Integration of equation (1.3) yields the analytical form of the

Gompertz model,

$$V(t) = V_0 e^{\frac{\alpha_0}{\beta}(1-e^{-\beta t})}.$$

According to this model, the tumour will approach a limiting asymptotic size, given by $K = V_0 e^{\frac{\alpha_0}{\beta}}$.

Despite lacking of a clear biological explanation, the Gompertz model was found to provide a good empirical description of tumour growth in several studies on animals [69, 74–76] and has often been used as basis for models incorporating the effect of treatment [10, 11].

1.4.2 Treatment

Skipper-Schabel-Wilcox model

One of the first quantitative studies of tumour growth in response to chemotherapy was carried out by Skipper, Schabel and Wilcox, who in the early 1960s proposed what became known as the log-kill model [71],

$$\frac{dV}{dt} = \alpha V(1 - k\,C(t)),$$

where $C(t)$ is the drug concentration at time t. This model is based on experimental observations that for tumours growing exponentially, a certain level of therapy will always kill a fixed fraction of tumour cells, regardless of the tumour size at the time of treatment. This means that if a given dose of a given drug reduces 10^6 cells to 10^5 cells, the same therapy applied to 10^4 cells will leave 10^3 cells alive (Figure 1.2). The concept of fractional kill thus implies that small tumours should be easily cured by repeated cycles of therapy. However, this prediction was not confirmed in the clinic, for example when the concept of fraction kill was applied to the treatment of micrometastases in early-stage breast cancer [77].

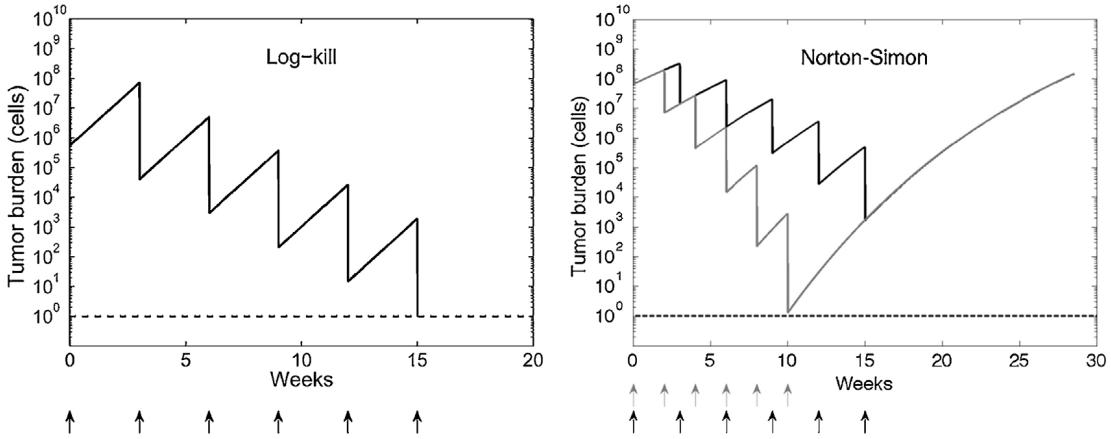

Figure 1.2 – Left: log-kill model. Each cycle of therapy produces a fixed fraction kill. Right: Norton-Simon model. This model suggests intensification of treatment schedules as the tumour shrinks. (Image from [78]).

Norton-Simon model

The log-kill model is based on the assumption of exponential growth, which is not realistic for the majority of human tumours [72, 73]. In the 1970s, Norton and Simon [10] proposed an alternative model to describe tumour regression in response to chemotherapy. The Norton-Simon model is based on Gompertzian growth and assumes a kill rate proportional to the growth rate of the untreated tumour, that is

$$\frac{dV}{dt} = \alpha_0 e^{-\beta t} V(1 - k\,C(t)).$$

This model implies that a given therapy will cause slower regression in very large and very small tumours than in histologically equivalent tumours of intermediate size. According to the Norton-Simon model, the best therapeutic strategy would be then to employ a moderate therapy initially (when the tumour is presumably of intermediate size) and a final intensification (Figure 1.2). This prediction was confirmed in several clinical trials where late intensification was accomplished either by increasing dose levels of the same agents (intensification) or by using new agents in an aggressive manner (cross-over intensification) [79, 80].

The model of Hahnfeldt

An extension of the Gompertz model has been proposed by Hahnfeldt *et al.* [11] to describe tumour growth dynamics under angiogenic control. This model differs from the classical Gompertz model in that it represents the effects of angiogenic control by means of a time-dependent carrying capacity, K:

$$\begin{cases} \frac{dV}{dt} = \alpha V \log\left(\frac{K}{V}\right) \\ \frac{dK}{dt} = -\lambda_2 K + bS(V,K) - dI(V,K) - eKC(t) \\ V(t=0) = V_0, \quad K(t=0) = K_0. \end{cases}$$

In the equation for K, the first term represents the spontaneous vascular loss; the second and third terms represent stimulation and inhibition due to the tumour cells; the last term represents inhibition due to the administered drugs, taken to be proportional to the concentration $C(t)$. The expressions for $S(V,K)$ and $I(V,K)$ are established on the basis of biological considerations. The authors used their model to analyse experimental data from mice bearing Lewis lung tumours treated with antiangiogenic agents (endostatin, angiostatin and TNP-470). The model predicted the existence of a limiting tumour size despite the presence of vasculature in the tumour. This plateau is due to the balance of endogenous stimulators and inhibitors and may be lowered by administering an inhibitor agent.

Models of combination of chemotherapy and antiagiogenic therapy

Models with varying carrying capacity have been applied in a number of works evaluating the synergetic interaction between antiangiogenic and cytotoxic agents [7, 81, 82]. These modelling works were motivated by studies suggesting a transient normalisation of the intratumoural vasculature induced by antiangiogenic agents [83, 84]. As chemotherapy reaches the tumour through the blood circulation, this fact can be exploited for a more efficient drug delivery.

In [7], Mollard *et al.* built a PK-PD model describing the evolution in time of the vascular quality under the effect of antiangiogenic agents. This model extends the model of Hahnfeldt by decomposing the time dependent carrying capacity $K(t)$ into a stable component $S(t)$ and an unstable component $U(t)$, representing respectively the mature and immature vessels components of the tumour vasculature. The effect of the cytotoxic drug is described with a transit compartment model [12] in order to account for the delay in the effect of the drug. The antiangiogenic drug is assumed to affect the unstable vessels component because it represents the new vessels generated through the process of angiogenesis. Simulations of the model suggested an optimal time gap of 3.4 days between the administration of bevacizumab and paclitaxel. The proposed scheduling was then tested experimentally on mice orthotopically xenografted with human breast cancer cells, where the sequential administration of bevacizumab and paclitaxel with a time lag of 3 days resulted in improved antitumour efficacy and reduced metastatic spreading.

In [82], the authors simplified the model presented in [7] to identify the optimal scheduling for the administration of bevacizumab and pemetrexed-cisplatin, using data from a mouse model of non-small cell lung cancer (NSCLC). The mathematical model predicted an optimal delay of 3 days between bevacizumab and chemotherapy. This model prediction was further confirmed in experiments comparing the proposed schedule against other sequential and concomitant administrations.

Models of the emergence of biochemical resistance

The Norton-Simon model explains failure of therapy through the concept of "kinetic resistance" by which treatment can lose its efficacy as the tumour shrinks. This phenomenon of kinetic resistance is different from the resistance acquired at the biochemical level due to genetic and/or epigenetic events. The problem of biochemical resistance was first addressed in a quantitative sense by Goldie and Coldman, who developed a mathematical model relating the drug sensitivity of a tumour to its spontaneous rate of mutations towards phenotypic drug resistance [85]. Their analysis indicated that the probability of

there being at least one resistant cell will rise dramatically during a very short interval in the growth history of the tumour. Based on this result, the authors suggested that to maximise the probability of cure, tumours should be treated as early as possible using as many effective drugs as possible. Moreover, the authors recommended that if several drugs cannot be administered simultaneously, they should be employed in a strict alternating sequence. The concept of alternating sequence was tested in numerous clinical trials. However, compared to sequential regimens, alternating regimens resulted in little or no benefit [86].

To investigate the problem of the emergence of resistance in non-small cell lung cancer (NSCLC) during treatment with the epidermal growth factor receptor (EGFR) inhibitor erlotinib, Chmielecki *et al.* [8] developed a mathematical model based on a stochastic branching process in which drug-sensitive and resistant cancer cells divide or die according to growth rates dependent on the drug concentration, and sensitive cells give birth at each division to a resistant cell with a certain probability. Model parameters were determined using a patient-derived cell line. The authors then used their model to select among a range of clinically tolerable schedules, the strategy that minimises the probability of resistance or the conditional expected number of resistant cells in the event that resistance has already emerged [87]. The optimal strategy identified by the model consists in combining a daily low dose with twice weekly high-dose pulses. This schedule was tested in patient in a phase I study [8]. The schedule selected by the model analysis did not delay the development of resistance, probably because the drug concentrations utilised in the preclinical models were not achievable in patients [8]. However, the clinical results indicated superiority of the pulse-continuous schedule in controlling central nervous system metastases.

1.4.3 Metastasis

Compared to the vast literature dedicated to the modelling of the growth of a single tumour, relatively few models have been proposed to describe the metastatic process. The reason for this may be partly due to the complexity of the metastatic process that makes

its modelling difficult as well as the limited availability of metastatic data. The study of Liotta *et al.* [13, 88] is one of the first modelling work that makes use of experimental data to model mathematically the metastatic process. The authors developed an ODE model consisting of a number of compartments representing key steps of the metastatic cascade. The model was parameterised using data from a mouse model of fibrosarcoma that developed pulmonary metastases and its predictions were found in agreement with the observed number of macroscopic metastases and the metastatic free survival in the animals.

To predict the number of tumour under the detectability limit, Iwata *et al.* [14] proposed a deterministic model describing the evolution in time of the size distribution of a population of metastatic tumours. The Iwata model is the model adopted in this thesis to model the metastatic process and will be described in the next chapter, along with its validations and extensions by other authors.

Hanin *et al.* have produced a number of works using a stochastic model of cancer progression, accounting for primary tumour growth, dissemination of metastases, latency and growth of metastases in secondary sites [15, 89]. Dissemination is modelled as a Poisson process with rate dependent on the primary tumour size through a power law, following the same assumption as Iwata *et al.* The model provides an explicit formula for the volume distribution of the metastatic tumours at a given site, which is used for estimating the identifiable parameters of the model from metastatic data. For example, in [15], the authors applied their model to the autopsy data of an untreated lung cancer patient with 428 metastases in the liver. Simulation results indicated that the first metastasis started growing before diagnosis, thus suggesting that the patient could not have been cured by surgery alone.

In a study by Heano *et al.* [16], the authors developed a mathematical model of pancreatic cancer progression using clinical data of pancreatic cancer patients. The model assumes exponential growth for primary tumour and metastases. Cancer cells follow a stochastic process, where at each time step a cell is chosen to divide or die. The probability of establishing a new colony at a distant site is assumed to be the product

of the probability for a cell of the primary tumour to acquire a mutation conferring the ability to metastasise and the probability for the mutated cells of being "exported" from the primary tumour. The authors calibrated their model using autopsy data from 101 pancreatic cancer patients and validated it on a independent cohort of 127 patients. The mathematical model was then used to evaluate the effects of resection and chemotherapy strategies on patient survival. Simulation results suggested that chemotherapy strategies able to effectively reduce the growth rate of primary and metastatic tumours are more efficient in extending survival of patients than surgical resection alone.

Another class of models aims at describing the most likely pattern of metastasis from a specific primary tumour. An example of such model is that of Newton *et al.* [17], who proposed a Markov chain based model to describe the metastatic spread from primary lung cancer. The model is based on a network of metastatic sites with a transition matrix whose coefficients were estimated from the empirical distribution of the metastatic locations in a population of 3827 deceased lung cancer patients. The calibrated model was used to analyse the timing of metastasis in each sites. For example, the estimated one-step and two-step transition probabilities allowed to classify metastatic sites as first-order and second-order sites, as well as the identification of stronger self-seeder sites. The authors also performed Monte Carlo simulations of the calibrated model in order to compute the mean first-passage time from the lung to any given metastatic site. They propose to use this quantity as a measure of metastatic progression, since according to the model, if a patient has metastases in one of those sites with largest mean first-passage times, then he is also likely to have metastases in other areas.

1.5 Motivations and objectives

This thesis contains two projects: the modelling study of neoadjuvant sunitinib on pre-clinical data and the development of a predictive model for the time to metastatic relapse on a clinical dataset of breast cancer patients. The following sections outline the motivations and the aims of each one of these works.

Modelling study of neoadjuvant sunitinib on preclinical data

Sunitinib is a drug with anti-angiogenic activity used in the treatment of patients with metastases from renal cell carcinoma or gastrointestinal tumours. However, recent preclinical studies have shown limited, or even opposing, efficacies in preventing metastatic spread, despite clear inhibition of primary tumour growth [25–27]. In addition, there are a number of preclinical and clinical studies suggesting that stopping antiangiogenic treatment may lead to rapid revascularisation and rebound tumour growth [28]. To date, the majority of mathematical models in oncology focus on the effects of treatment only on primary tumour dynamics. This work aims at i) extending an established model of the metastatic process [19] to describe primary tumour and metastatic dynamics in response to sunitinib in clinically relevant mouse models of metastatic cancers, ii) testing possible hypotheses for the reported differential effects of sunitinib on primary tumour and metastases, iii) evaluating different schedules of neoadjuvant sunitinib by simulations of the calibrated model, and iv) assessing the predictive power of biomarkers on the model parameters with the use of machine learning algorithms.

Development of a predictive model for the time to metastatic relapse

The second part of this thesis concerns the predictive modelling of the time to metastatic relapse in patients diagnosed with early-stage breast cancer. The proposed model is based on the biology of the metastatic process and is evaluated for its predictive power on a dataset of 642 breast cancer patients. The final objective is to develop a predictive model of clinical utility that, by providing estimates of the invisible metastatic burden at the time of diagnosis and forward simulations of metastatic growth, could be used as a personalised prediction tool to assist in the decision for adjuvant therapy.

1.6 Organisation of the thesis and summary of contributions

The biology of the metastatic development and the main anticancer treatments have been described in this chapter. Chapter 2 describes the datasets used in this thesis, the

mathematical model used to describe the metastatic process and the statistical techniques utilised for the analysis of longitudinal and time-to-event data, with a first example of modelling of tumour growth data. In Chapters 3 and 4, the metastatic model is extended and applied to analyse experimental data of primary tumour and metastatic dynamics from mice treated with neoadjuvant sunitinib therapy. In Chapter 5, the metastatic model is adapted to fit time-to-relapse data and its predictive performance evaluated and compared to Cox regression and machine learning algorithms. Finally, Chapter 6 summarises the thesis achievements, discusses the clinical implications of the results and suggests possible future works.

The study carried out in Chapter 3 and 4 is based on an existing code in Matlab to fit the Iwata model to primary tumour and metastatic burden data using a mixed-effects population approach. My personal contribution has been to i) confirm the validity on larger datasets of the models established in [19], ii) perform model simulations in Matlab to test the effect of therapy on metastases, iii) adapt the code to fit longitudinal data from treated animals, and iv) combine the mixed-effects framework with machine learning algorithms available within the R caret package [90] in order to assess the predictive power of biomarkers. The study of Chapter 3 has been presented in a poster at the AACR Annual Meeting 2018 [91], and has been accepted for two oral presentations, at the 28th PAGE meeting and the SMB Annual Meeting 2019. It is to be submitted to the journal *Cancer Research* [92] along with the study presented in Chapter 4 [93].

For the study of Chapter 5, I have utilised the extension of the R saemix package to right censored time-to-event data, developed by Belhal Karimi [39, 94]. My contribution has been to i) code in Python the structural model and the likelihood function for the mechanistic model of the time to metastatic relapse, and ii) make the connection between Python and R by using the R package reticulate. The mechanistic model applied to a dataset of early-stage breast cancer patients performs similarly to the state of the art approaches. In addition, it brings advances to the field of survival analysis, being the first attempt of mechanistic modelling for prediction of the time to metastatic relapse. This work has been presented during an oral session dedicated to applications of machine

learning in oncology at the 28th PAGE meeting and has been submitted to the *JCO Clinical Cancer Informatics* [95].

1.6.1 Scientific production

Papers to be submitted

- C. Nicolò, M. Mastri, J. ML Ebos, S. Benzekry. Machine learning combined to mechanistic modeling of differential effects of neoadjuvant Sunitinib on primary tumor and metastatic growth. *To be submitted to Cancer Res*
- M. Mastri, C. Nicolò, S. Benzekry and J. ML Ebos. Impact of treatment breaks and burst in the neo-adjuvant setting for anti-angiogenic therapy of kidney cancer. *To be submitted to Cancer Res*
- C. Nicolò, C. Perier, M. Prague, G. MacGrogan, C. Bellera, O. Saut, and S. Benzekry. Machine learning versus mechanistic modeling for prediction of metastatic relapse in breast cancer. *Submitted to JCO Clinical Cancer Informatics*

Oral communications

- July 2019, SMB Annual Meeting, Montréal, Québec, Canada. Machine learning combined to mechanistic modeling of differential effects of neo-adjuvant Sunitinib on primary tumor and metastatic growth. Oral (speaker)
- June 2019, Population Approach Group meeting in Europe (PAGE), Stockholm, Sweden. Machine learning combined to mechanistic modeling of differential effects of neo-adjuvant Sunitinib on primary tumor and metastatic growth. Oral (speaker)
- June 2019, Population Approach Group meeting in Europe (PAGE), Stockholm, Sweden. Machine learning versus mechanistic modeling for prediction of metastatic relapse in breast cancer. Oral
- April 2018, Annual meeting of the AACR, Chicago, USA. Mathematical modeling of differential effects of Sunitinib on primary tumor and metastatic growth. Poster

Chapter 2

Methods

2.1 Description of the data

2.1.1 Primary tumour and metastatic data in mouse models of cancers in response to neoadjuvant sunitinib

The experimental data used in this study were made available to us by Dr. John Ebos (Roswell Park Cancer Institute, Buffalo, USA) and were derived from two orthosurgical metastasis models representing competent and incompetent immune systems with luciferace-tagged human breast (LM2-4$^{\mathrm{LUC+}}$) and mouse kidney (RENCA$^{\mathrm{LUC+}}$) cell lines, respectively [19]. Cancer cells were implanted orthotopically in mice, namely into the right mammary fat pad for the breast model and into the left kidney for the kidney mouse model. Primary tumour burden was monitored with callipers, while post-surgical metastatic tumour burden was assessed by bioluminescence. Animals received neoadjuvant sunitinib treatment according to different schedules, starting 14 days before primary tumour removal (Figure 2.1). The dataset contains measurements for 230 animals (132 for the breast model and 98 for the kidney model). Besides longitudinal measurements of primary tumour and metastatic dynamics, it also comprises survival data and pre-surgical molecular and cellular biomarkers, including vascular cell Ki67 and CD31 expression, circulating tumour cells (CTCs) and myeloid derived suppressor cells

(MDSCs).

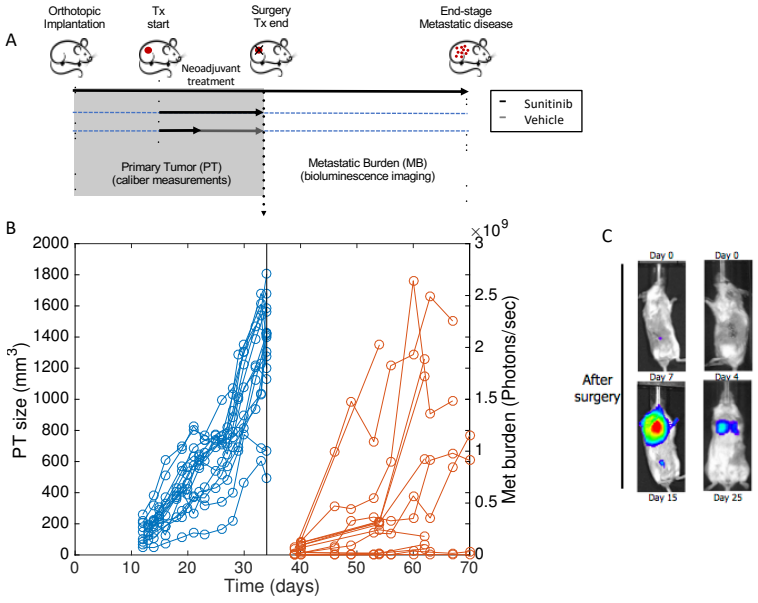

Figure 2.1 – A) Sketch of the experimental setting for the studying of neoadjuvant sunitinib in mouse models of breast and kidney cancers. B) Longitudinal data of primary tumour size and metastatic burden. C) Bioluminescence monitoring of post-surgical metastatic development. Data from Dr. John Ebos's lab (Roswell Park Cancer Institute, Buffalo, USA)

2.1.2 Metastatic relapse in early-stage breast cancer patients

This dataset contains data of time to metastatic relapse for 642 women diagnosed with primary operable invasive breast carcinoma and operated at the Bordeaux Bergonié institute between 1989 and 1993. The patients considered did not received any adjuvant treatment, with the exception of post-surgical local irradiation for 512 patients, thus allowing to assess the natural history of the course of metastasis. Figure 2.2 shows the Kaplan-Meier estimates of overall and distant metastasis-free survival for these patients. The latter was defined as the time from the date of diagnosis to the date of distant recurrence and patients with no metastasis were censored at the date of last news or death. Clinical/pathological variables available in the dataset included age and tumour size at diagnosis, menopausal status, grade, T and N stages, histological type and number of

invaded ganglions. In addition, ER and PR receptor, HER2, Ki67, basal markers, CD24, CD44, ALDH1, BCL2, E-Cadherin and Trio were recorded.

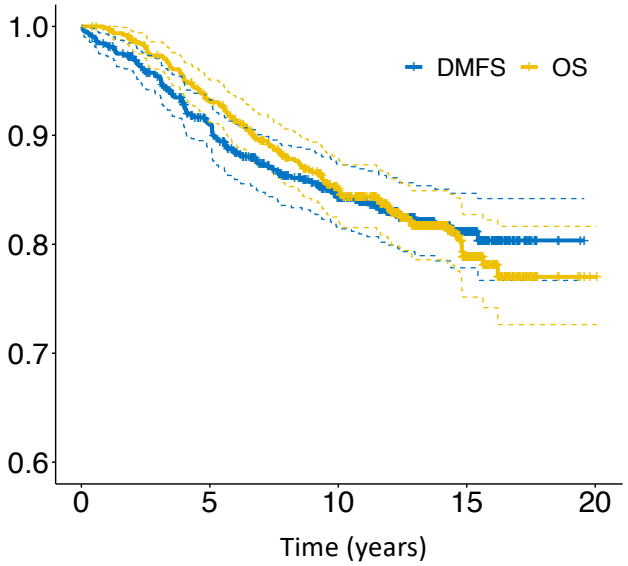

Figure 2.2 – Kaplan-Meier estimates of the distant metastasis-free survival (DMFS) and overall survival (OS) for the breast cancer patients of the Bergonié dataset. + : censored observations.

2.2 The Iwata model for the description of the metastatic process

2.2.1 Assumptions and equations

Iwata *et al.* [14] developed a mathematical model to describe the evolution in time of the size distribution of metastatic tumours. A schematic representation of the model is shown in Figure 2.3. In this model, the primary tumour is assumed to start from a single cell and to grow at rate $g_p(v)$, where v denotes the tumour size, expressed either in volume or in number of cells ($1\ \text{mm}^3 \simeq 10^6$ cells [96]). It is supposed that, while growing, the primary tumour emits metastatic single cells at rate $d(v)$. Each metastatic cell develops into a new tumour, that grows at rate $g(v)$ and also disseminates metastatic cells at rate $d(v)$. It is further assumed that the nuclei of colonisation are located far enough

from each other so that their ranges do not overlap and that no metastatic tumour is present at the initial time. The state of the metastatic process is described by means of a function $\rho(t, v)$, representing the distribution of metastatic tumours with size v at time t. This solves the following initial-boundary value problem (IBVP):

$$\begin{cases} \partial_t \rho(t,v) + \partial_v (g(v)\rho(t,v)) = 0, & t \in (0,+\infty),\ v \in (V_0,+\infty) \\ g(V_0)\rho(t,V_0) = d(V_p(t)) + \int_{V_0}^{+\infty} d(v)\rho(t,v)\,dv, & t \in (0,+\infty) \\ \rho(0,v) = 0, & v \in (V_0,+\infty) \end{cases} \tag{2.1}$$

where V_0 represents the size of one cell, and $V_p(t)$ is the size of the primary tumour at time t, which, by definition, solves

$$\begin{cases} \dfrac{dV_p(t)}{dt} = g_p(V_p) \\ V_p(0) = V_0. \end{cases} \tag{2.2}$$

The model equations (2.1) can be derived as follows. Let $P(t, v)$ be the number of metastases with size smaller than v at time t

$$P(t,v) = \int_{V_0}^{v} \rho(t,s)\,ds.$$

Passing from time t to time $t + dt$, this quantity has to satisfy the following balance equation:

$$P(t+dt, v+g(v)dt) = P(t,v) + \left[d(V_p(t)) + \int_{V_0}^{+\infty} d(v)\rho(t,v)\,dv \right] dt. \tag{2.3}$$

Expanding the l.h.s. of (2.3) with respect to dt and dv yields

$$P(t+dt, v+g(v)dt) \approx P(t,v) + \partial_t P(t,v)dt + \partial_v P(t,v)g(v)dt,$$

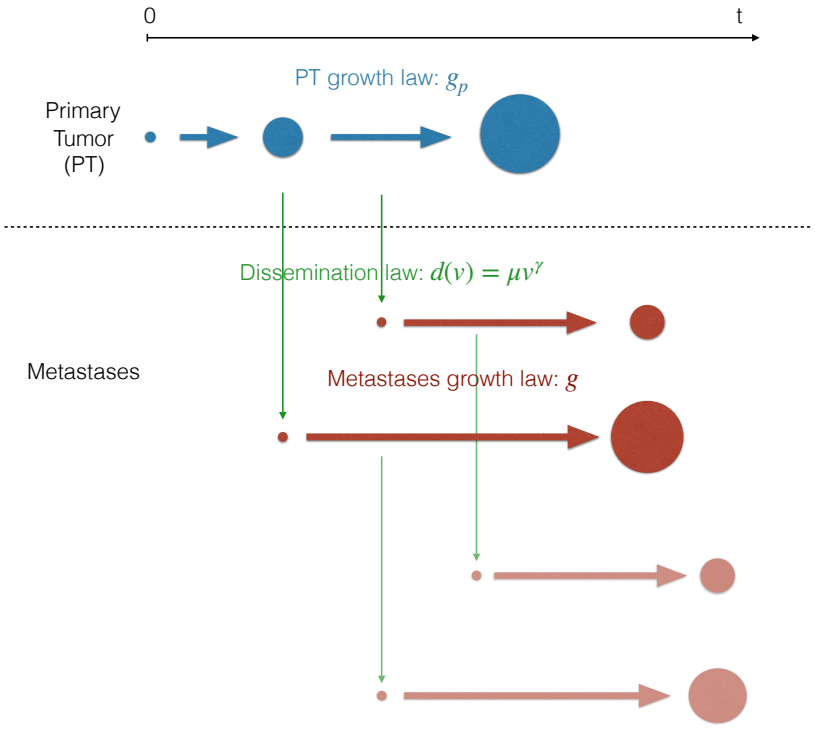

Figure 2.3 – Schematic representation of the mathematical metastatic model defined by (2.1) - (2.2). g_p and g are the growth rates of the primary tumour and metastases, respectively. d denotes the dissemination rate from the primary tumour and metastases. It depends on the tumour volume and two parameters μ and γ. The former characterises the metastatic aggressiveness of the tumour, whereas the latter can be interpreted as the fractal dimension of the vessels infiltrating the tumour [14].

so that one gets

$$\int_{V_0}^{v} \partial_t \rho(t,s)\, ds + g(v)\rho(t,v) = d(V_p(t)) + \int_{V_0}^{+\infty} d(v)\rho(t,v)\, dv.$$

Derivation of the above equation with respect to v yields

$$\partial_t \rho(t,v) + \partial_v (g(v)\rho(t,v)) = 0,$$

while setting $v = V_0$ provides the boundary condition

$$g(V_0)\rho(t, V_0) = d(V_p(t)) + \int_{V_0}^{+\infty} d(v)\rho(t, v)\, dv.$$

The former equation means that the number of metastases emitted in one time unit corresponds to the total rate of metastatic emission due to the primary tumour (first term of the r.h.s.) and the metastatic tumours (second term of the r.h.s).

The model presented in [14] assumed:

- the same Gompertzian growth rate for both primary and secondary tumours:

$$g_p(v) = g(v) = av \log \frac{b}{v},$$

  where a is a growth rate constant and b is the maximum reachable size (carrying capacity).

- a dissemination rate $d(v)$ of the following form:

$$d(v) = \mu v^{\gamma},$$

  where μ is the dissemination coefficient and γ is the fractal dimension of blood vessels infiltrating the tumour. A value of $\gamma = 1$ indicates that blood vessels are homogeneously distributed inside the tumour, whereas a value of $\gamma = 2/3$ indicates that the tumour vascularity is superficial [14].

2.2.2 Numerical discretisation

Macroscopic quantities

From the size distribution function $\rho(t, v)$, it is possible to derive some macroscopic quantities which are important when the model has to be compared against observed

data. Example of such quantities are the *total number of metastasis* at time t,

$$N(t) = \int_{V_0}^{+\infty} \rho(t, v)dv, \tag{2.4}$$

the *metastatic burden* (i.e. the total metastatic mass),

$$M(t) = \int_{V_0}^{+\infty} v\rho(t, v)dv, \tag{2.5}$$

and the *cumulative number of metastases*, that is the number of metastases of size larger than a given size $\bar{v}$:

$$N_{\bar{v}}(t) = \int_{\bar{v}}^{+\infty} \rho(t, v)dv. \tag{2.6}$$

More generally, we may rewrite the above quantities as weighted integrals

$$F_f(t) := \int_{V_0}^{+\infty} f(v)\rho(t, v)dv. \tag{2.7}$$

Proposition 1 (Hartung [97])**.** *If the metastatic growth rate g is autonomous, then the quantity defined in* (2.7) *satisfies*

$$F_f(t) = \int_0^t f(V(s)) \left[d(V_p(t-s)) + \int_{V_0}^{+\infty} d(v)\rho(t-v, v)dv \right] ds, \tag{2.8}$$

where V is defined as the solution of

$$\begin{cases} \frac{dV}{dt} = g(V), \\ V(t=0) = V_0. \end{cases} \tag{2.9}$$

Proof. If g does not depend on time, the first equation in (2.1) can be rewritten as

$$\partial_t(g(v)\rho(t, v)) + g(v)\partial_v(g(v)\rho(t, v)) = 0, \tag{2.10}$$

from which we see that $g(v)\rho(t, v)$ is constant along the characteristics associated to (2.10). The characteristic that solves (2.9) separates the domain into two subregions: to

the left of it, the solution depends on the boundary condition, whereas to the right of it, the solution depends on the initial condition, and thus is zero (Figure 2.4). Therefore, we have

$$F_f(t) = \int_{V_0}^{+\infty} f(v)\rho(t,v)dv = \int_{V_0}^{V(t)} f(v)\rho(t,v)dv.$$

Making the change of variables $v = V(s)$, $dv = g(V(s))ds$ and exploiting the conservation property along the characteristics, we obtain

$$\begin{aligned} F_f(t) &= \int_0^t f(V(s))\rho(t,V(s))g(V(s))ds \\ &= \int_0^t f(V(s))\rho(t-s,V_0)g(V_0)ds \\ &= \int_0^t f(V(s))\left[d(V_p(t-s)) + \int_{V_0}^{+\infty} d(v)\rho(t-s,v)\,dv\right]ds. \end{aligned}$$

□

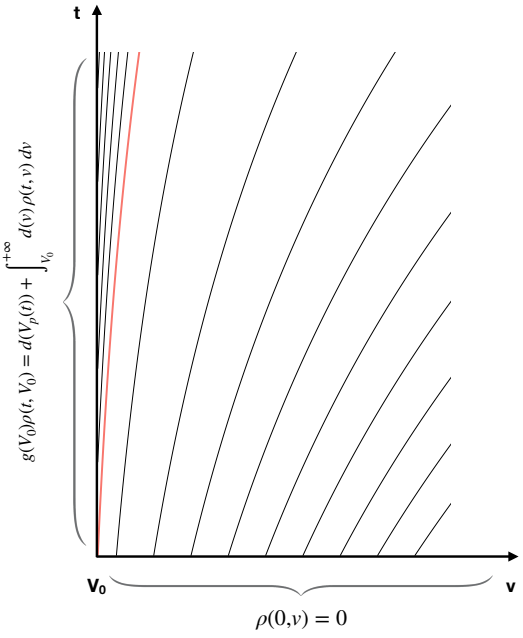

Figure 2.4 – Picture of the characteristics for the IBVP (2.1).

Remark 1. *If secondary dissemination is neglected,* (2.8) *reduces to*

$$F_f(t) = \int_0^t f(V(s))d(V_p(t-s))ds,$$

so that computation of $F_f(t)$ *does not require solving* (2.1)*. In particular, the total number of metastases* ($f \equiv 1$) *and the metastatic burden* ($f(v) = v$) *are respectively given by*

$$N(t) = \int_0^t d(V_p(s))ds, \qquad M(t) = \int_0^t V(s)d(V_p(t-s))ds.$$

The latter equation can be solved efficiently through the use of a fast Fourier transform algorithm [97].

To calibrate the mathematical model from primary tumour and metastatic burden data, simulations of the model required for the fitting algorithm were performed with a method based on the use of a fast Fourier transform algorithm [97]. This method cannot be applied when the metastatic growth rate depends on time, such as in the case where treatment is supposed to affect the growth of metastases. Simulations of the model in this case were performed using a numerical scheme based on the method of characteristics and involving a change of variables that, by straightening the characteristics, leads to the resolution of a simpler problem [98].

A discrete version of the model was used to simulate the cancer history in individual patients after model calibration (Section 5.3.4). In the discrete model, the appearance time of the i-th metastasis is defined by

$$T_i = \inf\{t > 0 : N(t) \geq i\}.$$

Its volume is then given by

$$\begin{cases} \dfrac{dV_i(t)}{dt} = g(V_i) \\ V_i(t = T_i) = V_0. \end{cases}$$

Both continuous and discrete versions of the Iwata model are implemented in the Matlab

library METAMATS developed by S. Benzekry.

2.2.3 Extensions and validations

Iwata *et al.* [14] assessed the practical applicability of their model by fitting the cumulative number of metastases (2.6) to CT scan data from a patient with hepatocellular carcinoma as primary tumour and multiple metastatic tumours in the liver. The model was found to reproduce well the behaviour of the observed data. In addition, since the estimated value for the fractal dimension parameter γ was close to $2/3$, the authors concluded that for that patient the tumour vascularity should have been nearly superficial.

A detailed mathematical analysis of the Iwata model has been conducted by Barbolosi *et al.* [99], who established the existence and uniqueness of solutions to the PDE and presented an appropriate numerical scheme.

A two-dimensional version of the metastatic model (2.1) has been proposed by Benzekry [98] in order to include the angiogenic process and model the effects of a combined cytotoxic/antiangiogenic therapy. The author performed a mathematical analysis of the model in the autonomous (model without treatment) and non-autonomous case (model with treatment), and introduced an adapted numerical scheme. Model simulations were then presented to illustrate possible applications of modelling to the clinic and compare different treatment modalities [100, 101]. Based on simulation results, the author suggests the use of a metronomic administration scheme [101]. Further extensions of the model were also derived to account for possible systemic interactions between tumours [102, 103].

In a work of Hartung *et al.* [18], the Iwata model has been validated against experimental data of primary tumour and metastatic burden dynamics from orthotopic breast tumor xenograft experiments conducted in mice.

Another validation of the Iwata model that uses data from mouse models was conducted by Benzekry *et al.* [19]. The main difference of this study is that it utilises data from orthosurgical mouse models in order to carry out a mathematical modelling analysis of the impact of surgery on metastasis. Validation was also extended to multiple

animal models (breast and kidney). In addition, the authors calibrated the Iwata model on a clinical dataset of metastatic relapse probability in breast cancer patients and used the estimated distribution of μ to analyse the relationships between resected primary tumour size and survival. The simulated relationship indicated two threshold for the primary tumour size: a lower threshold, below which metastatic risk is negligible, and an upper threshold, above which surgery has a negligible benefit. The authors pointed out that estimation of the model parameter μ in a patient specific manner would be of clinical relevance, since it would allow to use their model in practice as a diagnostic and prognostic tool.

2.3 Nonlinear regression

We suppose to dispose of a mathematical model that approximates the phenomenon under study and that this model can be expressed as a parametric function of time $f(t;\theta)$, which we will call the *structural model*. The next step to complete the model consists in determining an estimate of the unknown parameter θ by making use of available measurements. A model for continuous data is generally written as follows:

$$y_j = f(t_j;\theta) + e_j \quad 1 \leq j \leq n, \tag{2.11}$$

where $(y_j, 1 \leq j \leq n)$ are the observations collected at times $(t_j, 1 \leq j \leq n)$, and $(e_j, 1 \leq j \leq n)$ is a sequence of residual errors with $\mathbb{E}(e_j) = 0$. Two estimation methods commonly used in the context of parametric models are the least-squares method (Section 2.3.1) and the maximum likelihood method (Section 2.3.2).

Besides estimating the model parameters, it is also important to evaluate the precision of the estimates. This can be done by looking at the standard errors, i.e. the standard deviations of the components of the estimator. Standard errors can often be estimated using analytical formula based on asymptotic results. In more complicated cases, standard errors can be obtained using the bootstrap method [104, p. 108].

2.3.1 Least-Squares Estimation

Definition 1 (Least-squares estimator)**.** *Let θ^* be the true unknown value of θ. The least-squares estimate of θ^* is the value $\hat{\theta} = \hat{\theta}(y_1, \ldots, y_n)$ that minimises the residual sum of squares [105, p. 21]*

$$S(\theta) = \sum_{j=1}^{n} (y_j - f(t_j; \theta))^2. \tag{2.12}$$

The least-squares method does not provide any estimate for the variance of the residual errors. However, if the e_j are independent and identically distributed (i.i.d.) with variance σ^2, an *a posteriori* estimate of σ^2 is given by [105, p. 21]

$$\hat{\sigma}^2 = \frac{S(\hat{\theta})}{n - d}, \tag{2.13}$$

where d is the dimension of the parameter vector θ.

Theorem 1 (Asymptotic normality of the LSE)**.** *Under certain regularity conditions, for large n, the least-squares estimator has approximately a normal distribution [105, p. 24]*

$$\hat{\theta} \sim \mathcal{N}(\theta^*, C), \quad C = \sigma^2 (J(\theta^*)^T J(\theta^*))^{-1}, \tag{2.14}$$

where $J = \left[\left(\frac{\partial f(t_i;\theta)}{\partial \theta_j} \right) \right]$ is the jacobian matrix of the model.

The theorem above can be proved using a linear approximation [105, p. 23] and allows to estimate the standard error of the jth component of $\hat{\theta}$ as:

$$\widehat{se}(\hat{\theta}_j) = \sqrt{\hat{C}_{jj}}, \text{ with } \hat{C} = \hat{\sigma}^2 (J(\hat{\theta})^T J(\hat{\theta}))^{-1}. \tag{2.15}$$

2.3.2 Maximum Likelihood Estimation

Definition 2 (Likelihood function)**.** *Let $Y = (Y_1, \ldots, Y_n)$ be random variables with joint density function $p_Y(y_1, \ldots, y_n; \theta)$ and let $y = (y_1, \ldots, y_n)$ denote the observed values of*

Y. The likelihood *is a function of θ defined by*

$$\mathcal{L}_y(\theta) = p_Y(y_1, \ldots, y_n; \theta).$$

In particular, if Y_j, $j = 1, \ldots, n$, are independent, the likelihood is

$$\mathcal{L}_y(\theta) = \prod_{j=1}^{n} p_{Y_j}(y_j; \theta).$$

Definition 3 (Maximum likelihood estimator)**.** *The* maximum likelihood *(ML)* estimator *is the value of θ that maximises $\mathcal{L}_y(\theta)$.*

An estimate of the variance of the ML estimator can be computed analytically using the following asymptotic result [104, p. 129].

Theorem 2 (Asymptotic normality of the MLE)**.** *Let θ^* be the true value of θ. Under appropriate conditions, the ML estimator of θ has an asymptotic normal distribution with mean θ^* and covariance matrix $C = I_y^{-1}(\hat{\theta})$, where $I_y(\hat{\theta})$ is the* observed Fisher information matrix *(FIM)*

$$I_y(\hat{\theta}) = -\frac{\partial^2}{\partial \theta^2} \log(\mathcal{L}_y(\hat{\theta})).$$

Going back to (2.11), since e_j are random variables, y_j are random variables as well. For instance, if we assume that the e_j are independent and identically distributed (i.i.d) and that $e_j \sim \mathcal{N}(0, \sigma^2)$, then y_j are also independent and from (2.11) it follows that:

$$y_j \sim \mathcal{N}(f(t_j; \theta), \sigma^2), \quad 1 \leq j \leq n.$$

Thus, the corresponding likelihood function is:

$$\mathcal{L}_y(\theta, \sigma) = \frac{1}{(2\pi\sigma^2)^{n/2}} \exp\left\{ -\frac{1}{2} \sum_{j=1}^{n} \left(\frac{y_j - f(t_j; \theta)}{\sigma} \right)^2 \right\}.$$

To find the ML estimate of $\hat{\theta}$, we maximise the log-likelihood

$$\mathcal{LL}_y(\theta, \sigma) = -\frac{2}{n}\log 2\pi - n\log\sigma - \frac{1}{2\sigma^2}\sum_{j=1}^{n}\left(y_j - f(t_j;\theta)\right)^2,$$

from which we see that maximising the log-likelihood with respect to θ is the same as minimising the residual sums of squares (2.12). This shows that under the assumption of error normality and constant error model, the least squares estimator coincides with the maximum likelihood estimator.

Models for continuous data are usually stated in the more general form:

$$y_j = f(t_j;\theta) + g(t_j;\theta,\xi)\varepsilon_j \quad 1 \leq j \leq n,$$

where g is the residual error model and $(\varepsilon_1, \ldots, \varepsilon_n)$ are the standardised residual errors. In this case, the likelihood writes:

$$\mathcal{L}_y(\theta,\xi) = \frac{(2\pi)^{-n/2}}{\prod_{j=1}^{n} g(t_j;\theta,\xi)} \exp\left\{-\frac{1}{2}\sum_{j=1}^{n}\left(\frac{y_j - f(t_j;\theta)}{g(t_j;\theta,\xi)}\right)^2\right\}.$$

The residual error model g is a function that depends on a vector of parameter ξ. It may also be a function of time and of the structural parameters θ. Examples of residual error models are constant ($g = a$), proportional ($g = bf(t_j;\theta)$) and combined ($g = a + bf(t_j;\theta)$) error models.

2.3.3 Application example: practical identifiability study of the Gompertz and Iwata models

In this subsection, we apply the mathematical model and the statistical methods described above to analyse longitudinal data of brain metastases from a patient with a lung adenocarcinoma as primary tumour. Figure 2.5 shows the acquired data. A treatment with erlotinib was started after diagnosis of the primary tumour. This induced an initial regression in the primary tumour size followed by subsequent regrowth. A first

metastasis was detected in the brain 20 months after diagnosis of the primary tumour. Other 5 metastases were detected 40 months after diagnosis, and yet other 14 before date of last examination before death of the patient (47 months post-diagnosis).

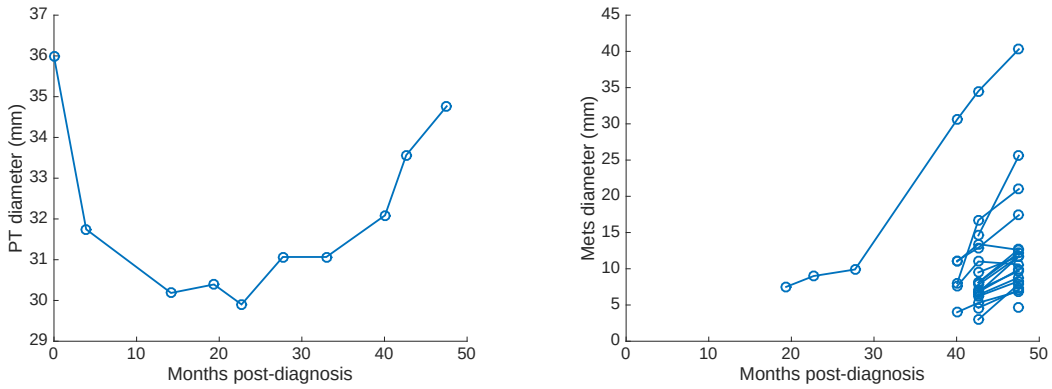

Figure 2.5 – Growth of the primary tumour (left) and of metastases (right) detected in the brain of a patient with primary lung adenocarcima. Data from Bergonié Institute [106].

Growth of a single metastasis

The data points plotted in Figure 2.6 represent the progression of the first detected brain metastasis in the patient. A Gompertz model

$$V(t;\alpha_0,\beta) = \exp\left[(\ln(V_i) - \alpha_0/\beta)\exp(-\beta(t-t_i)) + \alpha_0/\beta\right], \tag{2.16}$$

was used to fit these data. The left-most time point is the first measurement available for the metastatic tumour after diagnosis of the primary tumour and was used to fix $V(t=t_i) = V_i$ in the model. The Gompertz growth parameters were estimated through least-squares regression. The resulting values were $\alpha_0 = 3.79 \cdot 10^{-2}$ day^{-1} and $\beta = 1.43 \cdot 10^{-3}$ day^{-1}, and yielded an estimate for the origin of this metastasis of 325 days prior to diagnosis of the primary tumour.

Practical identifiability of the model parameters depends on the quantity and quality of data. To determine how many measurements are required, we evaluated the precision of the parameters estimated using only the first 4 and 5 data points. The resulting fits

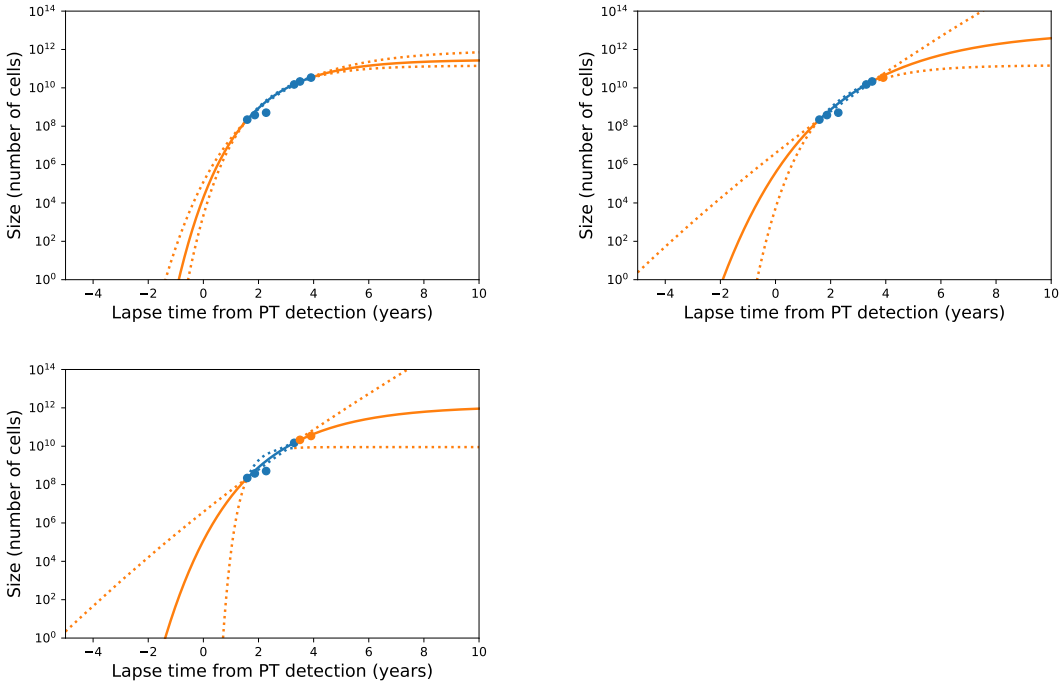

Figure 2.6 – Fits of the Gompertz model obtained varying the number of points used for estimating the model parameters, from 6 (top left) to 4. Points in blue are those used for the fit. Solid lines are least squares fits. Dashed lines depict 95 % confidence intervals for the prediction of $V(t)$.

Table 2.1 – Parameter values estimated using variable number of data points

Number of points	Parameter	Unit	Estimate	r.s.e. (%)
6	α_0	[day^{-1}]	$3.79 \cdot 10^{-2}$	9.86
	β	[day^{-1}]	$1.43 \cdot 10^{-3}$	11.5
	t_b	[day]	-325	23.3
5	α_0	[day^{-1}]	$2.40 \cdot 10^{-2}$	40.3
	β	[day^{-1}]	$8.05 \cdot 10^{-4}$	55.1
	t_b	[day]	-698	59.9
4	α_0	[day^{-1}]	$3.00 \cdot 10^{-2}$	158
	β	[day^{-1}]	$1.08 \cdot 10^{-3}$	202
	t_b	[day]	-505	108

are shown in Figure 2.6. Best fit parameter values, inferred times of inception, t_b, and estimated standard errors are reported in Table 2.1. In each case, the standard error of the inferred time of inception, t_b, was estimated by simulation. Namely, we generated a sample of parameter vectors $\theta_m = (\alpha_0, \beta)$, $m = 1, \ldots, M$, from the asymptotic distribution of the estimator (2.14), and computed the empirical standard deviation of $(t_b(\theta_1), \ldots, t_b(\theta_M))$. According to the estimated standard errors, six data points are sufficient to identify the model parameters and infer the time of origin of the metastatic tumour with good precision. However, while 5 data points still allow to obtain satisfactory estimates of the model parameters, 4 data points are insufficient.

Number of visible metastases and cumulative size distribution

Following [106], we modelled the unobserved pre-treatment phase of the primary tumour growth with a Gompertz model and utilised two exponential growth curves to describe the observed decrease and subsequent increase in tumour size.

Let $V_p(t)$ denote the number of cells in the primary tumour at time t. Assuming a dissemination rate of the form $d(V_p) = \mu V_p^\gamma$, and neglecting secondary dissemination, the cumulative number of metastases is given by

$$F(t, v) := \int_v^{+\infty} \rho(t, s) ds = \int_0^{t-\tau(v)} \mu V_p(s)^\gamma ds,$$

where $\tau(v)$ denotes the time needed for a metastatic tumour to reach size v. We assumed a Gompertz growth law for the metastatic tumours (i.e. equation (2.16) with $V_i = 1$ cell) and estimated α_0, β, μ and γ by fitting the cumulative distribution function to the observed cumulative number of metastases. Figure 2.7 compares the resulting cumulative distribution functions to the observed cumulative number of tumours at six successive times. While the fitted curves seem to agree well with the data, the high uncertainty in the estimated value of μ (see Table 2.2), indicates that the model with all free parameters might be structurally unidentifiable. Indeed, as shown in Table 2.3, fixing μ to different values resulted in equally good estimation of the remaining parameters. Moreover, a

decrease in μ is compensated by an increase in γ.

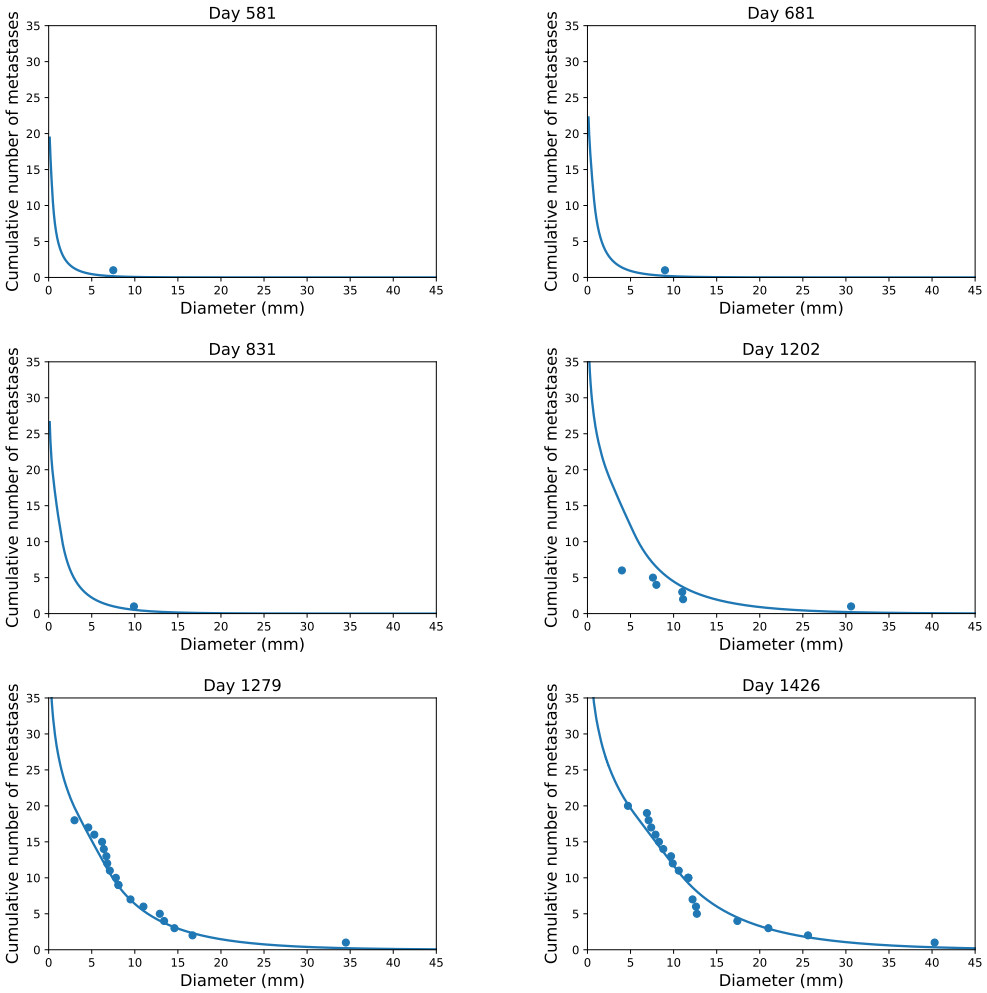

Figure 2.7 – Fit of the model to the observed cumulative size distribution.

Table 2.2 – Estimation of the model's parameters by fitting the theoretical cumulative size distribution to the observed cumulative numbers of metastases.

Number of points	Parameter	Estimate	r.s.e. (%)
47 (first 6 days)	α_0	2.28e-02	6
	β	7.36e-04	13
	μ	8.27e-09	398
	γ	6.47e-01	26
	σ	1.85	-

Table 2.3 – Parameter estimates (relative standard error (%)) obtained by fitting the theoretical cumulative size distribution with fixed value of μ.

	$\mu = 10^{-4}$	$\mu = 10^{-5}$	$\mu = 10^{-6}$	$\mu = 10^{-7}$	$\mu = 10^{-8}$	$\mu = 10^{-9}$
α_0	1.16e-02 (20.1)	2.16e-02 (2.67)	2.28e-02 (1.75)	2.28e-02 (0.78)	2.26e-02 (0.70)	2.24e-02 (0.68)
β	1.12e-04 (160)	7.27e-04 (6.45)	7.73e-04 (1.62)	7.51e-04 (0.55)	7.20e-04 (2.25)	6.96e-04 (0.47)
γ	2.83e-01 (5.66)	3.43e-01 (0.98)	4.41e-01 (0.93)	5.40e-01 (0.39)	6.40e-01 (0.47)	7.39e-01 (0.28)
σ	2.19	2.11	1.98	1.89	1.83	1.80

Figure 2.8 compares the observed number of metastases to the theoretical number of visible tumours ($N_{vis}(t) = \int_0^{t-\tau(V_{vis})} \mu V_p(s)^\gamma ds$, assuming a visible threshold V_{vis} of 5 mm in diameter) with parameter values obtained by fitting the theoretical cumulative size distribution to the data from the first 4, 5 and 6 follow up days. In all cases, the value of μ was fixed to 10^{-9}. By visual evaluation, the model calibrated on observations from the first 4 follow-up days only, does not allow to predict the number of visible tumour at days 2920 and 3067. On the contrary, these seem to be well predicted when also the data from the next the follow-up day are used.

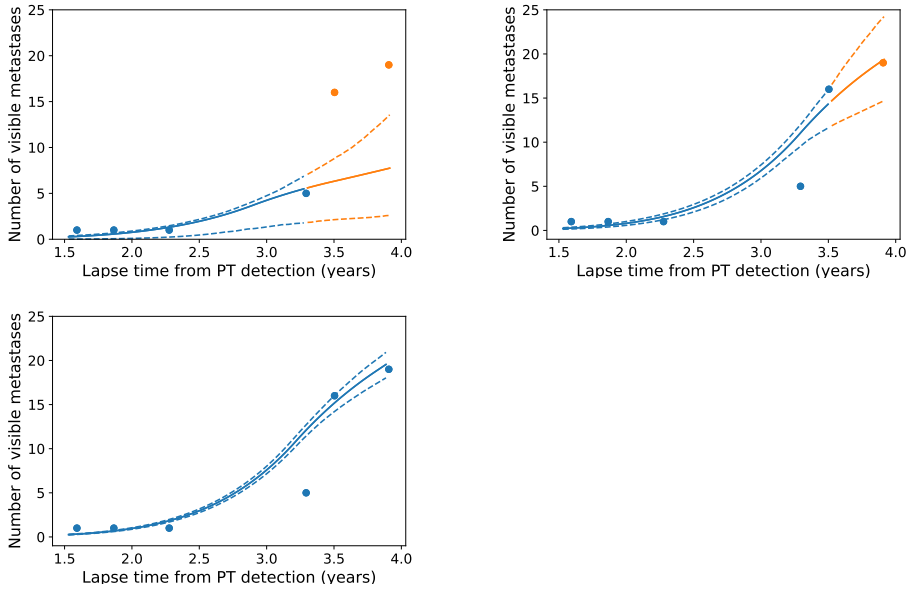

Figure 2.8 – Observed and predicted number of visible metastases. Predictions are obtained using the parameter estimated by fitting the cumulative size distribution to the data of the first 4, 5 and 6 follow-up days. In all cases, the value μ was fixed to 10^{-9}. Dashed lines depict 95 % CIs for $N_{vis}(t; \theta^*)$.

2.4 Machine learning regression algorithms

We have seen modelling approaches where the nonlinearity in the data is directly specified by a structural model. There are also regression techniques that, being intrinsically nonlinear, do not require to model the form of nonlinearity in the data and can be applied in situations where this is unknown. Neural networks and tree-based models are examples of such methods.

In what follows, we assume to have n pairs of observations $\{(x_1, y_1), \dots (x_n, y_n)\} \subset \mathbb{R}^p \times \mathbb{R}$, where y denotes the response (or outcome) variable and x is a vector of p predictor variables (or covariates). The response variable is related to the covariates by

$$y_i = f(x_i) + e_i, \qquad \mathbb{E}[e_i] = 0, \quad i = 1, \dots, n.$$

The goal of these algorithms is to estimate the regression function f.

2.4.1 Neural networks

In a neural network [33, p. 141] the outcome variable is modelled through a set of unobserved variables called hidden units. Each hidden unit is a linear combination of the predictor variables transformed by a nonlinear function, such as the logistic function:

$$h_k(x) = g\left(\beta_{0k} + \sum_{j=1}^{p} x_j \beta_{jk}\right), \quad \text{where} \quad g(u) = \frac{1}{1 - e^{-u}}.$$

A neural network usually contains multiple hidden units which are linked by a linear combination to the outcome (Figure 2.9):

$$f(x) = \gamma_0 + \sum_{k=1}^{H} \gamma_k h_k.$$

Thus, for a number of p predictors, a neural network with H hidden units requires the estimation of $H + 1 + H(p + 1)$ total parameters. These parameters are estimated by

minimising with an iterative algorithm the following objective function:

$$\sum_{i=1}^{n}(y_i - f(x_i))^2 + \lambda \sum_{k=1}^{H}\sum_{j=1}^{p}\beta_{jk}^2 + \lambda \sum_{k=0}^{H}\gamma_k^2,$$

where a *weight decay* λ is introduced to moderate overfitting by penalising large regression coefficients. Neural networks have two tuning parameters: the value of λ and the number of hidden units. Kuhn and Johnson [33] recommend to use values of λ between 0 and 0.1.

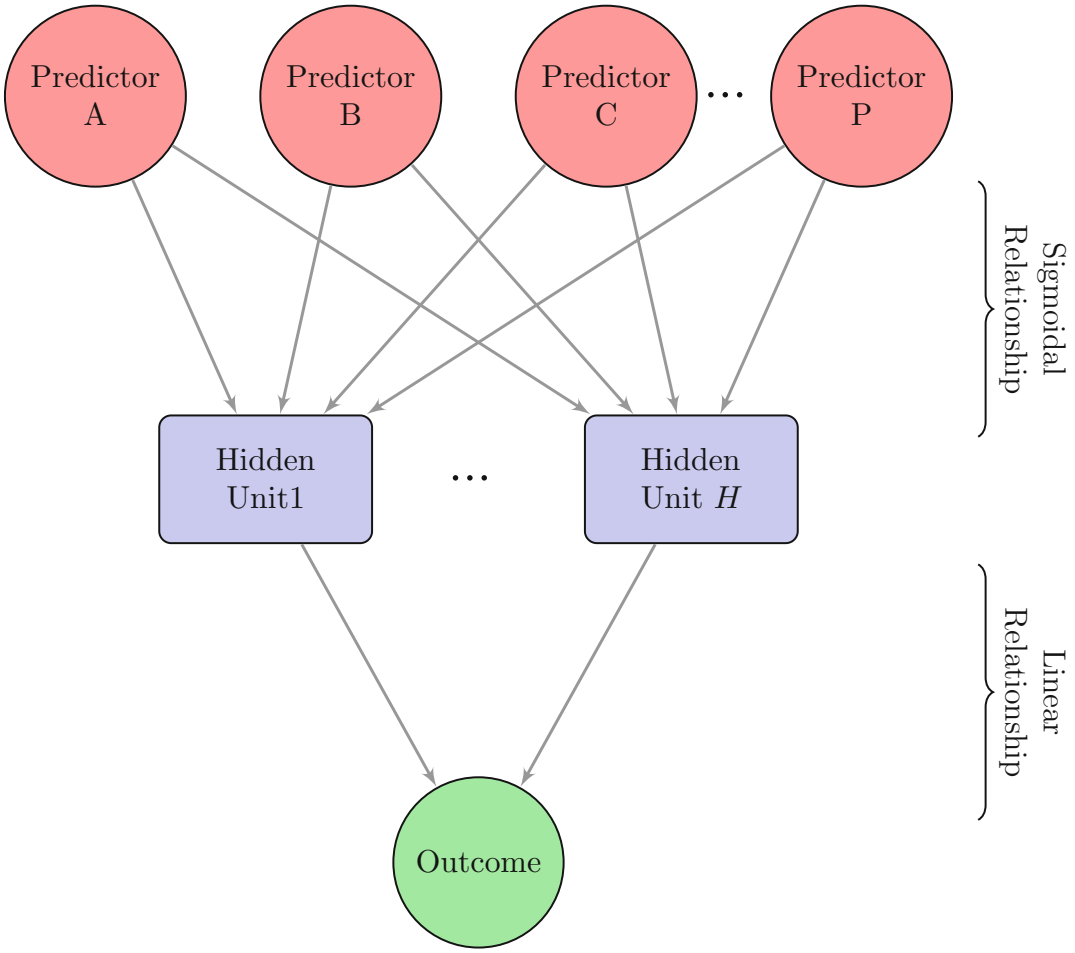

Figure 2.9 – Structure of a neural network with a single hidden layer. The hidden units are linear combinations of the predictor variables transformed by a sigmoidal function. The outcome variable is modelled as a linear combination of the hidden units. (From [33].)

2.4.2 Regression trees

Tree-based models [33, p. 175] partition the covariate space into disjoint subsets through a sequence of nested `if-then` statement. The outcome for a new sample is predicted by simply following the if-then statements for the sample's predictors down the tree.

One approach to construct regression trees is the classification and regression tree (CART) methodology introduced by Breiman *et al.* [107]. Starting from the entire dataset, $S = \{1, \ldots, n\}$, the algorithm forms two daughter nodes, S_1 and S_2, by finding the predictor $x^* \in \{x_1, \ldots x_P\}$ and the split value $c^* \in \mathbb{R}$ such that the overall sums of squared error are minimised:

$$SSE = \sum_{i \in S_1} (y_i - \bar{y}_1)^2 + \sum_{i \in S_2} (y_i - \bar{y}_2)^2,$$

where $S_1 = \{i \in S : x^* \leq c^*\}$, $S_2 = \{i \in S : x^* > c^*\}$ and $\bar{y}_i$ denotes the average of the training set outcomes within group S_i, $i = 1, 2$. This process is repeated within set S_1 and S_2 until the number of samples in the nodes falls below a given threshold. Predictions in terminal nodes are computed by averaging the training set outcomes within each node.

If the resulting tree is too large it is likely to overfit the training data. One strategy to reduce overfitting consists in removing unnecessary nodes by applying a pruning algorithm [33, p. 178].

A second technique to build regression trees is the *conditional inference trees* methodology of Horthorn *et al.* [108]. In these models, statistical tests are used to test the independence between any of the p variables and the response. If the global hypothesis can be rejected, the covariate with the strongest association with the response is selected and the optimal binary split is determined by maximising a statistic quantifying the discrepancy between the daughter nodes.

2.4.3 Bagged Trees and Random Forests

Ensemble methods are techniques that combine many models' prediction in order to make predictions more stable. In bagging (**B**ootstrap **agg**regat**ing**), m trees models are

grown using bootstrap samples of the original data. Each tree in the ensemble provides a prediction for a new sample and these m predictions are averaged to obtained the bagged model's prediction.

Besides making predictions more stable, bagging has the advantage of providing an internal measure of prediction error which has been shown to correlate well with the cross-validation error estimate [33, p. 197]. Indeed, when a bootstrap sample is generated, certain samples are left out. These samples are called *out-of-bag* samples and are used to evaluate the predictive performance of the tree built on the corresponding bootstrap sample. The performance metric for the entire ensemble is then estimated as the mean of the m out-of-bag metrics.

In bagging, generation of bootstrap samples induces a distribution of trees and thus a distribution of predictions for each sample. However, because all predictors are considered at each split, trees generated by different bootstrap samples tend to have similar structures. This phenomenon is known as tree correlation and in general weakens the performance of bagging. Reducing correlation can be done by introducing randomness in the tree construction process. The random forests algorithm is a generalisation of bagged tree models, where splits in each trees are done by considering a subset of m_{try} randomly selected covariates. Tuning parameters in random forests are the number m_{try} of covariates that are used at each split and the number `ntree` of trees in the forest. Base learners in random forests can be CART or conditional inference trees.

2.4.4 Evaluating predictive performance of regression models

Once a model has been built, one might be interested at knowing how good it is at predicting new samples. When predicting continuous outcomes, the root mean squared error (RMSE) and the coefficient of determination R^2, are metrics commonly used to evaluate model performance. The former can be interpreted as the average distance between observed and predicted data, while the latter quantifies the proportion of information explained by the model.

Evaluating the model on the calibration set is referred to as *apparent performance*

of the model. However, metrics of predictive performance are more useful if computed on samples that were not used for model building. If the data set at hand is not large enough for being split into a *training* and a *test* set, it is possible to build the model on all samples and estimate its predictive performance by splitting the data into multiple training and test sets using resampling techniques such as k-fold cross-validation or the bootstrap method.

k-Fold Cross-Validation. In k-fold cross-validation, the original data set is randomly partitioned into k sets, called *folds*, of approximately equal size. The model is fitted using all samples except those belonging to the first fold. The held-out samples are predicted by this model and used to compute the performance metric. This procedure is then repeated for each of the k folds. At the end, the k estimates of the performance metric are summarised, usually with mean and standard error. A schematic of the cross-validation process is shown in Figure 2.10.

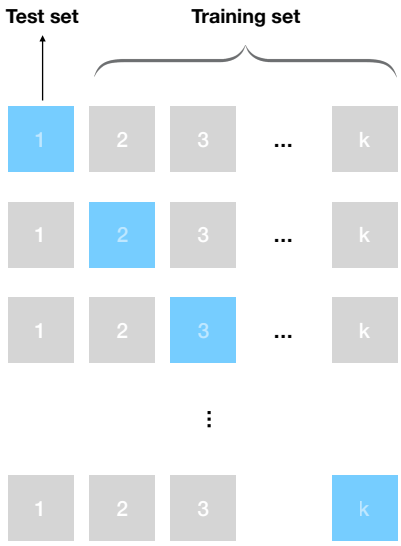

Figure 2.10 – A schematic of k-fold cross-validation. The original data are divided randomly into k sets. At each iteration, samples of the blue square (test est) are predicted using the model trained on the samples of the grey squares (training set).

Bootstrap. A bootstrap sample has the same size of the original data set and is generated by drawing data with replacement. Therefore, some observations will be included multiple times in a bootstrap sample, while others will not be selected. The samples that are left out are called *out-of-bag* samples. For a given iteration of bootstrap resampling, the model is fitted using the selected samples and the out-of-bag samples are used to estimate model performance.

2.5 The population approach

In this section, we assume that the data at hand consists of repeated measurements collected on several individuals from a population. The aim of the population approach is to build a model for the population as a whole while quantifying variability between subjects. As for the case of a single individual, we suppose that the structural model representing the biological phenomenon can be written as a parametric function of time $f(t;\psi)$.

Population models were originally developed by fitting the model against the combined data from all individuals, thus ignoring inter-individual variability (the "näive pooled approach"), or by fitting each individual's data separately and then combining the individual parameter estimates to derive population characteristics, estimated as the sample mean and the variance/covariance of the individual parameter estimates (the "two-stage approach") [109].

The mixed-effects approach allows to model explicitly intra- and inter-individual variabilities in a unique statistical model and to estimate the population characteristics from the whole data set in a one-step procedure. Unlike the two-stage approach, mixed-effects models can be developed even when relatively few data are available for each individual [32].

2.5.1 Nonlinear mixed-effects models

Let us consider a sequence of observations collected on a set of N individuals. We denote with $y_i = (y_{ij}, 1 \leq j \leq n_i)$ the observations taken on individual i at times $(t_{ij}, 1 \leq j \leq n_i)$. The statistical model for the observations is the following:

$$y_{ij} = f(t_{ij}; \psi_i) + g(\psi_i, \sigma, t_{ij})\varepsilon_{ij}, \tag{2.17}$$

where f and g are parametric functions defining the structural model and residual error model, respectively, and $\varepsilon_{ij} \sim_{i.i.d.} \mathcal{N}(0,1)$ are the standardised residual errors. In the population framework, it is further assumed that each individual can be represented by a vector of individual parameters ψ_i. This is modelled parametrically as a function of *fixed effects* ψ_{pop}, and individual *random effects* η_i:

$$h(\psi_i) = h(\psi_{pop}) + \eta_i, \quad \text{where } \eta_i \sim \mathcal{N}(0, \Omega), \tag{2.18}$$

where h is a transformation such that $h(\psi_i)$ can be assumed normally distributed. Common choices for h are the identity function (normal distribution for ψ) and the logarithmic function (log-normal distribution for ψ). Equation (2.17) provides the conditional distribution of the observations given the individual parameters, while equation (2.18) defines the distribution of the individual parameters. The model can then be represented in terms of probability distributions as follows:

$$p(\boldsymbol{y}, \boldsymbol{\psi}; \theta) = p(\boldsymbol{y}|\boldsymbol{\psi}; \sigma)p(\boldsymbol{\psi}; \psi_{pop}, \Omega),$$

where $\boldsymbol{y} = (y_1, \ldots, y_N)$ and $\boldsymbol{\psi} = (\psi_1, \ldots, \psi_N)$ are the observations and the parameter vector for the set of N individuals. The notation $p(\boldsymbol{y})$ is used for brevity to indicate the probability density function of a random variable $\boldsymbol{y}$; the semicolon is used to separate random variables from nonrandom ones.

2.5.2 Maximum likelihood estimation of the population parameters

The population model is completely defined by the vector of population parameter $\theta = (\psi_{pop}, \Omega, \sigma)$. This can be estimated by maximising with respect to θ the observed likelihood function:

$$\mathcal{L}_{\boldsymbol{y}}(\theta) := p(\boldsymbol{y}; \theta) = \int p(\boldsymbol{y}, \boldsymbol{\psi}; \theta) d\boldsymbol{\psi}. \tag{2.19}$$

In general, for nonlinear mixed-effects models the likelihood has no closed-form expression. To deal with its maximisation different methods have been proposed. These methods follow mainly three approaches: i) linearisation methods linearise the model or the likelihood to obtain a more tractable problem; ii) integral approximation methods approximate numerically the likelihood and then maximise it directly; iii) EM-type methods are iterative algorithms that maximise at each iteration an approximation of the conditional expectation of the complete log-likelihood function $\log p(\boldsymbol{y}, \boldsymbol{\psi}; \theta)$. This subsection provides a brief description of the EM algorithm and of its stochastic approximation version, namely the SAEM algorithm, which was used for parameter estimation of all population models considered in this thesis [110, 111].

The EM algorithm

The expectation-maximisation (EM) algorithm is an iterative algorithm to find a value of θ that maximise (2.19) given observed data $\boldsymbol{y}$. The explanation of the algorithm is provided in a classic paper of Dempster *et al.* [112]. Starting from an initial value θ_0, the kth iteration of the EM algorithm updates the current estimate θ_{k-1}^{EM} of θ with the following two steps:

- E-step: Compute $Q_k(\theta)^{EM} = \mathbb{E}\left(\log p(\boldsymbol{y}, \boldsymbol{\psi}; \theta) | \boldsymbol{y}; \theta_{k-1}^{EM}\right)$.
- M-step: Compute the value θ^k that maximises $Q_k(\theta)^{EM}$.

The idea is that if we could observe the individual parameters $\boldsymbol{\psi}$, we would estimate θ just by maximising $\log p(\boldsymbol{y}, \boldsymbol{\psi}; \theta)$. However, since we do not know $\log p(\boldsymbol{y}, \boldsymbol{\psi}; \theta)$, we maximise instead its current expectation given the data.

In [112], it is proved that each iteration of the EM algorithm increases the likelihood of the observations. The convergence properties of the EM algorithm have also been studied by Wu [113], who showed that the EM sequence of parameter estimates converges to a stationary point of the observed likelihood under general regularity conditions.

The main difficulty with the EM algorithm is that the E-step cannot be computed explicitly when the relationship between the observations $\boldsymbol{y}$ and the individual parameters $\boldsymbol{\psi}$ is nonlinear. To address this issue, other methods that approximate by simulation the E-step have been proposed. The Stochastic Approximation of EM (SAEM) [110] replaces the E-step with a stochastic approximation procedure. This algorithm is implemented in different tools, including MONOLIX, NONMEM, MATLAB (nlmefitsa function) and R (saemix package).

The SAEM algorithm

Given an initial value θ_0, at iteration k the estimate of θ is updated through the following three steps [32, p. 239]:

- Simulation step: For $i = 1, \ldots, N$ draw $\psi_i^{(k)}$ from the conditional distribution $p(\psi_i | y_i; \theta_{k-1})$.
- Stochastic approximation: Update $Q_{k-1}(\theta)$ with

$$Q_k(\theta) = Q_{k-1}(\theta) + \gamma_k(\log p(y, \psi^{(k)}; \theta) - Q_{k-1}(\theta)),$$

  where (γ_k) is a decreasing sequence of positive numbers with $\gamma_1 = 1$.
- Maximization step: Choose θ_k that maximises $Q_k(\theta)$.

Delyon *et al.* [110] showed that convergence of the SAEM algorithm requires that the sequence of γ_k satisfies $\sum_{k=1}^{\infty} \gamma_k = \infty$ and $\sum_{k=1}^{\infty} \gamma_k^2 < \infty$. Lavielle [32] recommends setting $\gamma_k = 1$ for the first K_1 iterations in order to converge quickly to a neighbourhood of a maximum of the likelihood, and $\gamma_k = 1/(k - K_1)$ for the remaining iterations to ensure almost sure convergence to the maximum likelihood estimate of θ. Usually for

nonlinear models, the individual parameters cannot be simulated exactly from the conditional distribution. For these cases, the Metropolis-Hastings algorithm can be used. This algorithm simulates data from a probability distribution by constructing a Markov chain having as stationary distribution the probability distribution one wants to simulate [114].

After obtaining an estimate $\hat{\theta}$ of θ, the Metropolis-Hastings algorithm can be used to obtain an empirical estimate of the conditional distribution $p(\psi_i|y_i;\hat{\theta})$ of each individual. The individual parameters can then be estimated as the conditional mean $\mathbb{E}[\psi_i|y_i;\hat{\theta}]$, or the conditional mode $\arg\max_{\psi_i} p(\psi_i|y_i;\hat{\theta})$. The latter estimates of the individual parameters are also called *empirical Bayes estimates* (EBEs).

2.5.3 Model evaluation

Standard errors

Standard errors of the population parameters can be obtained from the inverse of the observed Fisher information matrix:

$$I_{\boldsymbol{y}}(\hat{\theta}) := -\frac{\partial^2}{\partial\theta^2}\log(\mathcal{L}_{\boldsymbol{y}}(\hat{\theta})).$$

As for the likelihood function, the Fisher information matrix of nonlinear mixed-effects models has no closed-form expression. One method to estimate it consists in approximating the log-likelihood by linearisation of the model around the vector of estimated individual parameters and computing the partial derivatives numerically by finite difference. Alternatively, the Fisher information can be estimated using a stochastic approximation based on the Louis' formula [32, p. 259]. This formula expresses $\frac{\partial^2}{\partial\theta^2}\log(\mathcal{L}_{\boldsymbol{y}}(\hat{\theta}))$ as combination of conditional expectations that can be estimated by Monte Carlo simulations.

Diagnostic plots

Within the nonlinear-mixed effects modelling framework different graphical methods are used for model evaluation [115].

Population and individual fits. These are respectively obtained by superimposing the individual observations to the predicted profile given by the estimated population model $f(t;\hat{\psi}_{pop})$ and the estimated individual model $f(t;\hat{\psi}_i)$. They allow to assess whether the model can describe individual dynamics and how individual profiles differ from the population profile.

Observations vs. predictions. Population or individual predictions are plotted versus the observed data. If the model is correct, data points are expected to be scatter along the identify line. The 90 % prediction interval, which depends on the error model, can be displayed. An high proportion of data outside the prediction interval suggests that the model is misspecified.

Individual weighted residuals IWRES$_{ij}$. These are estimates of the standardised residuals ε_{ij} obtained from the individual predictions as

$$\text{IWRES}_{ij} = \frac{y_{ij} - f(t_{ij};\hat{\psi}_i)}{g(t_{ij};\hat{\psi}_i,\hat{\sigma})}.$$

IWRES are usually plotted versus time or model prediction to check for heteroscedasticity. If the model is correct, data points should be randomly scattered around the horizontal zero-line with the majority of them lying within (-1.96, 1.96).

Visual predictive check. A visual predictive check (VPC) compares the percentiles of the observations – usually the 10th, 50th and 90th percentiles – to the corresponding theoretical percentiles estimated from multiple Monte Carlo simulations. Predictions intervals are constructed using the theoretical percentiles computed from each simulations. If the model is correct, the observed percentiles should remain inside the corresponding prediction intervals.

Distribution of the individual parameters - shrinkage. Once the individual parameters have been estimated, the resulting histograms can be compared to the corre-

sponding theoretical distributions defined in the statistical model. Further information about the reliability of the individual parameter estimates can be obtained by computing the η-shrinkage which is defined as:

$$\eta\text{-shrinkage} = 1 - \frac{\mathrm{Var}(\hat{\eta}_i)}{\hat{\omega}^2},$$

where $\mathrm{Var}(\hat{\eta}_i)$ is the empirical variance of the estimated random effects $\hat{\eta}_i$'s and $\hat{\omega}^2$ denotes the estimated variance. A high shrinkage indicates that the individual data are not sufficient to correctly estimate the individual parameters. In this case, the individual parameter estimates, as well as the diagnostic plots base on them, cannot be considered reliable.

Correlation between random effects. This plot displays each pair of the estimated random effects against each other. It allows to check the appropriateness of the assumed covariance structure.

Model selection

A number of statistical tools have been proposed to aid selection among different plausible models. These include information criteria such as the Akaike information criteria (AIC) and the Bayesian information criteria (BIC), which are defined as

$$AIC = -2\log \mathcal{L}_{\boldsymbol{y}}(\hat{\theta}) + 2P,$$
$$BIC = -2\log \mathcal{L}_{\boldsymbol{y}}(\hat{\theta}) + \log(N)P,$$

where P is the total number of population parameters (i.e. fixed effects, random effects, and error model parameters) and N is the number of individuals. Both criteria include a penalty to compensate the improvement in the likelihood due to a larger number of parameters. According to [116], a drop in AIC or BIC of 2 can be taken as a threshold for selecting one model over another.

In addition, to compare nested models, the Wald test and the likelihood ratio test

(LRT) can also be used, in particular when one wants to assess whether a covariate should be added in the model (see Section 2.5.4).

The LRT evaluates if the difference between the likelihood under the more complex model and the base model is statistically significant. To compute the p-value, the LRT statistic is compared against a χ^2 distribution with degrees of freedom the difference in the number of parameters between the two nested models.

The Wald test requires computation of the standard error to test whether a fixed effect β is zero. In the univariate case, the Wald statistic is $\hat{\beta}/\text{se}(\hat{\beta})$ and is compared against a normal distribution $\mathcal{N}(0,1)$.

2.5.4 Models with covariates

Covariates can be introduced into the model in order to explain part of the variability in the individual parameters and consequently to obtain more individualised predictions. Although covariates may be included in the model through complex functions, for the sake of model identification and parameter estimation, the effect of covariates on the model parameters is usually modelled by a linear function:

$$h_k(\psi_{i,k}) = h_k(\psi_{pop,k}) + \beta \cdot c_i + \eta_{i,k}, \quad \eta_{i_k} \sim \mathcal{N}(0, \omega_k^2),$$

where c_i is a vector of individual covariates and the subscript k refers to the kth component of the vector of individual parameters ψ_i. In this context, the β's are additional population parameters to be estimated.

The plot showing the correlations between covariates and individual parameters may give a hint of which covariates trying on which parameter. Alternatively, the covariate model can be built automatically using a stepwise procedure. This method consists in a set of iteration of forward selection followed by a backward elimination step. During the forward selection, the relationship of individual parameters and covariates not yet included are evaluated in a univariate manner, and the model that improve some criteria (LRT or BIC) is chosen for the next iteration. Covariates are included one at a time in

this manner until the criteria stops improving. During the backward elimination step, covariates are removed in a univariate manner.

A faster method for automatic building of the covariate model is the COSSAC (COnditional Sampling use for Stepwise Approach based on Correlation tests) algorithm implemented in the Monolix software. Instead of trying all covariates, this algorithm uses samples from the a posteriori conditional distribution to calculate correlations between random effects and covariates and decide which covariates trying first [117].

2.6 Survival analysis

Survival analysis refers to a set of statistical techniques for analysing data in which the variable of interest is the time elapsed from a given origin to the occurrence of a particular event. The event can be death, disease occurrence, disease recurrence or any other experience of interest that might occur to an individual.
A common problem with survival data is that the time to event might not be observed for all individuals. This situation is called *censoring* and occurs when a patient has not experienced the event by the end of the study or is lost to follow-up.

Survival data are commonly modelled by means of probabilities. The survival function gives the probability that an individual survives beyond a specified time. Depending on the aim of the study, it can be estimated using different modelling approaches. This section gives a general overview of the most commonly used. After introducing the basic terminology and notation (Section 2.6.1), we describe the nonparametric Kaplan-Meier estimator (Section 2.6.2) and the semi-parametric Cox regression model (Section 2.6.3). Next, we present the parametric approach and how right-censoring is taken into account in writing the likelihood (Section 2.6.4). We conclude with the more recent Random Survival Forests model (Section 2.6.5).

2.6.1 Definitions and notation

Functions used in survival analysis

Let $T \geq 0$ be a random variable representing the time to event of an individual. The *survival function* $S(t)$ is the probability that an individual survives longer than time t:

$$S(t) = P(T > t).$$

The *hazard function* $h(t)$ represents the instantaneous event rate conditionally on surviving up to time t:

$$h(t) = \lim_{\Delta t \to 0^+} \frac{P(t \leq T < t + \Delta t \mid T \geq t)}{\Delta t}.$$

The cumulative hazard function $H(t)$ is defined as:

$$H(t) = \int_0^t h(u)du.$$

The survival and hazard functions are related by

$$h(t) = -\frac{d}{dt} \log S(t), \tag{2.20}$$

which is also equivalent to $S(t) = e^{-H(t)}$. Thus, the distribution of T is completely defined by either $S(t)$ or $h(t)$: knowing $h(t)$, one can determine the corresponding $S(t)$, and vice versa. However, survival models are usually defined by specifying the hazard function.

Censoring

The most common type of censoring in survival analysis is *right-censoring*. In this case, it is only known that the event will occur after a certain time C, called *censoring variable*.

In presence of right-censoring, the observations are $(\tilde{T}, \delta)$, where

$$\tilde{T} = \min(T, C), \tag{2.21}$$

and δ is an indicator variable

$$\delta = \begin{cases} 0 & \text{if } T > C, \\ 1 & \text{otherwise.} \end{cases} \tag{2.22}$$

2.6.2 The Kaplan-Meier estimator

The survival function can be estimated nonparametrically using the Kaplan-Meier estimator [118]. Let $(\tilde{T}_i, \delta_i)$, $i = 1, \ldots, n$, be i.i.d. right-censored observations and let $t_1 < \cdots < t_k$ denote the distinct times of events. The Kaplan-Meier estimator of $S(\cdot)$ is given by:

$$\hat{S}(t) = \prod_{j:t_j \leq t} \left(1 - \frac{d_j}{n_j}\right),$$

where d_j is the number of events that occurred at time t_j, and n_j is the number of individuals known to be "alive" (who have not yet had an event or have been censored) just before time t_j. The Kaplan-Meier estimator is a step function, with a jump at each time of event. Andersen et al. [119] showed that for large n, the distribution of $\hat{S}(t)$ is approximately $\mathcal{N}(S(t), \hat{\sigma}_t^2)$, where $\hat{\sigma}_t^2$ can be estimated using Greenwood's formula:

$$\hat{\sigma}_t^2 = \hat{S}(t)^2 \sum_{j:t_j \leq t} \frac{d_j}{n_j(n_j - d_j)}.$$

This property allows to estimate asymptotic confidence intervals for the survival probability.

Survival functions of two or more groups can be compared using the nonparametric log-rank test [120]. The log-rank test compares the number of events observed in each group to the corresponding expected number of events calculated under the null hypothesis that the survival functions are equal. The test statistic has approximately a χ^2 distribution with $g - 1$ degrees of freedom, where g is the number of groups. This

allows to compute a p-value to evaluate the significance of the difference between the survival curves of the groups.

A stratified log-rank test can be used to take into account the impact of a second covariate. However, to investigate the effect of several covariates simultaneously multivariate approaches are more appropriate.

2.6.3 The Cox proportional hazard model

The Cox proportional hazards (PH) model [121] assumes the following relationship between the hazard function $h(t)$ and a vector of p explanatory variables $Z = (Z_1, Z_2, \dots Z_p)^T$:

$$h(t; Z, \beta) = h_0(t) \exp(\beta^T Z),$$

where $\beta = (\beta_1, \dots, \beta_p)$ is the vector of regression coefficients and $h_0(t)$ is the baseline survival function, representing the hazard of a subject with all explanatory variables equal to zero. The name "proportional hazards" comes from the fact that given two vector of covariates Z_i and Z_j, the hazard ratio is constant over time:

$$\begin{aligned} \frac{h(t; Z_i, \beta)}{h(t; Z_j, \beta)} &= \frac{h_0(t) \exp(\beta^T Z_i)}{h_0(t) \exp(\beta^T Z_j)} \\ &= \frac{\exp(\beta^T Z_i)}{\exp(\beta^T Z_j)}, \end{aligned}$$

which is an assumption of the model whose validity has to be verified. A simple graphical method to check the proportional hazards assumption when comparing two groups consists in plotting the $\log[-\log(\hat{S}(t))]$ curves of the groups and checking if they are approximately parallel.

The Cox model is considered a semi-parametric model since it includes a non-parametric part $h_0(t)$ and a parametric part $\exp(\beta^T Z)$. The quantities $\exp(\beta_i)$ are called hazard ratios. A value of $\exp(\beta_i)$ greater than 1 indicates that the predictor variable Z_i is associated with higher risk. The vector β can be estimated by maximizing a partial likelihood which does not depend on $h_0(t)$, allowing to estimate the regression coefficients without

making any assumption on $h_0(t)$. Let $t_1 < t_2 < \cdots < t_k$ the distinct times of events. Assuming that times are not tied, the conditional probability that subject i undergoes the event at time t_i, knowing that he is at risk at this time, is:

$$p_i = \frac{h(t_i; Z_i, \beta)}{\sum_{l:\tilde{T}_l \geq t_i} h(t_i; Z_l, \beta)} = \frac{\exp(\beta^T Z_i)}{\sum_{l:\tilde{T}_l \geq t_i} \exp(\beta^T Z_l)}$$

The partial likelihood as defined by Cox [122] is given by the product of the above conditional probabilities calculated at each event time:

$$\mathcal{L}(\beta) = \prod_{i=1}^{k} p_i = \prod_{i=1}^{k} \frac{\exp(\beta^T Z_i)}{\sum_{l:\tilde{T}_l \geq t_i} \exp(\beta^T Z_l)}. \tag{2.23}$$

The maximum partial likelihood estimators of the regression coefficients are the values that maximise (2.23). They can be obtained using a Newton-like iterative method. Consistency and asymptotical normality also hold for the estimators based on the partial likelihood [123, 124], allowing to calculate asymptotic confidence intervals and use Wald tests for evaluating the significance of the explanatory variables.

2.6.4 Parametric survival models

Parametric survival models assume that the survival times follow a chosen distribution $f(t; \theta)$, whose parameters can be estimated by maximising the likelihood function. In the presence of right-censored observations, the likelihood for n individuals is given by

$$\mathcal{L}(\theta) = \prod_{i=1}^{n} f(\tilde{T}_i)^{\delta_i} S(\tilde{T}_i)^{(1-\delta_i)}, \tag{2.24}$$

where $(\tilde{T}_i, \delta_i)$, $i = 1, \ldots, n$, are defined by (2.21) and (2.22). We observe that if $\tilde{T}_i$ is not censored (i.e. $\delta_i = 1$), its contribution to the likelihood is the usual $f(\tilde{T}_i; \theta)$, while if it censored (i.e. $\delta_i = 0$), the contribution is $S(\tilde{T}_i; \theta)$. Recalling the relationship between

the hazard and survival functions (2.20), we can also write (2.24) as

$$\mathcal{L}(\theta) = \prod_{i=1}^{n} h(\tilde{T}_i)^{\delta_i} S(\tilde{T}_i). \tag{2.25}$$

Examples of classical distributions used in survival analysis are the exponential, Weibull and log-logistic distributions.

- The *exponential model* assumes a constant hazard function over time: $h(t;\lambda) = 1/\lambda$, where $\lambda > 0$. Its density and survival functions are:

$$f(t;\lambda) = \frac{1}{\lambda} e^{-\frac{t}{\lambda}}, \quad S(t;\lambda) = e^{-\frac{t}{\lambda}}.$$

- The *Weibull model* is defined by the following hazard function:

$$h(t;\lambda,s) = \frac{s}{\lambda}\left(\frac{t}{\lambda}\right)^{s-1},$$

  where $s > 0$ is the shape parameter and $\lambda > 0$ is the scale parameter. $h(t;\lambda,s)$ is an increasing function if $s > 1$, a constant function (exponential model) if $s = 1$ and a decreasing function if $0 < s < 1$. The probability density and survival functions of the Weibull distribution are:

$$f(t;\lambda,s) = \frac{s}{\lambda}\left(\frac{t}{\lambda}\right)^{s-1} e^{-(t/\lambda)^s}, \quad S(t;\lambda,s) = -e^{-(t/\lambda)^s}.$$

- The *log-logistic model* is defined by the following hazard function:

$$h(t;\lambda,s) = \frac{\frac{s}{\lambda}\left(\frac{t}{\lambda}\right)^{s-1}}{1+\left(\frac{t}{\lambda}\right)^{s}},$$

  where $s > 0$ is the shape parameter and $\lambda > 0$ is the scale parameter. If $s \leq 1$ the hazard function decreases monotonically, while if $\beta > 1$ is a non-monotonic function which has its maximum value at $t = \lambda(s-1)^{1/s}$. The probability density

and survival functions of the log-logistic distribution are:

$$f(t;\lambda,s)=\frac{\frac{s}{\lambda}\left(\frac{t}{\lambda}\right)^{s-1}}{\left(1+\left(\frac{t}{\lambda}\right)^{s}\right)^{2}},\quad S(t;\lambda,s)=\left[1+\left(\frac{t}{\lambda}\right)^{s}\right]^{-1}.$$

2.6.5 Random survival forests

Random Survival Forests (RSF) are a relatively recent extension of the random forests methodology for the analysis of right-censored survival data [125]. An implementation of the RSF algorithm is provided in the R software package `randomForestSRC` [40]. As in RF, trees are grown using `ntree` bootstrap samples of the data, and at each node of a tree, `mtry` covariates are randomly selected as candidate for splitting. A split on a given covariate Z is of the form $Z \leq c$ and $Z > c$. The best split is determined by finding the candidate covariate and the split value that maximise survival difference between daughter nodes. Survival splitting criteria available within the `randomForestSRC` package are the log-rank splitting rule (the default rule) [126] and the log-rank score rule [127]. Each tree is grown to full size under the constraint that terminal nodes should have no less than `nodesize` unique deaths. The `randomForestSRC` algorithm generates an ensemble estimate of the cumulative hazard function. This estimate is constructed by combining information from the `ntree` trees grown from the bootstrap samples. More precisely, cumulative hazard estimates are calculated at each terminal node using the Nelson-Aalen estimator:

$$\widehat{H}_m(t)=\sum_{j:t_{j,m}\leq t}\frac{d_{j,m}}{n_{j,m}},$$

where $\{t_{j,m}\}$ are the distinct times in a specific node m, and $d_{j,m}$ and $n_{j,m}$ denote the number of deaths and individual at risks at time $t_{j,m}$. Estimates $\widehat{H}_b(t|Z_i)$ for individual i are computed for each tree $b = 1, \ldots$ `ntree`, by simply dropping Z_i down the tree. The ensemble cumulative hazard estimator is then derived by averaging the cumulative

hazard estimates over all trees:

$$\widehat{H}_e(t|Z_i) = \frac{1}{\texttt{ntree}} \sum_{b=1}^{\texttt{ntree}} \widehat{H}_b(t|Z_i).$$

One advantage of the RSF algorithm is that it can account for complex nonlinear effects without making any model assumption. One disadvantage is that the resulting model is much less interpretable than models constructed with standard survival methods. However, covariate predictiveness can be evaluated using the *minimal depth* statistic proposed by Ishwaran *et al.* [128], which quantifies the importance of a variable based on its positioning in a tree. The minimal depth for a given covariate ν is defined as the distance D_ν from the root node to the first node that splits on ν. This quantity is computed for each tree and then averaged over the forest. The smaller the minimal depth, the higher the importance of a covariate on survival.

2.6.6 Assessing the predictive ability of survival models

To be of practical utility, a survival model must be able to i) generate predicted probabilities that agree numerically with the actual outcomes and ii) distinguish patients with different outcomes. To characterise these components of predictive ability, two type of measures are used: calibration and discrimination.

Calibration

Calibration of probability predictions can be assessed using a *calibration plot*. For a given time t, this plot shows an estimate of the observed probability of surviving until time t versus the corresponding model predicted probability. One way to construct this plot is to bin the individuals into groups based on their predicted probabilities. Then, for each bin, the Kaplan-Meier survival estimate is computed at time t, and plotted versus the mean value of the bin [129].

Discrimination

Discrimination can be assessed using the concordance index proposed by Harrell [129]. This index does not depend on a chosen time to evaluate the model and takes into account censored observations [128]. It is computed by considering all possible pairs of patients in which at least one of them has experienced the event. Pairs are considered unusable if the shorter event time is censored or if both patients experienced the event at the same time. A pair of observations is said to be concordant if the predicted survival time is shorter for the patient who had the event sooner. To define concordant pairs, instead of the predicted survival times, the predicted survival probabilities at any fixed time point can be used interchangeably, provided that the two estimates of the survival curves do not cross. This is true for instance if the proportional hazard assumptions are satisfied [129]. The C-index is defined as the proportion of all usable pairs in which the predictions and outcomes are concordant. This quantity gives an estimate of the probability of concordance between predictions and outcomes. A value of 0.5 means that model predictions are no better than random guessing, whereas a value of 1 indicates perfect discrimination.

Chapter 3

Modelling the differential effects of Sunitinib on primary tumour and metastatic growth

3.1 Introduction

Despite proven clinical action of antiangiogenic inhibitors [24], recent experimental studies have suggested differential effects of these drugs on primary and secondary tumours [25–27]. A study by Pàez-Ribez *et al.* [25] reported that VEGF inhibitors suppressed the growth of the primary tumour in mouse models of pancreatic neuroendocrine carcinoma and glioblastoma, but concomitantly increased lymphatic and distant metastasis. Ebos *et al.* [26] reported that in mouse models of breast cancer and melanoma, sunitinib significantly suppressed the growth of orthotopically implanted primary tumours. However, administration of sunitinib increased tumour burden in various metastasis assays, including after intravenous injection of tumour cells and after surgical removal of primary orthotopically grown tumours (Figure 3.1). Motivated by these alarming findings, Blagoev *et al.* [130] conducted a retrospective analysis of data from the randomised phase III trial that led to sunitinib's approval in the United States and in Europe for the

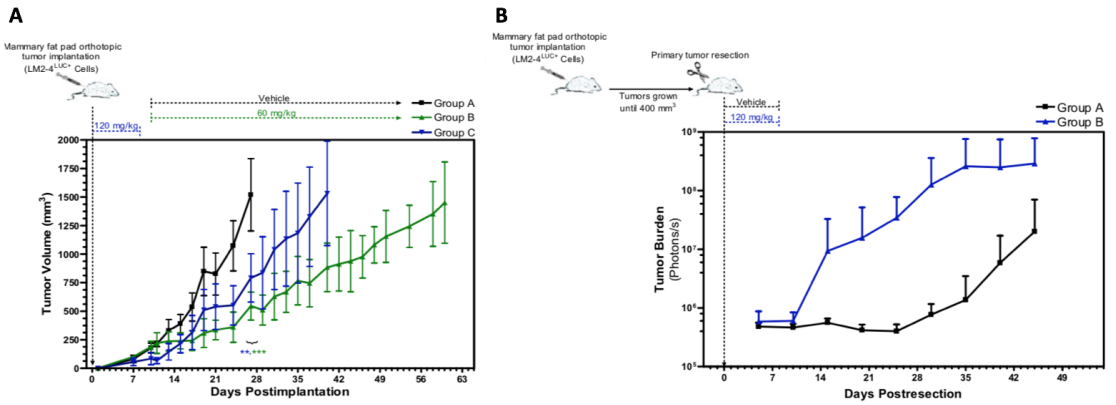

Figure 3.1 – Differential efficacies of sunitinib on primary and metastatic disease, taken from [26]. A) Sunitinib treated groups had significantly reduction in primary tumour volume compared to control animals. B) Quantification by bioluminescence showed increased metastasis in sunitinib treated animals.

treatment of mRCC [53]. The authors found no evidence of accelerated tumour growth and shortened survival, concluding that sunitinib is not harmful in humans.

The preclinical results however highlight the need to further investigate tumour response to these drugs. In this context, mathematical models may be useful to verify different theories by assessing the agreement of model predictions with the experimental observations. Mathematical models may also help establishing predictive biomarkers that would enable to tailor therapies for individual patients.

This study extends a previous mechanistic model [19] to integrate the effect of neoadjuvant sunitinib therapy. The model is calibrated using the nonlinear mixed-effects statistical framework on a large dataset of 104 mice treated with multiple scheduling strategies. The usability of the biomarkers to predict the mathematical model parameters is further investigated by means of artificial intelligence techniques. Finally, a survival model is used to investigate the predictive power of the acquired biomarkers and of the mathematical model's parameters.

Table 3.1 – Treatment schedules of neoadjuvant sunitinib. Groups written in red were used to calibrate the K-PD model.

Schedules	Surgery (days post-implantation)	Number of animals
Vehicle	34	27
60 mg/kg for 3 days	34	15
60 mg/kg for 7 days	34	6
60 mg/kg for 14 days	34	21
120 mg/kg for 3 days	34	20
120 mg/kg for 3 days / 60 mg/kg for 11 days	34	15
Vehicle	38	6
120 mg/kg for 3 days	38	6
120 mg/kg for 3 days / 60 mg/kg for 4 days	38	6
120 mg/kg for 3 days / 60 mg/kg for 8 days	38	6
120 mg/kg for 3 days / 60 mg/kg for 11 days	38	4

3.2 Materials and methods

3.2.1 Animal experiments

Human breast LM2-4 cancer cells (1×10^6 cells) expressing luciferase were implanted into the right inguinal mammary fat pad of female SCID mice. Primary tumour burden was monitored with Vernier callipers using the formula $\text{width}^2(\text{length} \times 0.5)$. Treatments started 14 days before primary tumours were surgically removed (34 or 38 days post-implantation). All animals were treated daily with sunitinib followed by vehicle for a total of 14-day treatment. Animals treated daily with vehicle for 14 days were used as controls. Treatment schedules utilised in this study are reported in Table 3.1. Post-surgical metastatic tumour burden was assessed by BLI and overall survival was monitored based on signs of end stage disease. Circulating tumour cells and myeloid derived suppressor cells levels were quantified on blood samples collected one day before surgical resection. CD31+ cells (% area), Ki67+ cells (% cells) and Ki76+/CD31+ cells (proliferating endothelial cells) were quantified on sections of the resected tumours.

3.2.2 Mechanistic model of metastatic dissemination and growth

The primary tumour (PT) volume, $V_p(t)$, was modelled as the solution of

$$\begin{cases} \dfrac{dV_p}{dt} = g_p(t, V_p) \\ V_p(t=0) = V_i, \end{cases}$$

where $g_p(t, v)$ is the PT growth rate, defined below. The initial condition V_i was the volume corresponding to the number of cells injected in the animals (= 1 mm^3 based on the conversion rule 1 $mm^3 \simeq 10^6$ cells [96]). It was assumed that metastases started from the volume V_0 of a single cell and that all grew at the same rate $g(t, v)$.

Emission of metastases was assumed to occur from the PT at the following volume-dependent rate [19]:

$$d(V_p) = \mu V_p,$$

where parameter μ can be interpreted as the daily probability that a cell from the PT successfully establishes a metastasis [19].

The state of the metastatic process was described through a function $\rho(t, v)$ representing the distribution of metastatic tumors with size v at time t. It solves the following initial boundary value problem [14]:

$$\begin{cases} \partial_t \rho(t, v) + \partial_v (g(t, v)\rho(t, v)) = 0, & t \in (0, +\infty),\ v \in (V_0, +\infty) \\ g(t, V_0)\rho(t, V_0) = d(V_p(t)), & t \in (0, +\infty) \\ \rho(0, v) = 0, & v \in (V_0, +\infty). \end{cases}$$

The first equation derives from a balance equation on the number of metastases; the second equation is a boundary condition for the rate of newly created metastases; the third equation is the initial condition (no metastases exists at the initial time).

The total metastatic burden (MB) at time t was then given by

$$M(t) = \int_{V_0}^{+\infty} v\rho(t, v)dv.$$

In the particular case of an autonomous metastatic growth rate $g(v)$ (i.e. with no effect of the therapy on the growth of the metastases), the previous quantity satisfies the following convolution formula [97]

$$M(t) = \int_0^t d(V_p(t-s))V(s)ds,$$

which can be solved efficiently through the use of a fast Fourier transform algorithm. In the previous equation, $V(s)$ represents the volume reached by a metastatic tumour after a period of time s from its emission, when growing with growth rate g.

Untreated animals

As previously shown [19], the metastatic process in vehicle-treated animals from the same ortho-surgical breast cancer mouse model can be adequately described using a Gomp-Exp growth model [68] with same parameter values for both primary tumour and metastases:

$$g_p(v) = g(v) = \min\left(\lambda v, \left(\alpha - \beta \log\left(\frac{v}{V_0}\right)\right) v\right).$$

In this modification of the Gompertz model, the tumour growth rate is limited by an experimentally determined *in vitro* proliferation rate λ [19]. This is done to avoid biologically unrealistic fast growth rates for small volumes. Parameters α and β define the Gompertz growth phase: the former is the specific growth rate at the size V_0 of one cell, the latter represents the exponential decay rate of the relative growth rate.

Sunitinib treated animals

The model we developed for the sunitinib treated animals assumed that the drug reduces the primary tumour growth rate by a term proportional to its concentration, $C(t)$:

$$g_p(t, v) = \min\left(\lambda v, \left(\alpha - \beta \log\left(\frac{v}{V_0}\right)\right) v\right)(1 - k\, C(t)),$$

where k is a parameter of drug efficacy. As no pharmacokinetic data were available, we used a kinetics-pharmacodynamics (K-PD) approach. Namely, we considered that the drug concentration decays exponentially after each dose,

$$C(t) = \frac{1}{V_d} \sum_{i=1}^{n} D_i e^{-k_e(t-\tau_i)} \mathbb{1}_{t>\tau_i},$$

where D_i indicates the dose administered at time τ_i; the volume of distribution V_d and the elimination rate constant k_e were fixed to the values reported in [131]. Inclusion of treatment effect on metastatic growth was considered in the model development phase; however, this led to model predictions which could not explain the behaviour of the experimental data. Therefore, the final model considered that the antiangiogenic agent did not affect growth of metastases, that is:

$$g(v) = \min\left(\lambda v, \left(\alpha - \beta \log\left(\frac{v}{V_0}\right)\right) v\right).$$

3.2.3 Calibration and validation of the mathematical metastatic model

The mathematical metastatic model was fitted to the experimental data using a nonlinear mixed-effects modelling approach [32]. Briefly, this consists in modelling inter-animal variability by assuming a parametric distribution for the model parameters. All individual primary tumour and metastatic burden longitudinal data can then be pooled together in a population model, whose parameters are estimated by likelihood maximisation [32]. The observed data were log-transformed and a proportional error model was used. For the vector of individual parameters, a log-normal distribution with full covariance matrix was assumed. Maximum likelihood estimates of the population parameters were obtained using the Stochastic Approximation of Expectation-Maximization (SAEM) algorithm implemented in the nlmefitsa Matlab function [132]. PT and MB data were fitted simultaneously for vehicle and sunitinib-treated animals. Visual predictive checks (VPC), individual fits and standard diagnostic graphical tools based on individual parameters were used for evaluating the adequacy of the different model components.

3.2.4 Machine learning algorithms

Effects of covariates on the model parameters were assessed using linear regression and a number of machine learning regression techniques (artificial neural networks, support vector regression, random forest models) using the train function of the R caret package [90, 133]. Except for the random forest models, data were centred and scaled prior to modelling. Tuning parameter values of the regression models were selected to minimise the root mean squared error (RMSE) using five replicates of a 10-fold cross-validation.

Partial least squares

Partial least squares (PLS) uses an iterative procedure to build linear combinations of the original predictors that have maximum correlation with the response. These new variables are called *components*. We evaluated PLS models with 1 through 7 components. The optimal RMSE was obtained with 1 component, either when the outcome variable was the metastatic potential parameter μ or its log-transformed.

Neural networks

Neural networks model the outcome variable by means of a set of intermediate variables called *hidden units*. The model parameters are estimated by a modified version of the least squares regression where a weight decay λ is introduced to penalise large regression coefficients. Using cross-validation, we evaluated models with three different weight decays ($\lambda = 0, 0.01, 0.1$) and a number of hidden units ranging from 1 to 10. For each instance, five different neural networks were generated using different initial parameters values, and the resulting predictions were averaged in order to reduce model instability. The optimal models for predicting $\log \mu$ and μ used a weight decay value $\lambda = 0.1$ and a number of 1 and 10 hidden units, respectively.

Support vector regression

Support vector regression uses an objective function that ignores data points with residuals smaller than a certain threshold and simultaneously penalises large residuals by means of a cost parameter that is set by the user. A support vector regression model with radial basis function kernel was evaluated over cost parameter values ranging from to 0.25 to $1.3 \cdot 10^5$. The final value of the cost parameter was $C = 0.25$ in both models for predicting $\log \mu$ and μ .

Random forests

A random forest is trained by drawing *ntree* bootstrap samples of the original data and by growing a tree on each bootstrap data set. At each node of the tree, *mtry* predictors are randomly selected as candidate variables for splitting. For a given sample, the forest's prediction is then obtained by averaging the samples predictions across trees. Based learner in random forests can be either classification and regression trees (CART) or conditional inference trees. We evaluated these two models using 1000 trees. In all cases, the optimal value for *mtry* was 2.

3.2.5 Survival analysis

Survival times were analysed using the Monolix software [134]. To model these data a log-logistic distribution was used. Its hazard function is defined by

$$h(t; T_e, s) = \frac{\frac{s}{T_e}\left(\frac{t}{T_e}\right)^{s-1}}{1 + \left(\frac{t}{T_e}\right)^{s}}, \quad t \in [0, +\infty),$$

where $T_e > 0$ is the scale parameter and $s > 0$ is the shape parameter. The scale parameter was assumed to vary from individual to individual and to model this variability a log-normal distribution was used. We utilized the COSSAC (**Co**nditional **S**ampling for **S**tepwise **A**pproach based on **C**orrelation tests) covariate selection algorithm imple-

mented in the Rsmlx package [135] for automatic building of the covariate model. This algorithm uses a stepwise approach, adding first covariates with lowest p-value from the Pearson's correlation test (continuous covariate) or ANOVA (categorical covariate), and confirming each step using a likelihood ratio test. Simulations of the final model were performed using the simulx function of the mlxR R package [136].

3.3 Results

3.3.1 Simulations of the effect of neoadjuvant sunitinib treatment on metastases suggested no effect on growth of metastases

We investigated possible mechanistic explanations of the reported differential effects of neo-adjuvant Sunitinib on primary and secondary disease [26, 27]. The overall effect of therapy on metastasis is the combined result of two phenomena: 1) reduction of metastatic spread from the effect on the primary tumour and 2) impact of metastatic growth itself. To disentangle the two, we generated model predictions under the assumptions of effect (A) or no effect of therapy on metastatic growth (B) (Figure 5.2). Thus, in scenario (B), only indirect metastatic effect is present, through limitation of dissemination due to reduced primary tumour size. Of important note, to do so we used parameter values estimated from a previous study on control groups [19]. In other words, the model simulations were agnostic to the data and represent pure mechanistic predictions. Simulations are reported in Figure 5.2. In first approximation, we modelled the inhibitory effect of the anti-angiogenic drug by setting the tumour growth rate to zero during the phase of treatment, which was able to describe the primary tumour data reasonably well. Population distributions obtained under the hypothesis A (effect of therapy on metastatic growth) failed to describe the data (Figures 5.2 and S1). On the other hand, simulations under hypothesis B reproduced the behaviour of the experimental data notably well. This was observed in all the treated groups (Figure S1) and suggested rejection of the assumption A, with B being a valid possible alternative.

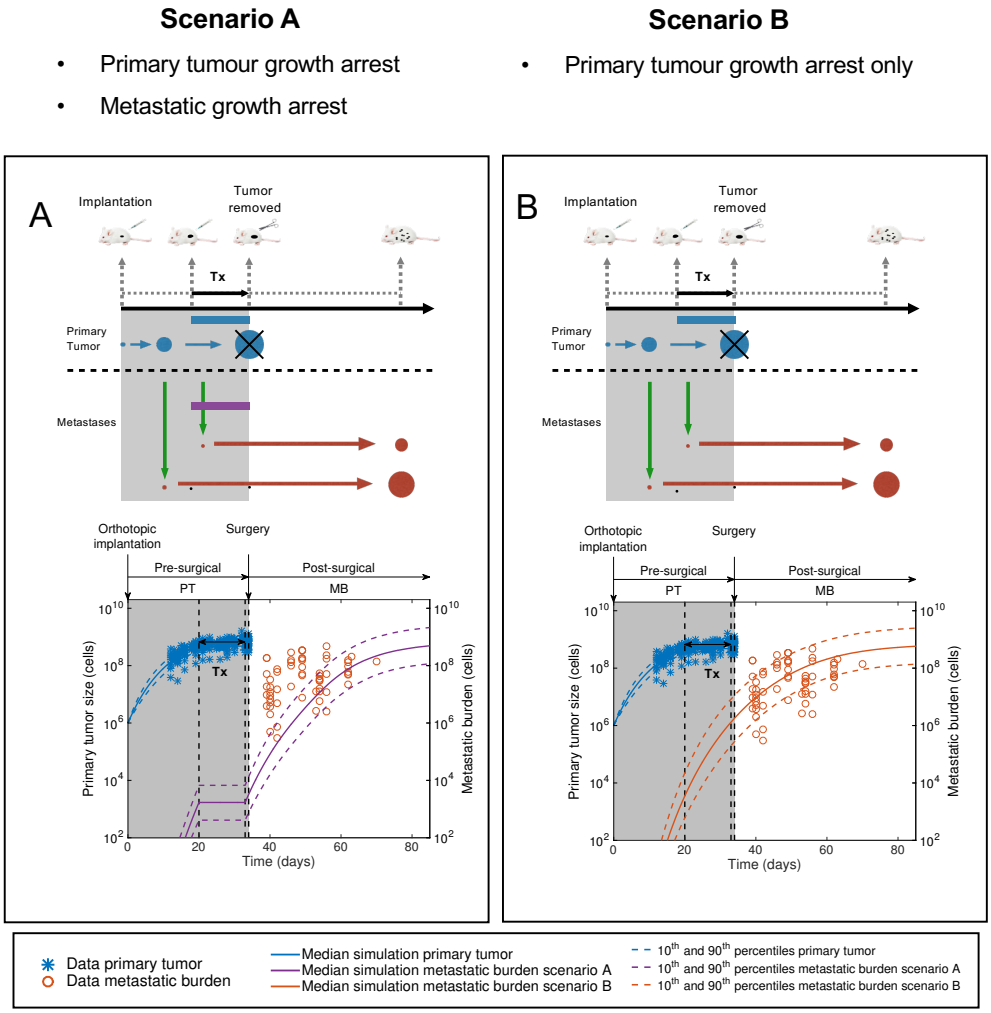

Figure 3.2 – Using mechanistic mathematical modelling to test hypotheses of differential effects of Sunitinib on primary tumour versus metastatic growth and dissemination. A mathematical model previously developed and calibrated for pre- and post-surgical metastatic growth without therapeutic intervention [19] was used to simulate the effect of neoadjuvant Sunitinib therapy by assuming growth arrest on either both the primary and the metastases (A) or only the primary tumour (B). Tx = treatment.

3.3.2 Calibration and validation of the K-PD mechanistic model

We developed a K-PD model (see methods) in order to account for differences between treatment schedules and evaluated its descriptive abilities using the data of 104 mice which received vehicle or neoadjuvant sunitinib treatment according to different schedules (see Table 3.1). Estimates of the model parameters are reported in Table 3.2. These

Table 3.2 – Parameter estimates of the K-PD model obtained by likelihood maximisation via the SAEM algorithm. Abbreviations: CV, coefficient of variation computed as the ratio of the standard deviation and the median of the estimated parameter distribution; r.s.e., relative standard error.

Parameter (Unit)	Meaning	Median	CV (%)	r.s.e. (%)
μ (cell$^{-1}\cdot$ day^{-1})	dissemination coefficient	$2.12 \cdot 10^{-11}$	$1.48 \cdot 10^{3}$	17.3
α (day^{-1})	gompertzian growth parameter	1.94	18.1	2
β (day^{-1})	gompertzian growth parameter	0.0911	19.7	2.21
λ (day^{-1})	in vitro proliferation rate	0.837 (fixed)	-	-
k (L/mg)	drug efficacy	0.446	32.1	6.34
k_e (day^{-1})	drug elimination rate	3.26 (fixed)	-	-
V_d (L/kg)	volume of distribution	12 (fixed)	-	-

were identified with good precision (relative standard error $\leq 17\%$) thanks to the large number of animals considered in the population fit. Confirming previous results [19], the metastatic potential parameter μ was found to be the parameter which varies most among individuals (largest coefficient of variation).

Figure 3.3 A shows the visual predictive checks (VPCs) for the vehicle group and two representative treated group. Other groups are reported in Figure S2. The calibrated model was able to describe both the structural dynamics and inter-subject variability of the experimental data in both vehicle and treated animals. Representative individual fits are shown in Figures 3.3 B and S3. These were in agreement with the experimental data, indicating that the model could also describe individual dynamics.

Further model diagnostic plots are shown in Figures 3.4 - 3.6. From these, no clear misspecification of the structural and residual error model could be detected. Points in the observations versus individual predictions plots were evenly distributed around the identity line (Figure 3.4 A) and the individual weighted residuals appeared to be approximately normal (Figure 3.4 B and 3.4 C).

The distributions of the empirical Bayes estimates were in agreement with the theoretical distributions defined in the statistical model (Figure 3.5). Moreover, the η-shrinkage was $\leq 20\%$ for each parameter, meaning that the individual parameter estimates and the diagnostic tools based on them can be considered reliable [137]. Finally, correlations found between the estimated random effects (Figure 3.6) confirmed the appropriateness

of a full covariance matrix in the assumed distribution of the individual parameters. The model could also predict PT and MB dynamics of five independent groups with different time of surgery and drug schedules that were not used to estimate the model parameters (Figure 3.7).

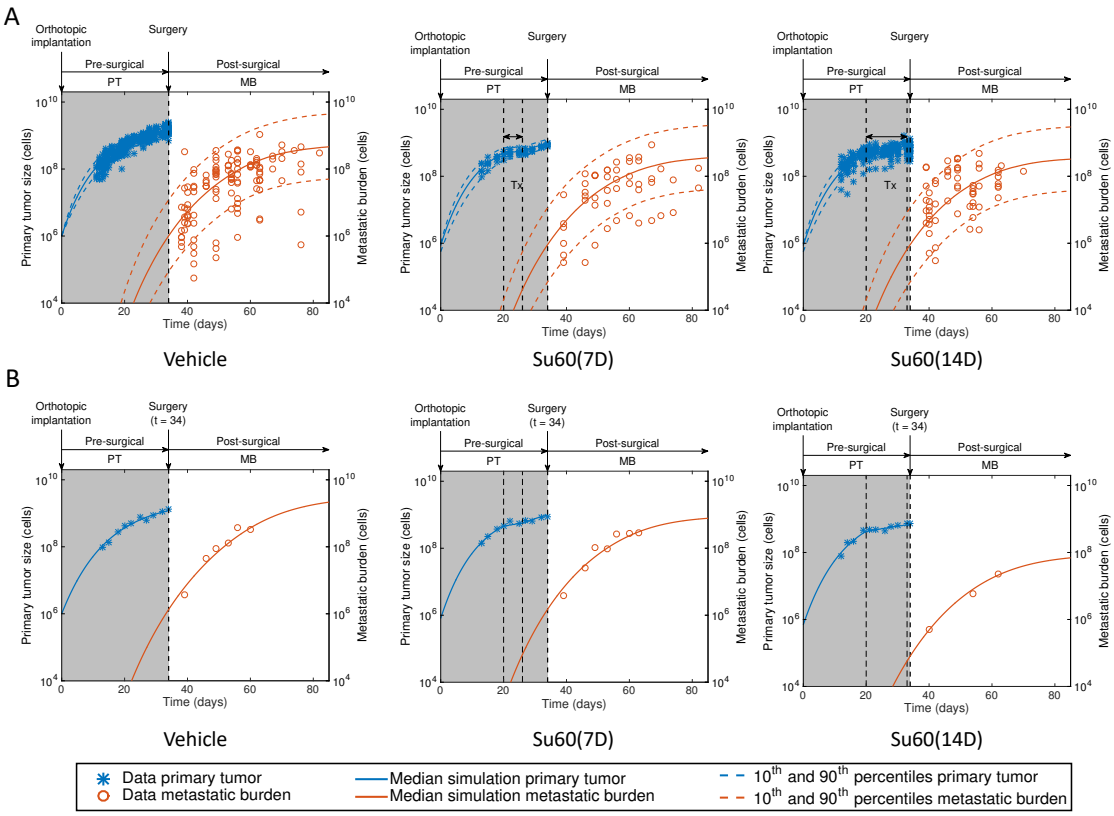

Figure 3.3 – Calibration and validation of a K-PD mathematical model for primary tumour growth and metastatic development (dissemination and growth) under neoadjuvant Sunitinib treatment. The mathematical model was fitted to the experimental data using a mixed-effects population approach. Maximum likelihood estimates of the population parameters were obtained simultaneously for vehicle and treated groups using the SAEM algorithm (n=104 animals in total). A) Comparison of the simulated model distribution for vehicle, 7 and 14 days Su (60mg/kg) treatment to the corresponding datasets. B) Examples of individual dynamics.

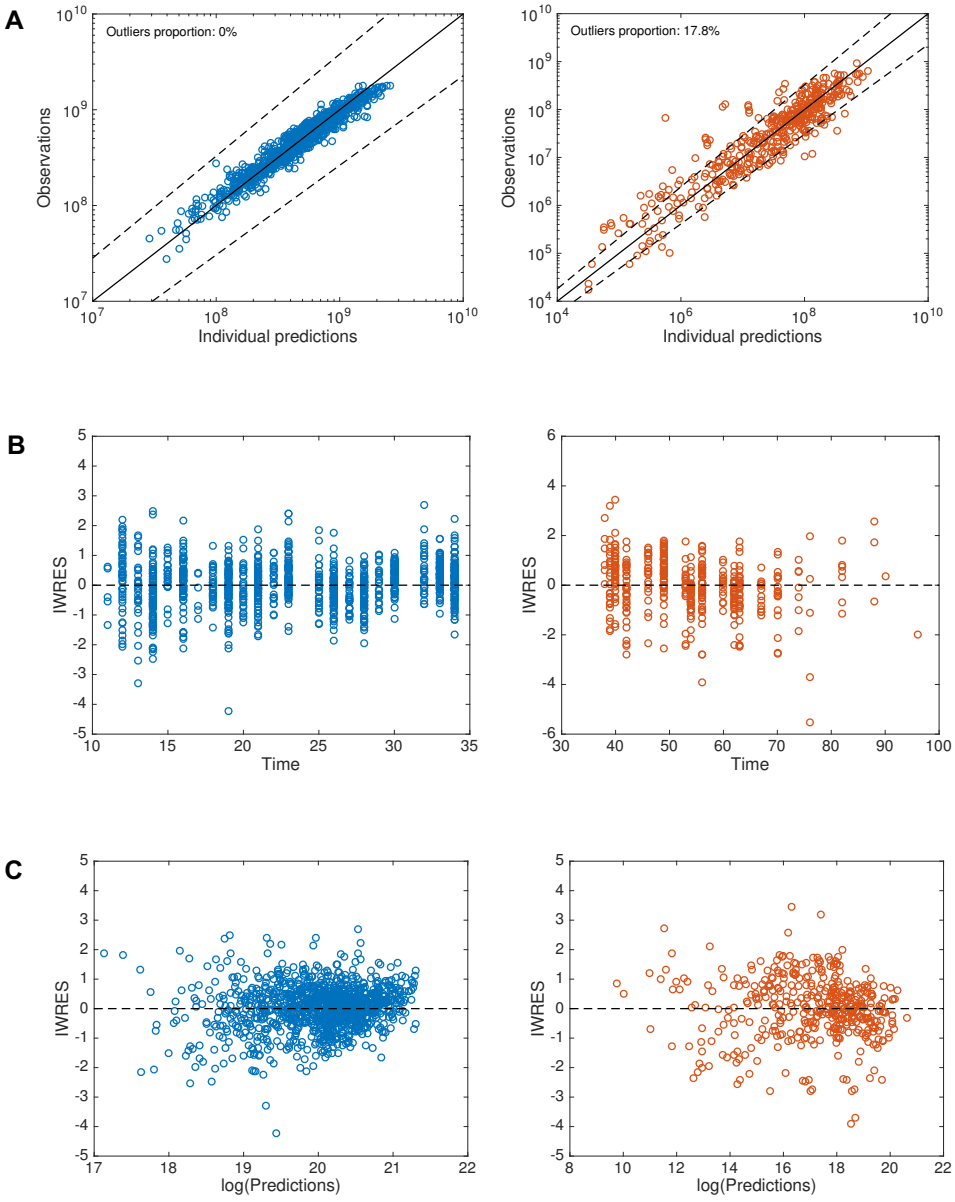

Figure 3.4 – Model diagnostic plots. A) Observation vs. individual prediction. Solid lines are identity lines. Dashed lines represent 90% prediction intervals. B) Individual weighted residuals (IWRES) vs time. C) Individual weighted residuals vs log-transformed individual predictions.

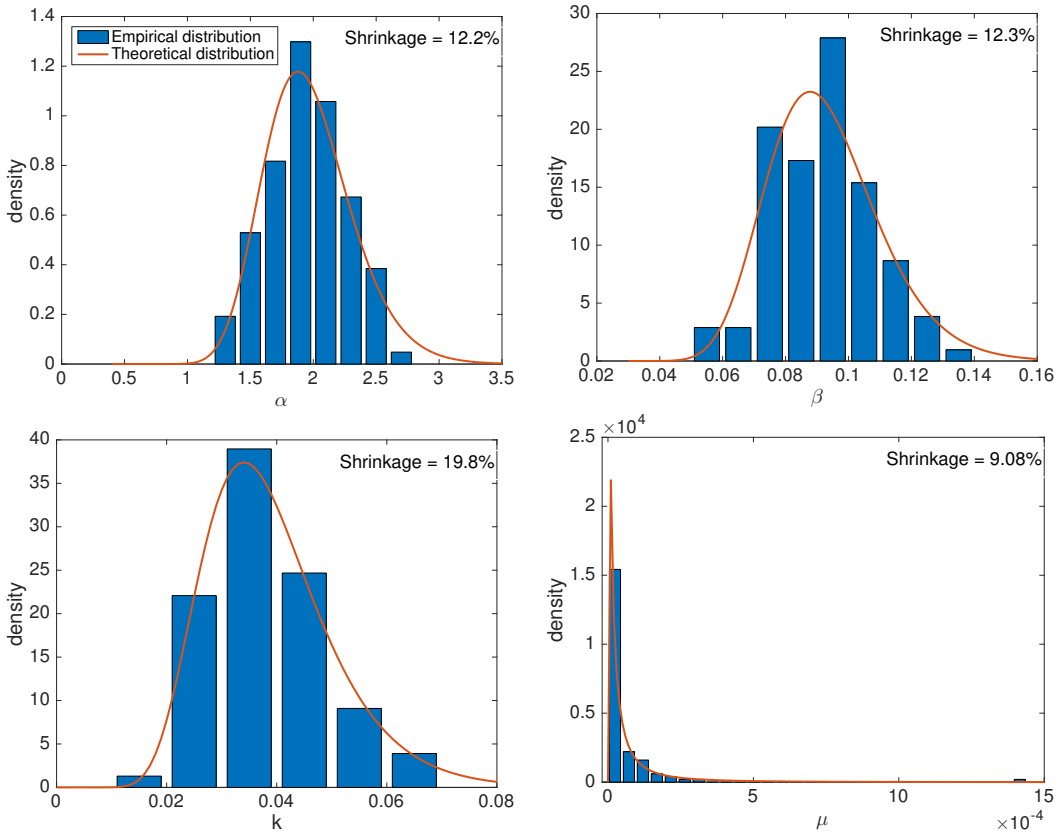

Figure 3.5 – Distribution of the individual parameters.

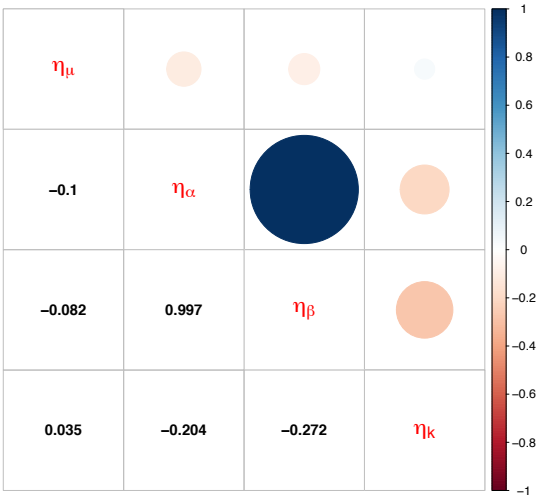

Figure 3.6 – Correlations between random effects.

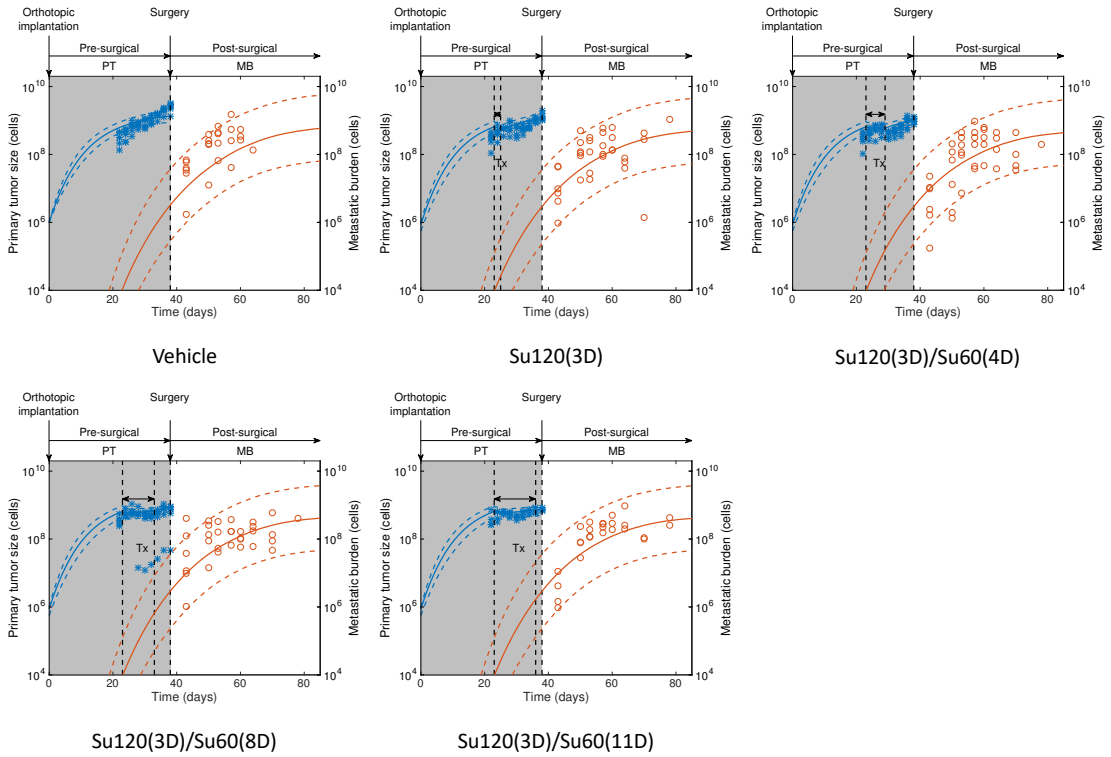

Figure 3.7 – Model predictions in independent datasets (surgery at day 38).

3.3.3 Machine learning for covariate analysis

Pre-surgical immunohistochemical measurements of tumour Ki67 and CD31, as well as MDSC and CTC levels were available for a number of 66 animals. We investigated whether these molecular and cellular biomarkers might help to explain part of the variability in the individual parameters. In particular, we looked for correlations between biomarkers and parameter μ, whose large variability indicated that there might exist subpopulations with different metastatic potential values. We first examined correlations between biomarkers in order to identify potential redundancies in the data (Figure 3.8). High correlations were found between Ki67 and Ki67$^+$/CD31$^-$ ($r = 0.979, p < 10^{-12}$) and CTC and gMDSC ($r = 0.678, p = 3.95 \cdot 10^{-10}$). We next investigated the value of these measurements as predictive biomarkers of the mechanistic parameters: α and β capture growth kinetics, k the effect of treatment and μ metastatic dissemination. Figure 3.9 A

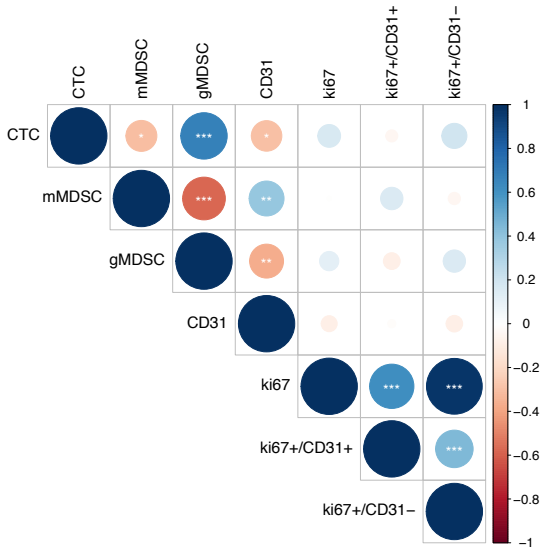

Figure 3.8 – Correlations between biomarkers (Pearson correlation coefficient). Significance code: '***' 0.001 '**' 0.01 '*' 0.05

shows the correlation matrix for biomarkers and the individual parameter estimates. As the individual growth parameters α and β were highly correlated ($r = 0.997, p < 10^{-5}$), we used the tumour doubling time at the volume $V_i = 1$ mm^3 to assess the impact of covariates on the tumour growth parameters. It is defined by

$$DT = -\frac{1}{\beta} \log\left(\frac{\log 2 + A}{A}\right), \quad \text{with } A = \log\left(\frac{V_i}{V_0}\right) - \frac{\alpha}{\beta}.$$

A weak correlation was found between $\log(DT)$ and mMDSC levels (Figure 3.9 A, $r = 0.275, p = 0.0257$). However, none of the available biomarkers was found to correlate either with μ or $\log \mu$ (Figure S4).

Partial least squares and a number of different machine learning regression algorithms were tested in order to identify possible relationships between covariates and individual estimates of the metastatic potential parameter. These included neural networks, support vector regression (SVR) and random forest models [33]. Cross-validation results for the RMSE of the final regression models were compared against the estimate of this metric for the intercept-only model, i.e. the model were prediction is the same for all animals and given by the median value in the population μ_{pop}. As shown in Figure 3.9 B, none of the

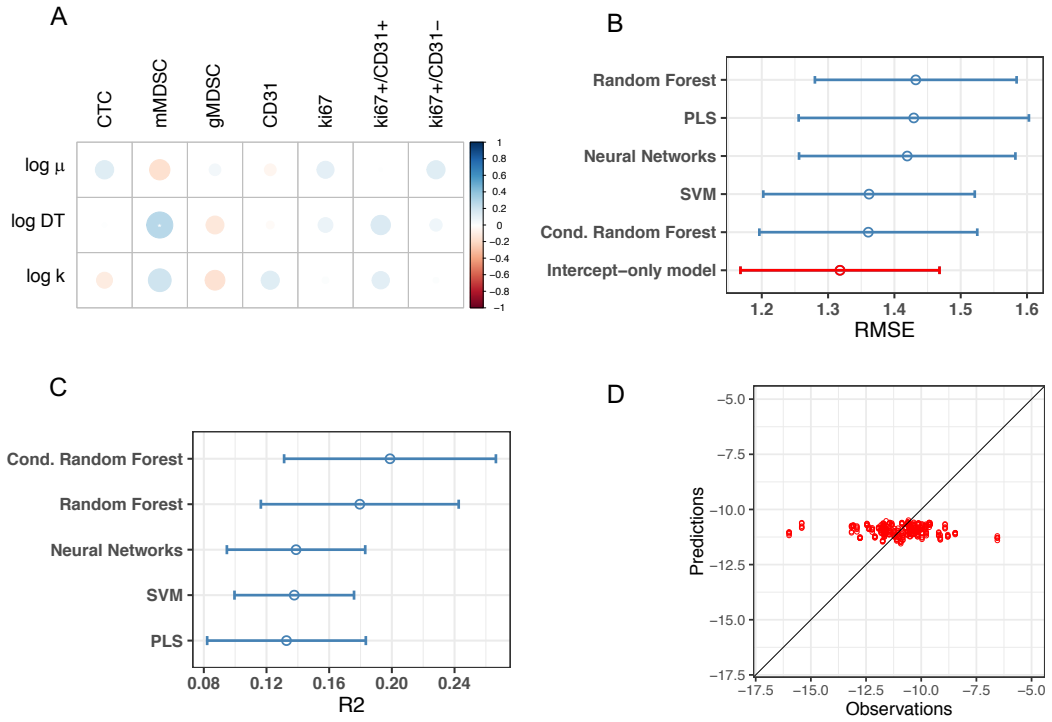

Figure 3.9 – Machine learning algorithms for prediction of the dissemination mechanistic parameter μ. A) Univariate correlations between the biomarkers and the mathematical parameters. B) Predictions versus observations for the Support Vector Machines algorithm. C) Cross-validated RMSE across different regression models utilising the values of the biomarkers for obtaining individual estimates of the metastatic potential μ. To assess the significance of the covariate in the models, RMSE were compared against the value of this metric obtained using a only-intercept model. Bars are 95% confidence intervals. D) Cross-validated R2 with 95% confidence intervals

fitted models had RMSE significantly different from the intercept-only model, suggesting that the biomarkers might not be important predictors of metastatic potential as defined by μ. Values of R^2 ranged from 0.133 to 0.199 across the models (3.9 C), with the highest value reached by the conditional random forest model. Lowest RMSE was achieved by the intercept-only model (1.32). Prediction error on $\log \mu$ ranged from 9.83% $\pm$ 10.7% for the best model (conditional random forests) to 10.6% $\pm$ 11.3% for the worse (random forests, mean $\pm$ std), which was not superior to the predictive power of the intercept-only model (9.71% $\pm$ 10.1%). Plotting the observed versus predicted values (Figure 3.9 D and S5) confirmed that the fitted algorithms were unable to explain the variability of parameter μ.

Table 3.3 – Parameter estimates of survival model with $\log \mu$ included as covariate on the scale parameter T_e: $\log(T_e) = \log(T_{e,pop}) + \beta \log \mu + \eta$.
Displayed is the p-value of the Wald test, testing the significance of the covariate in the model.

Parameter (Unit)	Meaning	Median	CV (%)	r.s.e. (%)	p-value
T_e (day)	scale parameter	32.3	11.5	11.4	
β_μ (unitless)	covariate coefficient	-0.066	-	15.8	$2.33 \cdot 10^{-10}$
s (unitless)	shape parameter	17.9	-	21.6	

3.3.4 Survival analysis

We first analysed the survival data of the subgroup of 66 animals for which biomarkers measurements were available. We fitted the log-logistic model and investigated the significance of covariates on survival by automatic covariate selection using the COSSAC algorithm. Searched covariates were the acquired biomarkers, treatment, and the logarithm of the individual parameters, μ, α, β, estimated from the fit of the mathematical metastatic model. Only covariate $\log \mu$ was selected by the COSSAC algorithm, indicating that biomarkers and treatment differences were insignificant for prediction of survival. Significance of the metastatic potential on survival was further confirmed on the entire group of 104 animals by fitting the survival model ($p = 2.33 \cdot 10^{-10}$, Wald test) and by direct assessment of the correlation between $\log \mu$ and the observed survival values (Figure 3.10 A). The model calibrated on the entire survival data was in agreement with the empirical Kaplan-Meier estimate (Figure 3.10 B). Parameter estimates obtained from this fit are reported in Table 3.3. To visualise the impact of the metastatic potential parameter on survival, we simulated two populations characterised by low and high value of μ, respectively (10th and 90th percentiles of the estimated distribution). Survival curves of the simulated populations and individual dynamics for animals with high and low metastatic potentials are shown in Figure 3.10 C and D, respectively.

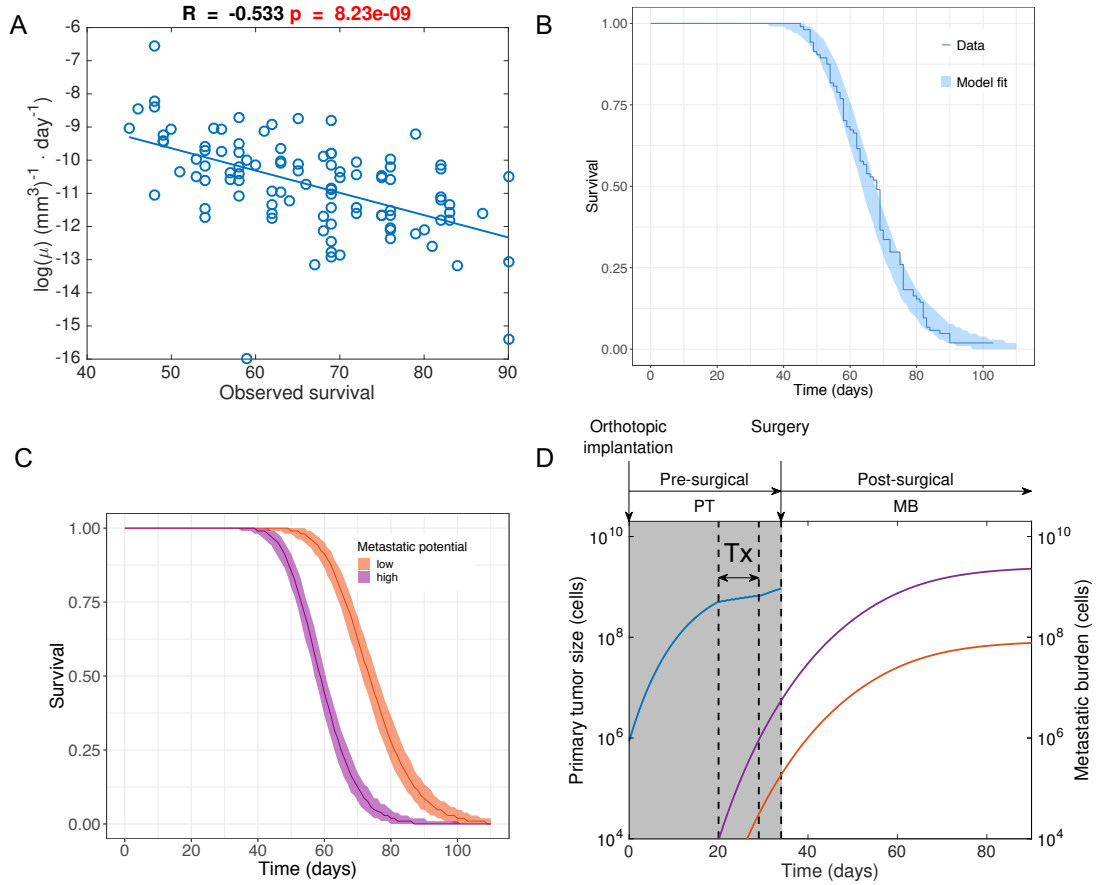

Figure 3.10 – Impact of μ on survival. A) Correlation between $\log(\mu)$ and the observed survival B) Visual predictive check for the survival model. Displayed are the empirical Kaplan-Meier curve with the 90% prediction interval calculated by model simulations. C) Survival curves with events simulated for two groups with high (90th percentile of the estimated distribution for μ, $\mu = 1.19 \cdot 10^{-4}$ mm^{-3} day^{-1}) and low metastatic potential (10th percentile, $\mu = 3.99 \cdot 10^{-6}$ mm^{-3} day^{-1}) and D) Corresponding individual dynamics obtained using the median values of parameters α, β and k.

3.4 Discussion

We extended a previously established mathematical model to integrate the effect of neoadjuvant antiangiogenic treatment on primary and metastatic growth dynamics in an orthosurgical mouse model of spontaneous metastatic breast cancer. **Analysis of a large data set using a non-linear mixed-effects modelling approach revealed a highly heterogeneous population in terms of the metastatic potential parameter** μ. Identifying biological predictors of μ able to reduce this variability would be of critical clinical interest by providing more individualised predictions of metastatic dynamics and survival. **According to our analysis of the biomarkers as covariates in the model, expression of Ki67 and CD31 in the primary tumour, and presurgical CTC and MDSC levels are not significant predictors of metastatic potential and survival in the breast model**. Although likely to depend on the animal model of cancer, these results highlight the need to investigate other molecular and cellular markers. In this regard, a recent clinical study comparing tumour gene expression profiling data in breast cancer patients at diagnosis and after 14 days of sunitinib neoadjuvant treatment, revealed a set of significantly differentially expressed genes between the two times, among which TIMP3 (tissue inhibitor of metalloproteinase 3), the metalloproteinase AD-AMSTS12, DLL4 (delta-like 4), FLT1 (vascular endothelial growth factor receptor 1), immunoglobulins and inflammatory mediators [138]. Ideally, longitudinal measurement of biomarkers could be included as time-varying covariates in the mathematical model, allowing to explain variations in the metastatic potential associated to therapy.

The mathematical models integrate the effect of treatment only on PT growth since preliminary model simulations including treatment effects also on metastases generated model predictions that were in contradiction with the experimental data from the breast model. This made it possible to use the convolution formula for the computation of the metastatic burden. However, if treatment effects are also modelled on metastases, the metastatic burden solves a Volterra equation

which is no more of convolution type and efficient quadrature techniques other than fast Fourier transform algorithms have to be applied (see [97] and the references therein).

Our results confirm a number of preclinical studies showing differential effect of antiangiogenic drugs on localised tumours compared to secondary disease [25–27]. These could be explained by the fact that micrometastatic tumours would rely on different mechanisms of vascularisation. Supporting this explanation, a recent study showed that lung metastasis from breast, colorectal and renal cancers, tend to co-opt the preexisting vasculature rather than inducing angiogenesis [65].

Given the increasingly diverse arsenal of systemic anticancer therapies available with the approval of immune-checkpoint inhibitors, the questions of treatment sequence [82, 139] and dosing regimen [140, 141] are becoming crucial. The proposed model could be used and extended to guide the rational design of treatment schedules and modes of combination before preclinical or clinical testing.

Chapter 4

Modelling the effect of sunitinib treatment breaks in the neoadjuvant setting

4.1 Introduction

Preclinical and clinical studies have suggested that discontinuous administration of VEGF-inhibitors may lead to rapid revascularization and tumour re-growth [28]. Such rebounds have been observed during treatment breaks with sunitinib in patients with metastatic renal cell carcinoma [29, 30], and with bevacizumab in patients with colorectal cancer [31], suggesting that prolonged administration of anti-VEGF therapy might be required to achieve therapeutic benefit. Although tumour rebounds have not been reported in all studies [142], further investigation of the effect of treatment breaks is critical, since treatment is frequently discontinued in practice because of drug toxicities.

Here we adapt the analysis of the previous chapter to investigate the effects of treatment discontinuation in the neoadjuvant setting. The mathematical metastatic model is developed using data from an orthosurgical mouse model of metastatic kidney cancer. Simulations of the calibrated model are then used to investigate the impact of treatment

Table 4.1 – Treatment schedules of neoadjuvant sunitinib.

Schedules	Surgery (days post-implantation)	Number of animals
Vehicle	30	16
Vehicle	26	6
Vehicle	23	6
60 mg/kg for 3 days	30	14
60 mg/kg for 7 days	30	6
60 mg/kg for 14 days	30	17
60 mg/kg for 14 days	26	6
120 mg/kg for 3 days	30	13
120 mg/kg for 3 days / 60 mg/kg for 11 days	30	14

breaks on primary tumour and metastatic dynamics. The predictive power of biomarkers and numerical parameters is also investigated through survival analysis.

4.2 Materials and methods

4.2.1 Animal experiments

RENCA$^{\mathrm{LUC+}}$ cells (4×10^4 cells) were implanted into left kidney of Balb/c mice. Primary tumour burden was monitored with Vernier callipers using the formula width^2(length $\times$ 0.5). Treatments started 14 days before primary tumours were surgically removed (23, 26 or 30 days post-implantation for the kidney model). All animals were treated daily with sunitinib followed by vehicle for a total of 14-day treatment. Animals treated daily with vehicle for 14 days were used as controls. Treatment schedules utilised in this study are summarised in Table 4.1. Post-surgical metastatic tumour burden was assessed by BLI and overall survival was monitored based on signs of end stage disease.

Myeloid derived suppressor cells levels were quantified on blood samples collected one day before surgical resection.

4.2.2 Mechanistic model of metastatic dissemination and growth

As previously shown [19], the metastatic process in vehicle-treated animals from the same ortho-surgical mouse kidney model can be adequately described assuming an exponential

growth law with different parameter values for primary tumour and metastastases:

$$g_p(v) = \alpha_p v, \quad g(v) = \alpha v.$$

This model was adapted to include the effect of neoadjuvant sunitinib therapy as follows. The primary tumour volume, $V_p(t)$, was modelled as the solution of

$$\frac{dV_p}{dt} = \begin{cases} \alpha_p V_p & t \leq \tau_{start} \\ \alpha_p(1 - k\,C(t))V_p & \tau_{start} < t \leq \tau_{end} \\ \alpha_{reb} V_p & t \geq \tau_{end} \end{cases}$$

$$V_p(t = 0) = V_i,$$

where V_i is the tumour volume at the time of injection, $[\tau_{start}, \tau_{end}]$ is the time interval in which treatment was administered, and α_p, α_{reb} denote the pre-treatment and post-treatment growth rates, respectively (this model, therefore, includes the possibility of post-treatment growth rebound). We assumed that the drug reduces the primary tumour growth rate by a term proportional to its concentration $C(t)$, where k is a parameter of drug efficacy. Concerning metastatic growth, it was supposed that the antiangiogenic drug does not affect the growth of metastases on the basis of simulations of the breast model, where inclusion of treatment on metastatic growth yielded model predictions in contradiction with the experimental data (Section 3.3.1).

The structural mathematical model contains six parameters – $V_i, \alpha_p, k, \alpha_{reb}, \mu$ and α. A log-normal distribution was used for $\alpha_p, k, \alpha_{reb}, \mu, \alpha$, while parameter V_i was considered without random effect. As done in the analysis of the breast data set, the observations were log-transformed and a proportional error model was used.

A number of model structures have been considered during the model development phase, including a model with same pre- and post-treatment growth parameters for the primary tumour. The latter assumption, however, resulted in larger uncertainty on the

Table 4.2 – Estimated population parameters for the kidney isograft data under different models.

Model	Parameter (Unit)	Meaning	Median	CV (%)	r.s.e. (%)
Same pre- and post-treatment PT growth	V_i (cell)	initial "take"	$1.44 \cdot 10^6$	-	8.73
	α_p (day^{-1})	PT growth rate	0.149	62.4	6.58
	k (L/mg)	drug efficacy	0.036	$3.49 \cdot 10^3$	114
	k_e (day^{-1})	drug elimination rate	3.26 (fixed)	-	-
	V_d (L/kg)	volume of distribution	12 (fixed)	-	-
	μ (cell$^{-1}\cdot$ day^{-1})	dissemination coefficient	0.02	130	19.3
	α (day^{-1})	metastatic growth rate	0.077	60.4	10.4
Different pre- and post-treatment PT growth	V_i (cell)	initial "take"	$1.58 \cdot 10^6$	-	9.3
	α_p (day^{-1})	pre-treatment PT growth rate	0.142	66.6	7.58
	k (L/mg)	drug efficacy	0.168	458	42.6
	k_e (day^{-1})	drug elimination rate	3.26 (fixed)	-	-
	V_d (L/kg)	volume of distribution	12 (fixed)	-	-
	α_{reb} (day^{-1})	post-treatment PT growth rate	0.214	48.3	11.8
	μ (cell$^{-1}\cdot$ day^{-1})	dissemination coefficient	0.02	166	19.9
	α (day^{-1})	metastatic growth rate	0.074	68.3	10.8

estimated parameters. Therefore, the model with different pre- and post-treatment primary tumour growth rates was considered more appropriate for describing the observed data.

4.3 Results

4.3.1 Calibration and validation of the K-PD model

We developed the K-PD model described above using a dataset containing 98 mice which received vehicle or neoadjuvant sunitinib treatment according to different schedules (Table 4.1). Parameters were estimated under two models: a first model, assuming that growth of the primary tumour reverts to the pre-treatment phase when the drug concentration becomes negligible, and a second model allowing for different pre- and post-treatment growth rates of the primary tumour. Values of the estimated parameters under these two models are given in Table 4.2. While V_i, α_p, μ and α were estimated with good precision in both cases, the uncertainty in parameter k was much higher in the model with same pre- and post-treatment growth rates, which was also rejected according to the Akaike and Bayesian information criteria (ΔAIC = -23.8, ΔBIC = -18.6). The model with different pre- and post-treatment growth rates was then selected. It was able to

describe the entire dataset both at the population and individual levels. VPCs of vehicle and two treated groups with representative individual fits are shown in Figure 4.1. Other groups and individual fits are reported in Figure S1 and Figure S2. Inter-animal variability was mainly explained by the variability in metastatic potential and the variability of response to therapy, as quantified by the coefficient of variation of parameters μ and k. Observations vs model predictions and weighted residuals are shown in Figure 4.2. From these, no clear misspecification of the structural and residual error model could be detected. Substantial η-shrinkage was present for parameter α_{reb} (91.9%), k (70.7%) and μ (62.8%), indicating that the data do not contain enough information to recover the individual estimates of these parameters, which therefore should not be used for covariate screening.

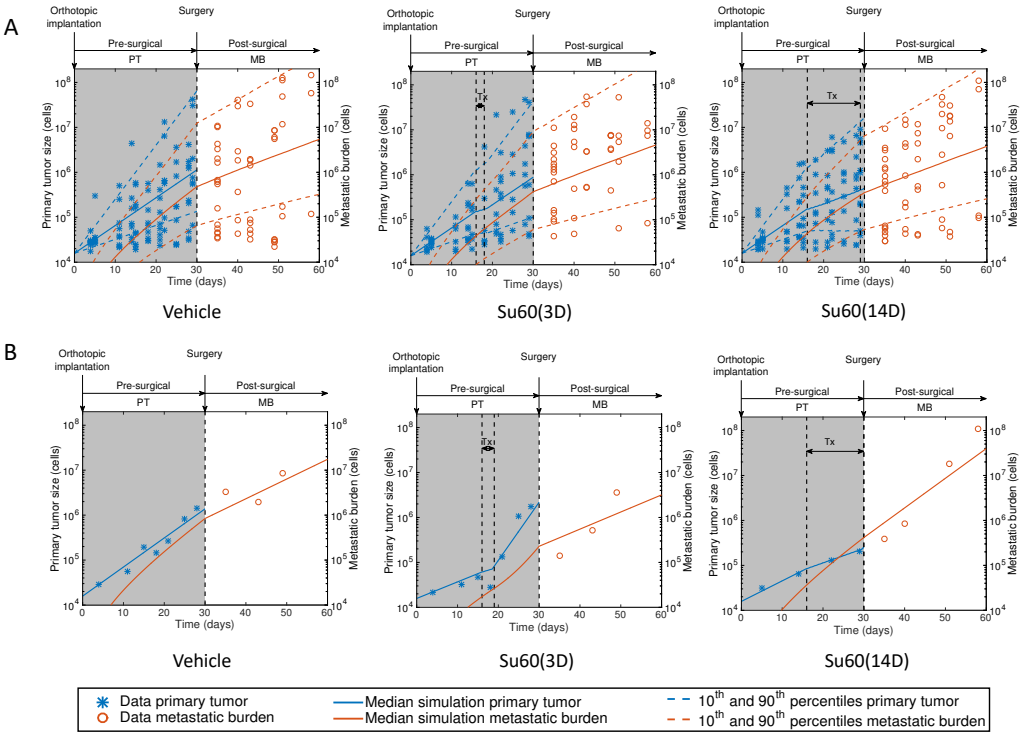

Figure 4.1 – Calibration and validation of a K-PD mathematical model for primary tumour growth and metastatic development (dissemination and growth) under neoadjuvant Sunitinib treatment. The mathematical model was fitted simultaneously to the data of vehicle and treated groups (n=98 animals in total). A) Comparison of the simulated model distribution for vehicle, 3 and 14 days Su (60mg/kg) treatment to the corresponding datasets. B) Examples of individual dynamics.

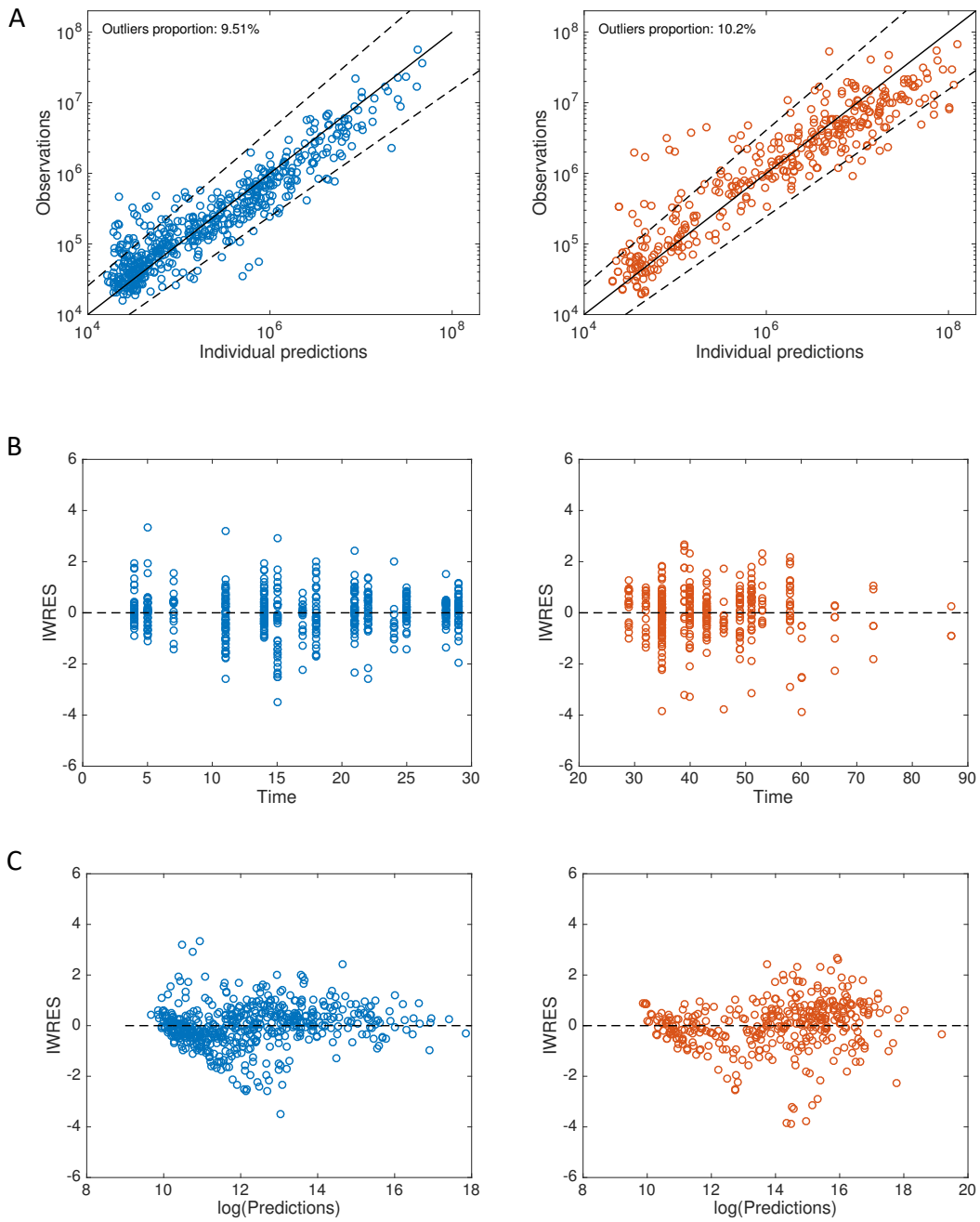

Figure 4.2 – Model diagnostic plots. A) Observation vs individual prediction. Solid lines are identity lines. Dashed lines represent 90% prediction intervals. B) Individual weighted residuals (IWRES) vs time. C) Individual weighted residuals vs log-transformed individual predictions.

Table 4.3 – Effect of the length of break on primary tumour and metastatic burden. Reported are the median change in volume compared to control.

Schedules	PT volume (% vehicle)	Metastatic burden (% vehicle)
13 days break	214	69
12 days break	163	47
11 days break	125	22
10 days break	101	11
9 days break	62	-1
8 days break	44	-10
7 days break	28	-6
6 days break	5	-11
5 days break	-10	-17
4 days break	-26	-18
3 days break	-36	-24
2 days break	-47	-29
1 days break	-54	-22
0 days break	-62	-28

4.3.2 Simulation of the impact of breaks

Simulations of the calibrated K-PD model were then used to compare treatment strategies with breaks of different length. Treatment was assumed to start 14 days before surgery, as in the preclinical experiments. Breaks of length from 0 to 13 days were considered, assuming a daily dose of 60 mg/kg. The effect of treatment on PT and metastatic burden was quantified by the percent change of tumour volume compared to vehicle at surgery and the final simulation time, respectively. Results from these simulations are summarised in Table 4.3 and Figure 4.3. These show that rebound in primary tumour growth caused by treatment cessation may result in increased metastatic burden compared to vehicle, and suggest that break should not be longer than 9 days in order to have a reduction of the metastatic burden.

4.3.3 Survival analysis

We analysed the survival data of 76 animals for which MDSC levels were available. A Gompertz survival model with delay was found to appropriately describe these data. Its

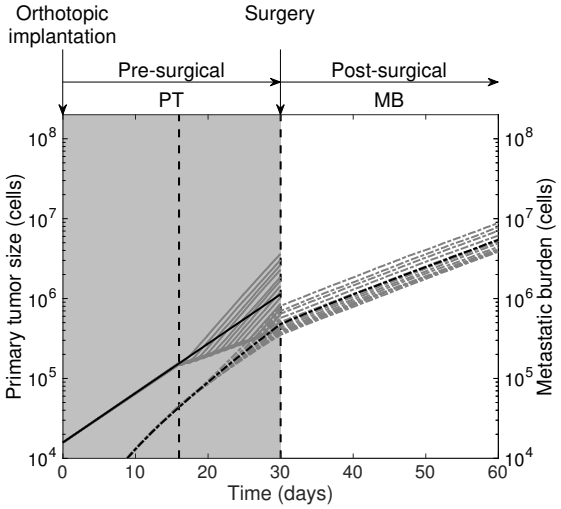

Figure 4.3 – Simulations of the calibrated model comparing vehicle (black line) versus treatments of increasing duration given at dose 60 mg/kg/day (grey lines).

hazard function is defined by

$$h(t;T_e,s) = \begin{cases} 0 & \text{if } t < t_{del} \\ \dfrac{s}{T'_e}\,\exp\left(\dfrac{t-t_{del}}{T'_e}\right) & \text{otherwise,} \end{cases}$$

where t_{del} is the delay after which the survival function starts to decrease; T_e and s are the scale and shape parameter, respectively, and the following re-parametrisation is used:

$$T'_e = \frac{T_e}{\log(1+\frac{\log 2}{s})}.$$

Only parameter T_e was assumed to vary between individuals and for this a log-normal distribution was assumed. The VPC of the fitted model is shown is Figure 4.4 A. Impact of covariates on survival was assessed by automatic building of the covariate model using the COSSAC algorithm of Monolix [117]. Besides MDSC levels, searched covariates were also the logarithm of the individual parameters α_p and α estimated from the fit of the mathematical metastatic model. The final survival model included granulocytic MDSC and $\log \alpha_p$ as covariates on parameter T_e (Table 4.4). Predictions of the developed model for simulated populations with high or low values (around the 10th and 90th percentile)

Table 4.4 – Parameter estimates of the survival model for the kidney data set.

Parameter (Unit)	Meaning	Median	CV (%)	r.s.e. (%)	p-value
T_e (day)	scale parameter	11.3	56.2	42.3	
β_{gMDSC} (unitless)	covariate coefficient	-0.173	-	25.4	$8.44{\cdot}10^{-5}$
β_{α_p} (unitless)	covariate coefficient	-0.683	-	25.2	$7.29{\cdot}10^{-5}$
s (unitless)	shape parameter	0.0334	-	20.7	
t_{del} (day)	delay	42.3	-	2.16	

of one of the two covariates are shown in Figure 4.4.

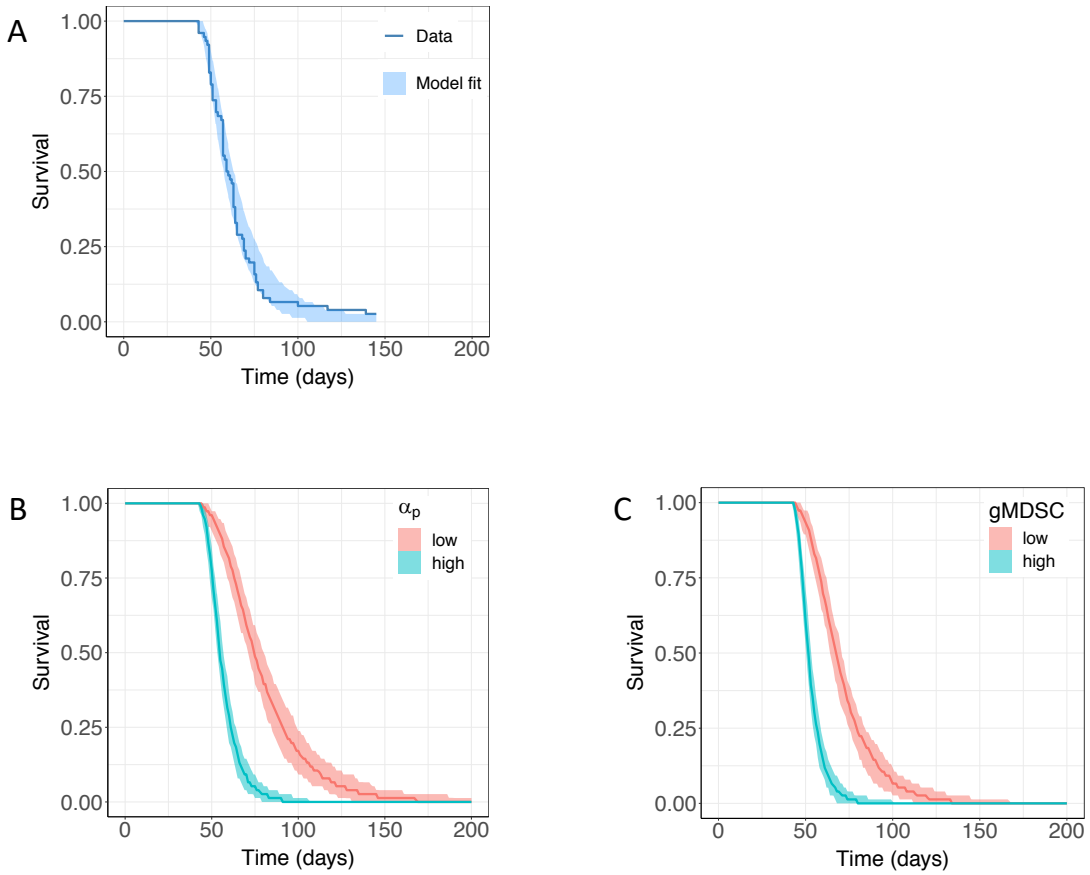

Figure 4.4 – Survival analysis for the kidney data set. A) Visual predictive check for the survival model. Displayed are the empirical Kaplan-Meier curve with the 90% prediction interval calculated by model simulations. B) Survival curves with events simulated for two groups with high (8.08 ± 2.1) and low (2.39 ± 0.88) gMDSC levels and median value of the estimated distribution of $\log \alpha_p$ (-1.89). C) Survival curves with events simulated for two groups with high (-1.34 ± 0.32) and low (0.07 ± 0.12) values of $\log \alpha_p$ and median value of gMDSC (4.13).

4.4 Concluding remarks

Antiangiogenic drugs, such as sunitinib and axitinib, are used for the treatment of patients with metastatic renal cell carcinoma [24]. However, duration and scheduling of therapy with these drugs remain controversial, as rapid revascularization during treatment break has been reported in a number of preclinical studies, and rebound tumour growth has been observed in patients after treatment withdrawal.

In this study, we developed a mathematical model to investigate the effect of discontinuous administration of neoadjuvant sunitinib in a clinically relevant orthosurgical mouse model of spontaneous metastatic kidney cancer. **Our model-based analysis of the data indicated a more rapid growth of the primary tumour after treatment cessation and data-calibrated simulations suggested that prolonged therapy may be needed to achieve therapeutic benefit on metastasis.**

The survival analysis performed here identified the primary tumour growth rate before treatment and granulocytic MDSC levels as predictive marker of survival for kidney cancer. The growth rate constant after treatment cessation might also correlate with survival. However, its predictive value could not be assessed due to the uncertainty in the individual estimates of this parameter as indicated by the large η-shrinkage.

The proposed model could be improved with the integration of pharmacokinetic data. It could also be scaled to human pharmacodynamics and used as a simulation tool to identify schedules that may improve post-surgical outcome.

Chapter 5

Prediction of metastatic relapse in clinical breast cancer

5.1 Introduction

Breast cancer is the most frequent cancer and the second leading cause of cancer death in women [34]. In the majority of cases, the disease is diagnosed in the early stages, when all detectable lesions confined to the breast or nearby lymph nodes can be removed by surgical intervention [35]. However, approximately 20-30% of patients are reported to relapse with distant metastases after surgery [36], suggesting that clinically occult micrometastases might already be present at the time of surgery. Because at present no treatments are effective against metastatic breast cancer, to lower the risk of relapse, adjuvant therapy, such as chemotherapy, hormone therapy and/or target therapy, is usually administered in addition to surgery [143]. Accurate prediction of the risk of metastatic relapse is therefore of critical clinical importance in order to personalise adjuvant treatment and avoid use of toxic and costly therapies when not needed.

Several prognostic tools have been developed to quantitatively evaluate the risk of recurrence in early-stage breast cancer patients. Online tools that calculate individualized survival probabilities and risk of recurrence are based on multivariate analysis and

integrate clinical variables such as age, tumour size, histological grade, hormone receptor and nodal status. Examples of these tools include the online Adjuvant! program [20, 144] and the PREDICT model [22]. Genomic test, such as MammaPrint and Oncotype DX utilise gene expression signatures determined on tumour samples to classify patients as being either at low or high risk of breast cancer recurrence [145]. All these tools, however, are based on purely statistical models, such as Cox proportional hazards models [21, 22] and machine learning algorithms [37, 38], relating predictor variables to the outcome, without integrating any available knowledge of the underlying biological processes.

Mechanistic modeling approaches are playing an increasingly significant role in cancer research and have been used to investigate many aspects of tumor development and metastasis, as well as treatment responses and resistance [4]. However, despite a number of mathematical models have been developed to describe metastatic dynamics [14–17], none of them have been validated as predictive tools to assess the extent of invisible metastases and predicting metastatic recurrence in individual patients. This might be due to the scarcity of data collected in clinical studies, which are often limited to time-to-event data and do not include longitudinal measurements of tumour size.

In [19], the authors extended the mathematical formalism first introduced by Iwata *et al.* [14] for describing metastatic dissemination and growth to account for surgery and validated the model using experimental data from clinically relevant orthosurgical mouse models of breast and kidney cancers. They demonstrated that a model with same growth kinetics for both primary and secondary tumours was able to accurately describe the data of post-surgical metastatic burden in the breast model. Furthermore, the model could also describe the size-dependent probability of 20-years metastatic recurrence in a historical dataset of 2,648 breast cancer patients [146].

In the current work, we developed and validated our mechanistic model for individualized prediction of distant metastasis free survival (DMFS) using a dataset containing DMFS and clinical/pathological characteristics of women that were diagnosed with early operable breast cancer at the Bordeaux Bergonié institute between 1989 and 1993. Patients included in this dataset did not receive any kind of therapy in addition to surgery

and localised radiation of the primary tumour, thus allowing to assess the natural history of the course of metastasis. Model parameters were estimated using a mixed-effects approach, using the stochastic approximation of the expectation-maximization (SAEM) algorithm [32] to maximise the resulting likelihood function. We used the random survival forest algorithm [147] to build a first predictive model and preselect the most predictive covariates to test in the mechanistic model. For comparison, we also applied more traditional approaches, such as Cox regression, and machine learning classification algorithms for predicting 5-year outcome. Predictive performance of all different models was internally evaluated by cross-validation using the concordance index and calibration plots.

We finally illustrate the possible value of the mechanistic approach by performing data-calibrated simulations of the entire cancer history of real patients. Our aim was to derive a model that not only estimates the likelihood of relapse, but also provides personalised predictions of the state of metastasis at the time of diagnosis and of future growth of metastases.

5.2 Methods

5.2.1 Description of the data

We used the data of 642 women diagnosed with primary operable invasive breast carcinoma and operated at the Bordeaux Bergonié institute between 1989 and 1993, which has previously been comprehensively analysed using standard statistical tools (Cox regression) [148]. The patients considered did not received any adjuvant treatment. The time to relapse variable was defined as the time from the date of diagnosis to the date of distant recurrence and patients with no metastasis were censored at the date of last news or death. Clinical/pathological variables available in the dataset included age and tumour size at diagnosis, menopausal status, grade, T and N stages, histological type and number of invaded ganglions. In addition, ER and PR receptor, HER2, Ki67, basal markers, CD24, CD44, ALDH1, BCL2, E-Cadherin and Trio were recorded.

Missing covariate (Figure S1) values were imputed before model building using the *missForest* imputation algorithm implemented in the missForest R package [149]. Using the default value of 100 trees per forest, continuous and categorical covariates were imputed with a 4.4% and 7.1% error, respectively, according to the out-of-bag (OOB) estimate of the imputation error returned by the missForest function.

5.2.2 Random survival forests analysis

The random survival forest (RSF) algorithm is an extension of Breiman's random forest for the analysis of right-censored time-to-event data [125]. The algorithm consists in drawing *ntree* bootstrap samples from the original data and growing a survival tree on each bootstrapped data set by using a survival splitting criterion. An ensemble estimate of the cumulative hazard function is then obtained for each individual by averaging the cumulative hazard estimates from all trees [125].

We utilised the RSF implementation of the randomForestSRC R package [40]. All RSF models were fitted using 1000 trees, with the log-rank splitting rule [125]. The optimal values of the tuning parameters, namely the *mtry* number of variables to be sampled at each split and the minimum number of data points in a terminal node, were selected to maximise the concordance index calculated on the OOB data, using the tune function provided within the randomForestSRC package.

Impact of covariates on DMFS was assessed using the forest-averaged minimal depth [128], which quantifies the predictiveness of a covariate in a tree by its distance from the root node to the first node where it is used to split (smaller minimal depth values correspond to more predictive covariates). Covariates were then ordered on the basis of minimal depth and selected by running a nested analysis.

Partial dependence plots were used to further examine the effect of each covariate on the predicted DMFS, after averaging the effects of all other variables in the model.

5.2.3 Mechanistic model of metastatic dissemination and growth

The individual primary tumour (PT) kinetics in individual i were described by the Gompertz model

$$V_p^i(t) = e^{\frac{\alpha^i}{\beta^i}(1-e^{-\beta^i t})}, \tag{5.1}$$

where $V_p^i(t)$ is the number of cells within the PT at time t, and α^i and β^i are the Gompertzian growth parameters. Under this model, the tumour volume converges to a theoretical upper limit $K = e^{\alpha^i/\beta^i}$. This was fixed to 10^{12} cells according to the value reported in [150], leaving α^i as the only free parameter driving growth. PT size reported as a diameter in the data was converted in number of cells assuming spherical shape and the classical assumption 1 $mm^3 = 10^6$ cells [96].

Considering a dissemination rate from the primary tumour given by [19]

$$d^i(V_p^i) = \mu^i V_p^i,$$

the total number of metastases at a given time t is

$$N^i(t) = \int_0^t d^i(V_p^i(s))ds = \int_0^t \mu^i V_p^i(s)ds.$$

Each metastasis was assumed to start from a single cell and to grow at the same rate of the primary tumour,

$$g^i(v) = \left(\alpha^i - \beta^i \log v\right) v.$$

The state of the metastatic process was then described by a function $\rho^i(t, v)$, representing the distribution of metastatic tumour with size v at time t. Its evolution in time is described by the following transport equation [14]

$$\partial_t \rho^i(t, v) + \partial_v(g^i(v)\rho^i(t, v)) = 0, \quad t \in (0, +\infty),\ v \in (1, +\infty), \tag{5.2}$$

with boundary and initial condition

$$\begin{aligned} g^i(1)\rho^i(t,1) &= d^i(V_p(t)), \quad t \in (0,+\infty), \\ \rho^i(0,v) &= 0, \qquad\qquad\quad v \in (1,+\infty). \end{aligned} \tag{5.3}$$

5.2.4 Mechanistic modelling of time-to-relapse

To calibrate the metastatic model on time-to-relapse data, we defined the theoretical time to relapse as illustrated in Figure 5.1. More precisely, assuming a value V_{vis} as detection threshold, the time τ_{vis} for a tumour to reach this size was given from the assumption of Gompertzian growth, i.e.

$$\tau_{vis} = -\frac{1}{\beta^i}\log\left(1 - \frac{\beta^i}{\alpha^i}\log\left(V_{vis}\right)\right).$$

In an analogous way, the time from the first cancer cell to the detection of the primary tumour, t^i_{diag}, was determined from the known size of the primary tumour at diagnosis, V^i_{diag}:

$$t^i_{diag} = -\frac{1}{\beta^i}\log\left(1 - \frac{\beta^i}{\alpha^i}\log\left(V^i_{diag}\right)\right).$$

A visibility threshold V_{vis} corresponding to 5 mm in diameter was assumed.

Since metastases of size larger than V_{vis} at time t, must have been emitted in the time interval $(0, t - \tau^i_{vis})$, the number of visible metastases at time t can be obtained as

$$N^i_{vis}(t) = N(t - \tau^i_{vis}).$$

The theoretical time-to-relapse was then defined as

$$TTR(V^i_{diag}; \alpha^i, \mu^i) = \begin{cases} \inf\left\{t > 0 : N^i_{vis}(t^i_{diag} + t) \geq 1\right\} & \text{if } N^i(t^i_{diag}) \geq 1, \\ +\infty & \text{otherwise.} \end{cases} \tag{5.4}$$

That is, the time elapsed from diagnosis to the appearance of the first visible metastasis, if, according to the model, at least a metastasis was present before diagnosis; otherwise it was considered as infinitive.

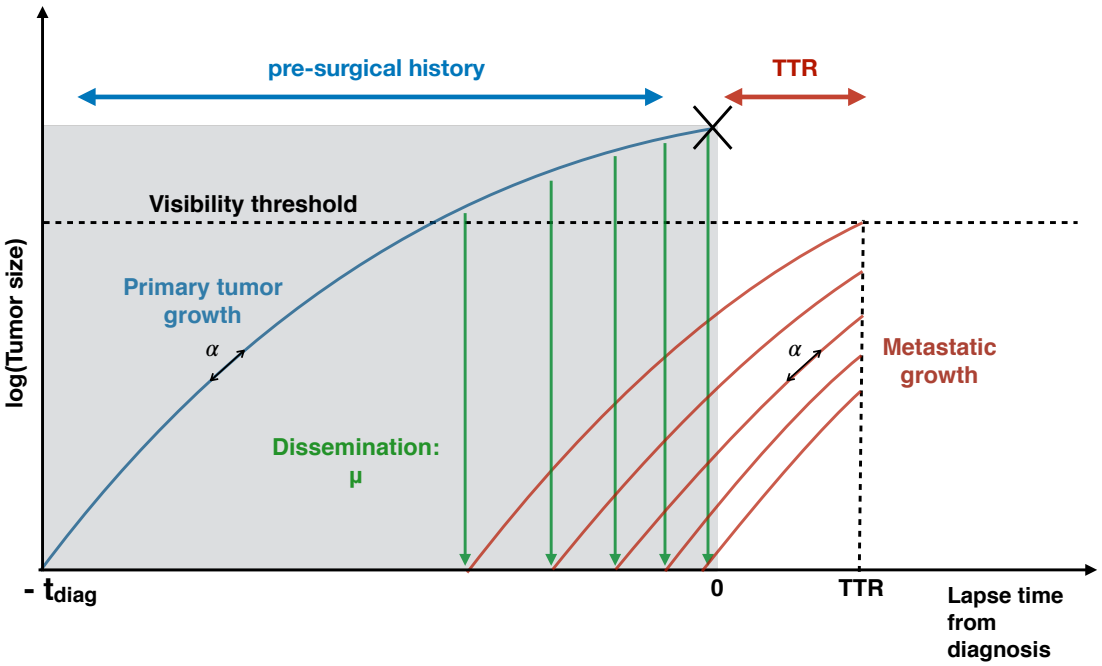

Figure 5.1 – Scheme of the mechanistic model for the time-to-relapse. Growth of primary and metastatic tumours are characterised by a common growth parameter α. Emission of metastases from the primary tumour occurs at a rate that depends on the primary tumour volume and on a parameter of metastatic potential μ. The time-to-relapse is defined as the lapse time from diagnosis at which the first emitted metastasis reaches the visible size.

5.2.5 Calibration of the mechanistic model using mixed-effects learning

The mathematical model for the individual time-to-relapse was thus defined as a function of V^i_{diag} and a vector of structural parameters $\psi^i = (\alpha^i, \mu^i)$. It was fitted to the time-to-relapse data using a mixed-effects modelling approach, as described below.

Let T^i denote the time-to-relapse variable for patient i. A constant error model was

assumed on the log-transformed data:

$$\log(T^i) = \log\left(TTR(V^i_{diag};\psi^i)\right) + e_i, \tag{5.5}$$

where e_i is the residual error following a normal distribution with mean 0 and variance σ^2. The individual parameters were assumed to be log-normally distributed and a linear covariate model was used:

$$\begin{aligned} \log\alpha^i &= \log(\alpha_{pop}) + \beta_\alpha \cdot x^i_\alpha + \eta^i_\alpha, \qquad \eta^i_\alpha \sim \mathcal{N}(0,\omega^2_\alpha) \\ \log\mu^i &= \log(\mu_{pop}) + \beta_\mu \cdot x^i_\mu + \eta^i_\mu, \qquad \eta^i_\mu \sim \mathcal{N}(0,\omega^2_\mu) \end{aligned} \tag{5.6}$$

where x^i_α and x^i_μ are vectors of subject-specific covariates, which might be identical, or partially or completely different.

The statistical model for the observations (5.5), implicitly defines for each individual i the probability density function of T^i conditionally on the individual parameters ψ^i. The corresponding survival and hazard functions can then be obtained as follows:

$$\begin{aligned} S(t \mid \psi^i; V^i_{diag}) &= \mathbb{P}(T^i > t \mid \psi^i) = \mathbb{P}(\log T^i > \log t \mid \psi^i) \\ &= \mathbb{P}\left(\frac{\log T^i - \log\left(TTR(V^i_{diag};\psi^i)\right)}{\sigma} > \frac{\log t - \log\left(TTR(V^i_{diag};\psi^i)\right)}{\sigma} \mid \psi^i\right) \\ &= 1 - \Phi\left(\frac{\log t - \log\left(TTR(V^i_{diag};\psi^i)\right)}{\sigma} \mid \psi^i\right), \end{aligned}$$

$$h(t \mid \psi^i; V^i_{diag}) = -\frac{d}{dt}\log S(t \mid \psi^i) = \frac{1}{\sigma t S(t \mid \psi^i)}\phi\left(\frac{\log t - \log\left(TTR(V^i_{diag};\psi^i)\right)}{\sigma} \mid \psi^i\right),$$

where Φ and ϕ are the cumulative distribution and probability density functions of the standard normal distribution, respectively.

Let C_i denote the censoring variable for individual i. With right-censoring, the observations are $(\widetilde{T}_i, \delta_i)$, where $\widetilde{T}_i = \min(T_i, C_i)$ and $\delta_i = \mathbb{1}_{T_i \le C_i}$ is the indicator variable.

The contribution of individual i to the likelihood is then given by [151]

$$\mathcal{L}^i(\theta) = \int h(\widetilde{T}^i \mid \psi^i;\theta)_i^\delta S(\widetilde{T}^i \mid \psi^i;\theta) p(\psi^i;\theta) d\psi^i,$$

where $\theta = (\alpha_{pop}, \mu_{pop}, \beta_\alpha, \beta_\mu, \omega_\alpha, \omega_\mu, \sigma)$ are the parameters to be estimated and $p(\psi^i;\theta)$ is the probability density function of the individual parameters, defined by (5.6).

The likelihood function was maximised using the Stochastic Approximation of the EM (SAEM) algorithm [32] implemented in the R saemix package [39]. Standard errors of the estimated parameters were obtained with the bootstrap method using 100 bootstrap sample, and significance of covariates was assessed using the Wald test.

Only covariates selected through the RSF analysis were tested in the mechanistic model. A backward elimination procedure was used to build the covariate model, by removing covariates with the highest p-value and refitting until all remaining covariates had p-value lower than 0.2.

To assess the overall fit of the base model, the mean of the conditional survival functions was compared to the Kaplan-Meier estimate of the survival curve. The former was estimated as

$$\frac{1}{N}\sum_{i=1}^{N} S(t \mid \psi^i; V_{diag}^i),$$

with $(\psi^1, \ldots, \psi^N)$ and $(V_{diag}^1, \ldots, V_{diag}^N)$ drawn respectively from the estimated distribution of the individual parameters and the values of V_{diag} in the data.

5.2.6 Evaluation of the model predictive performance

Discrimination and calibration of all models were internally validated using 10-folds cross-validation. Discrimination was quantified by the Harrell's concordance index [129]. Calibration of the models was examined graphically by comparing the model predicted probabilities against the Kaplan-Meier estimates of the DMFS, after binning individuals into quantiles groups according to their predicted probabilities [129].

5.3 Results

5.3.1 Random survival forests (RSF) multivariate analysis

We performed a RSF analysis [147] to identify covariates most predictive of DMFS. Cross-validated C-index for the nested RSF models with variables ordered on the basis of minimal depth (Figure 5.2 A) are shown in Figure 5.2 B. This metric improved as the size of the model increased, reaching a maximum with a number of variables between 5 and 8. Beyond the size, adding more variables did not improve discrimination. Therefore, we chose the RSF model with the 8 top covariates. In order of importance, these were Ki67, tumour size, age, HER2, CD44, EGFR, TRIO and PR. The cross-validation estimate of the C-index for this model was 0.69 (95% CI, 0.67-0.71). Calibration plots for 2-, 5- and 10-year outcome are shown in Figure 5.2 C. Overall there was a good agreement between the observed and model predicted probabilities of DMFS, but with underprediction of DMFS in higher risk groups.

Partial dependence plots for the selected covariates are displayed in Figure 5.3. These plots indicated strong nonlinear relationships between covariates and DMFS, with a non-monotonic behaviour for age and tumour size. Moreover, response/covariates relationships looked flatter at 2 years, suggesting that the examined covariates were more predictive of late than early relapse.

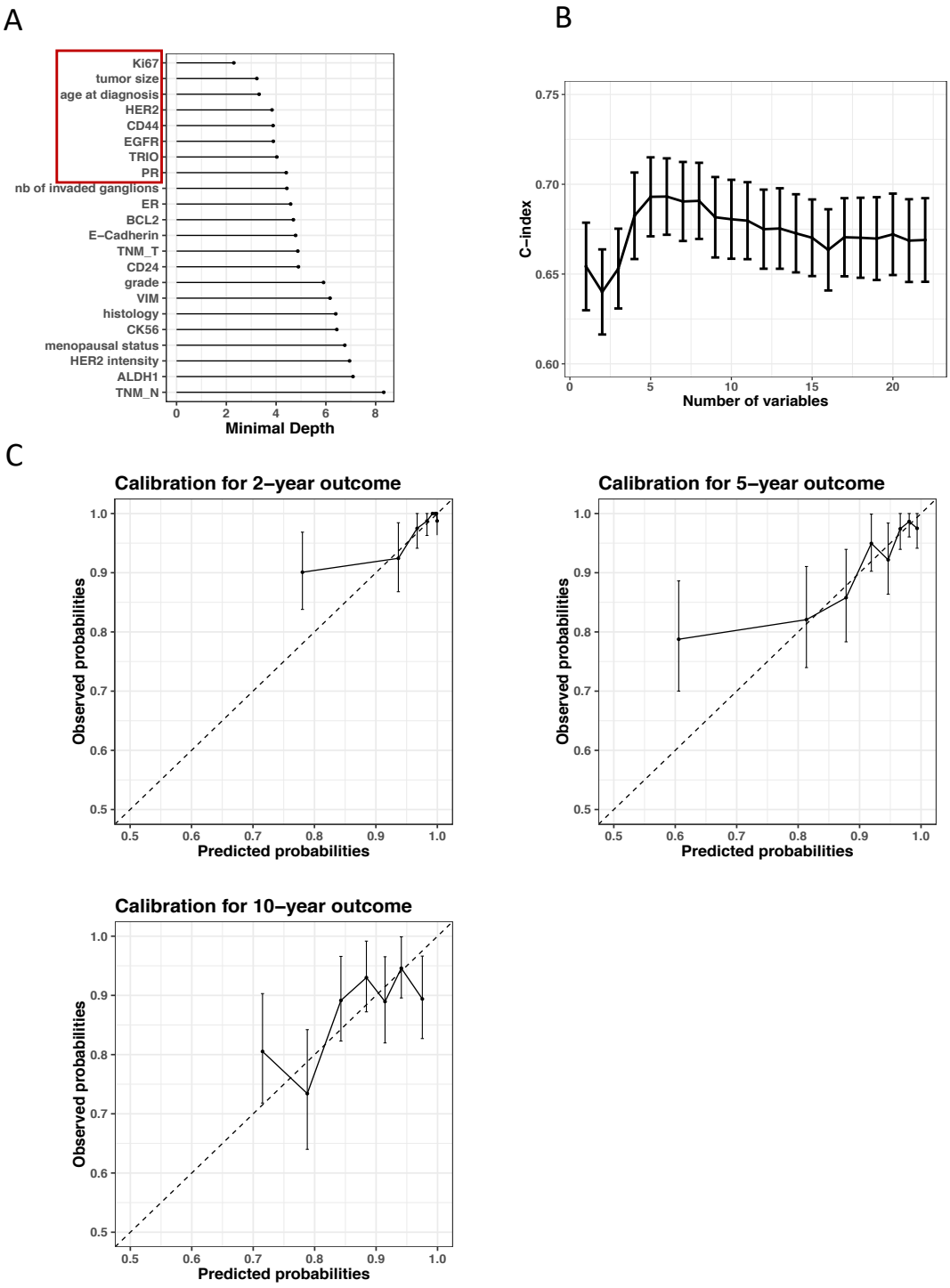

Figure 5.2 – Survival random forest and covariate selection. A) Minimal depth ranking of covariates. B) Apparent and cross-validated Harrell's C-index under sequentially fit RSF models with variables ordered by importance using minimal depth. Bars are 95% confidence intervals. C) Calibration plots for the RSF model with the 8 top variables (red box in figure A). Bars are 95% confidence intervals.

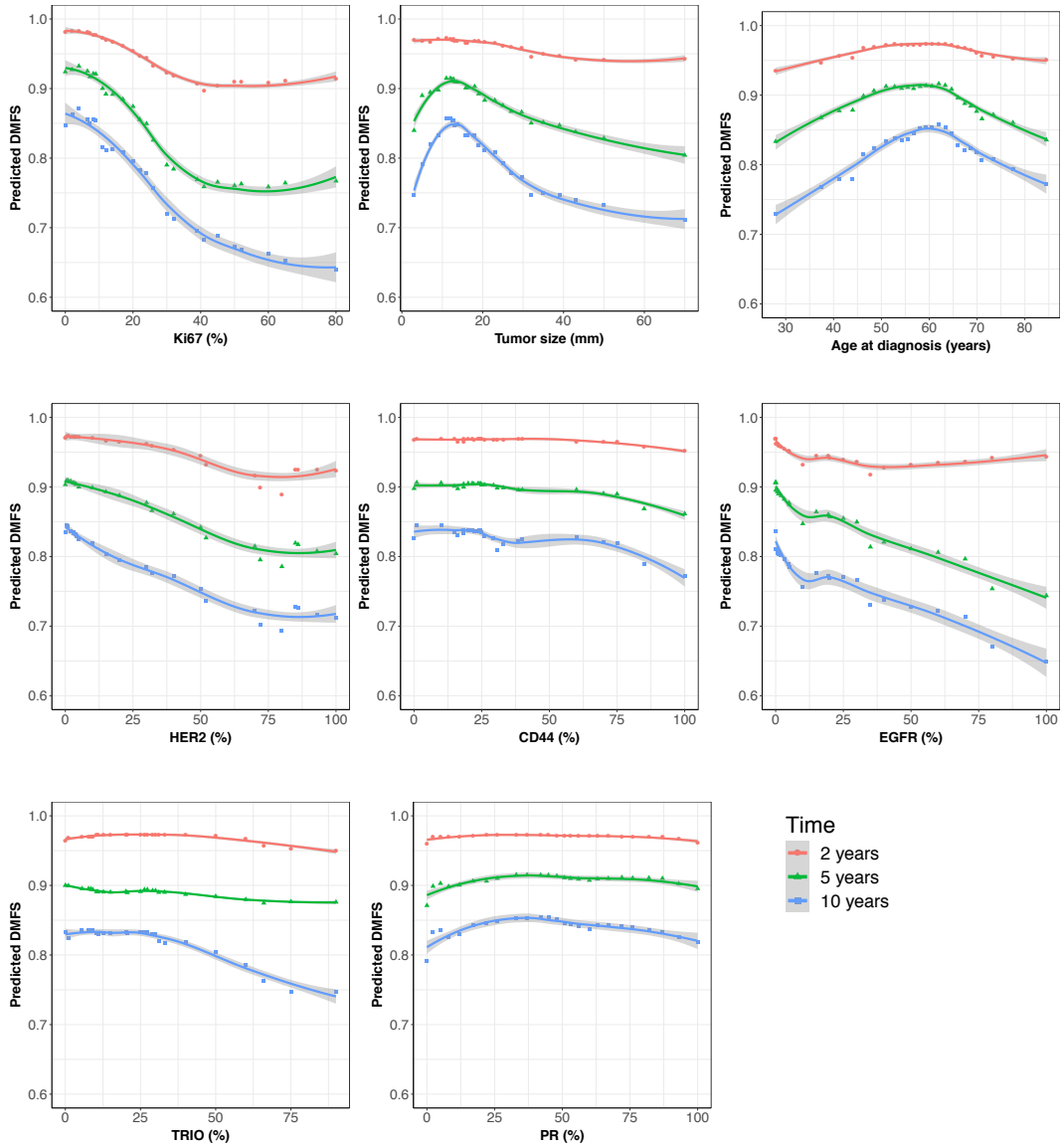

Figure 5.3 – Partial dependence plots of the random forest predicted DMFS as a function of the top eight predictors according to the minimal depth ranking. Symbols are partial dependence points estimates. Loess smooth line are added to indicate trends.

Table 5.1 – Parameter estimates of the mechanistic model for the time-to-relapse. Abbreviation: r.s.e., relative standard error.

Parameter	Estimate	r.s.e. (%)
$\log \alpha_{pop}$	-6.337	12.635
$\log \mu_{pop}$	-26.814	3.683
σ	0.542	28.409
ω_α	3.373	36.435
ω_μ	3.780	15.876

5.3.2 Calibration and validation of the mechanistic model

We first evaluated the ability of the mechanistic model to describe the time-to-relapse data without using any covariates, except for tumour size, which is a variable deeply encoded in the structural model. Estimates of the population parameters obtained with the SAEM algorithm are reported in Table 5.1. Both fixed and random effects were identified with satisfactory precision (relative standard error $< 36.4\%$). Moreover, the median value of μ was consistent with the value estimated in a previous work using data of metastatic relapse probabilities from a cohort of breast cancer patients [19]. Figure 5.4 compares the model estimation of the DMFS function to the empirical Kaplan-Meier estimate of the DMFS function with its 95% confidence interval. Despite a slight underestimation for smaller times, the model well captured the shape of the Kaplan-Meier estimate. To further verify the agreement between model and data, we also compared model curves and the Kaplan-Meier curves for different values of the tumour size at diagnosis. Although the model curves remained within the Kaplan-Meier confidence interval in all cases, we observed that model predictions tended to be less accurate as the tumour size increased, with overestimation of the risk of relapse for large PT sizes.

5.3.3 Mechanistic covariate analysis and predictive power of the mathematical model

We next tested the covariates selected by the RSF analysis in the mechanistic model. We built the covariate model using a backward elimination procedure, starting with the full model containing all covariates on both parameters α and μ. Notably, the analysis

Table 5.2 – Parameter estimates of the final model for the time-to-relapse with covariates.

Parameter	Estimate	r.s.e. (%)	p-value
$\log \alpha_{pop}$	-8.883	10.151	
$\beta_{\text{Ki67},\alpha}$	0.086	27.376	$2.59 \cdot 10^{-4}$
$\beta_{\text{HER2},\alpha}$	0.029	42.833	0.020
$\beta_{\text{CD44},\alpha}$	0.011	60.816	0.1
$\beta_{\text{TRIO},\alpha}$	0.016	58.119	0.085
$\log \mu_{pop}$	-26.342	3.696	
$\beta_{\text{EGFR},\mu}$	0.039	47.527	0.035
σ	0.606	23.104	
ω_α	2.062	22.715	
ω_μ	3.563	16.759	

confirmed the predictive value of Ki67 (a proliferation index) and revealed this biomarker as strongly correlated with the growth parameter α ($p < 0.001$, Table 5.2). The final model included Ki67, HER2, CD44 and TRIO on the growth parameter α, and EGFR on the dissemination parameter μ (Table 5.2). Moreover, the largest values of the coefficient associated to Ki67 and HER2 suggest that levels of these covariates have largest impact on growth than levels of CD44 and TRIO. The cross-validated C-index for this model was 0.67 (95% CI, 0.63-0.70). Calibration plots for 2-, 5- and 10-year outcome are shown in Figure 5.5 and demonstrate good predictive accuracy of the model. Nevertheless, as for the RSF model, DMFS was underestimated in high risk groups.

5.3.4 Predictive simulations of the mechanistic model

Once the mechanistic model has been calibrated and predictive covariates identified, the model can be used to perform simulations for new patients by using their individual covariates values. We used the calibrated model to simulate the natural cancer history for a number of representative patients of our dataset. Simulations were performed using a discrete version of the metastatic model (see [19] for details). Results of the simulations are reported in Figures 5.6 and S2, along with the size of the primary tumour at diagnosis and the covariate values predicting the growth and metastatic potential parameters α and μ (the remaining unexplained variability was neglected for these predictions). Im-

portantly, all simulations shown here represent pure predictions, since for each patient, they were generated using the model calibrated on the corresponding cross-validation, independent, training set.

These examples illustrate the possible utility of the mechanistic approach. For instance, for patients 47 and 255 (Figure 5.6), the model predicts a time from one cell to detection of 601 (1.65 years) and 4214 (11.5 years) days, respectively. At diagnosis, patient 47 is predicted to have a total of 9 invisible metastases. The largest metastasis is formed by $2.07 \cdot 10^3$ cells, while the smallest by 2.08 cells. According to this simulation, the first metastasis in this patient is emitted 490 days (1.34 years) after the first cell of the PT. The model predicts relapse 447 days (1.23 years) after diagnosis, with a prediction error of 292 days. Patient 255 is predicted to have 19 invisible metastases at the time of diagnosis. The largest metastasis contains $1.73 \cdot 10^4$ cells, while the smallest by 1.41 cells. The largest metastasis in this patient is emitted 3170 days (8.68 years) after the first cell of the PT. The model predicts relapse 1609 days (4.41 years) after diagnosis, making a prediction error of 202 days. The differences in PT and metastatic dynamics for these two patients are due to the different covariates values (Table in Figure 5.6). Levels of Ki67 and HER2 are higher in patient 47, causing faster tumour growth. Moreover, unlike patient 255, the tumour of patient 47 expresses EGFR, which according to our model, is associated with a higher metastatic potential.

Model predictions are also informative in the case of individuals that were censored at the last follow-up visit. For instance, patient 486 (see Figure S2) was censored at 12.6 years after diagnosis. According to the model prediction, this patient is free of disease and does not relapse (TTR = $+\infty$).

5.4 Discussion

We propose a mechanistic model for prediction of metastatic recurrence after surgical intervention in patients with early-stage breast cancer **which, for the first time, is able to simulate pre- and post-diagnosis history of the disease only**

Table 5.3 – Cox regression using the first 8 covariates selected by minimal depth with the random survival forest model.

	HR	95% CI	p-value
Ki67	1.02	[1.01, 1.03]	$1.71 \cdot 10^{-4}$
Tumor size	1.01	[0.99, 1.03]	0.46
Age	0.99	[0.98, 1.01]	0.49
HER2	1.01	[1.00, 1.01]	0.05
CD44	1.00	[1.00, 1.01]	0.47
EGFR	1.01	[1.00, 1.02]	0.06
TRIO	1.01	[1.00, 1.01]	0.12
PR	1.00	[0.99, 1.00]	0.80

from data available at diagnosis. Grounded on the biology of the metastatic process (simplified here in two determinants: growth and dissemination), **our model provides biological insights that machine learning algorithms and classical methods for the analysis of time-to-event data do not. For instance, it allows to test whether covariates are associated with growth and/or dissemination**. For these data, Ki67 and HER2 were found significant for predicting the proliferation rate parameter α, whereas EGFR was found associated with the metastatic potential parameter μ. Another advantage of the mechanistic model is that, once validated, it can be used to perform patient-specific simulations able to assess the extent of invisible metastases at the time of diagnosis and to predict future growth of metastases. In turn, this might aid selecting patients that will most benefit from extended adjuvant therapy. Notably, **with a concordance index of 0.67 (95% CI, 0.63 - 0.70), the mechanistic model was found to perform similarly to the RSF algorithm (95% CI, 0.67-0.71) and a Cox regression model (95% CI, 0.67-0.72, see Table 5.3)**. Comparable results were also obtained in terms of performance metrics of 5-year outcome between the mechanistic model, RSF, Cox regression and classification machine learning algorithms (Table 5.4). The latter were tested by Cynthia Périer and included logistic regression (LR), support vector machines, random forests (RF), k-nearest neighbours and gradient boosting. Here only metrics for the best performing machine learning classification algorithms are reported. We refer to [95] for more details.

Table 5.4 – Performance metrics for prediction of 5-year DMFS. Abbreviations: AUROC, area under the receiving operating curve; PPV, positive predicted value; NPV, negative predicted value

	AUROC	Accuracy	PPV	NPV	F1 score
RF	0.70	0.64	0.66	0.62	0.61
LR	0.71	0.66	0.71	0.63	0.61
RSF	0.75	0.71	0.71	0.71	0.71
Mechanistic model	0.73	0.73	0.72	0.70	0.70
Cox	0.75	0.79	0.77	0.71	0.72

One limitation of the mechanistic model is that it relies on a linear covariate model, which may not be appropriate when complex relationships exist between covariates and outcome. Indeed, the partial plots produced by the RSF predictions indicated nonlinear effects of covariates, especially for age at diagnosis, and this might explain why some covariates identified as predictive in the RSF analysis were then lost when assessed for significance on the parameters of the mechanistic model.

The proposed mechanistic model for the time to relapse represents a first attempt of a mechanistic, individual-level, predictive metastatic model and might be improved in a number of ways. For instance, unexplained variability remained despite the inclusion of covariates, suggesting that biomarkers other than those tested might improve model predictions. In this regard, models including gene signature have been shown to have higher predictive power compared to models based on standard histological and clinical variables [152]. The mechanistic model could also be refined by including the phenomenon of dormancy on metastases, which has been proposed to explain relapse occurring after many years from surgery [153, 154]. Finally, to be applied in the clinic, the model predictive performance should be further evaluated on external data sets.

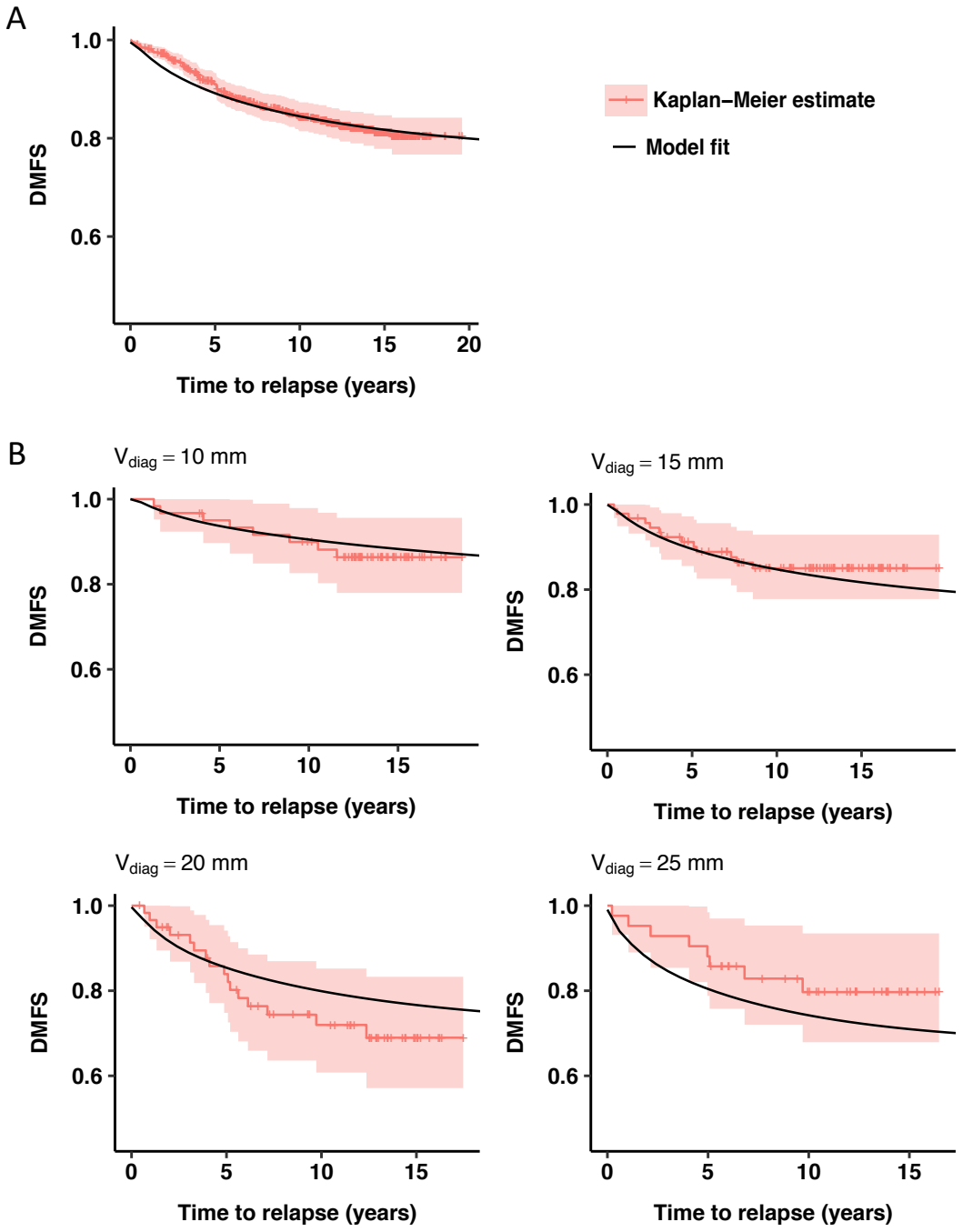

Figure 5.4 – A) Mean of the conditional DMFS functions from the mechanistic model and Kaplan-Meier DMFS estimate with 95% confidence interval. B) DMFS predictions of the mechanistic model and Kaplan-Meier estimates with 95% confidence intervals stratified by values of the primary tumour size at diagnosis.

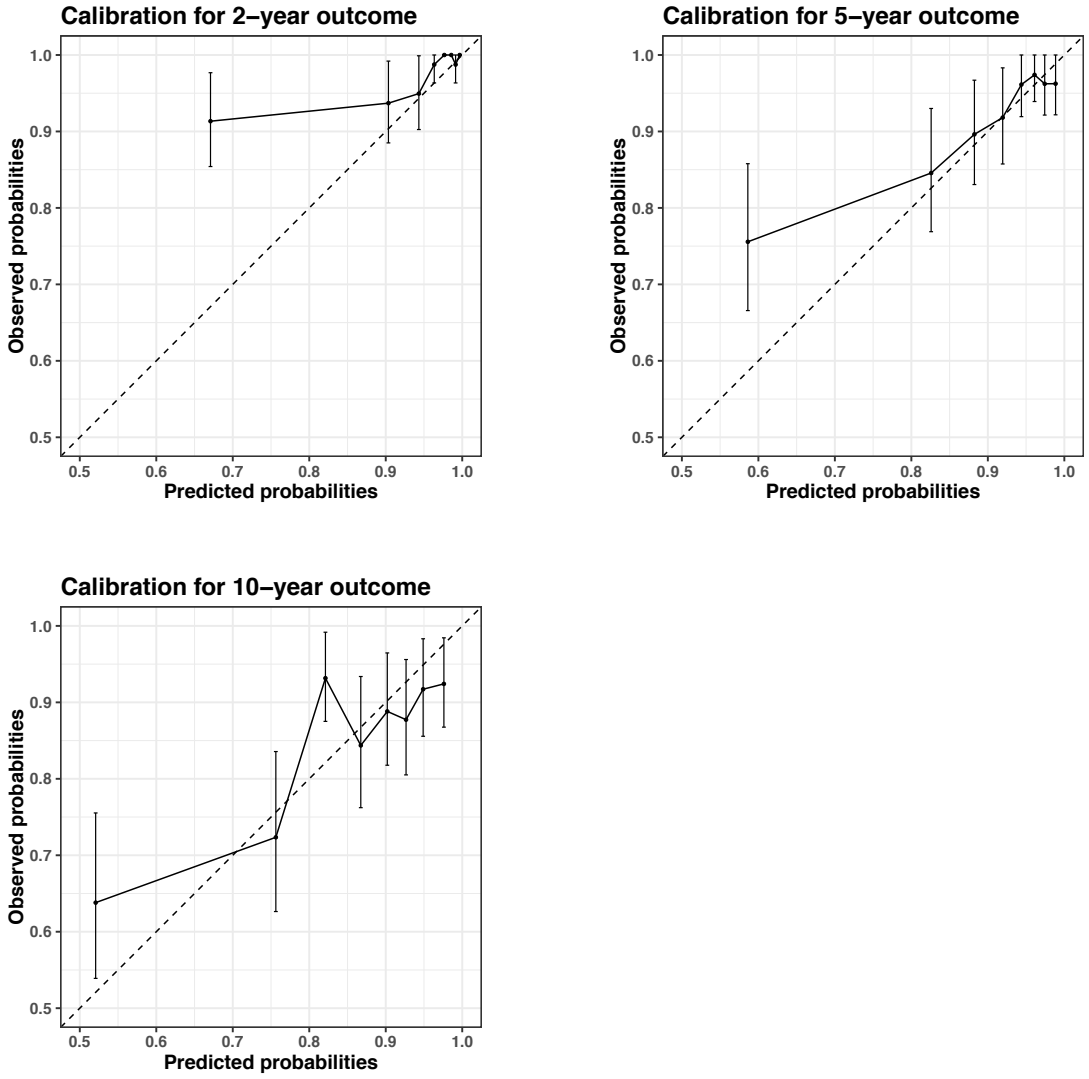

Figure 5.5 – Calibration plots of DMFS for the final mechanistic model with covariates.

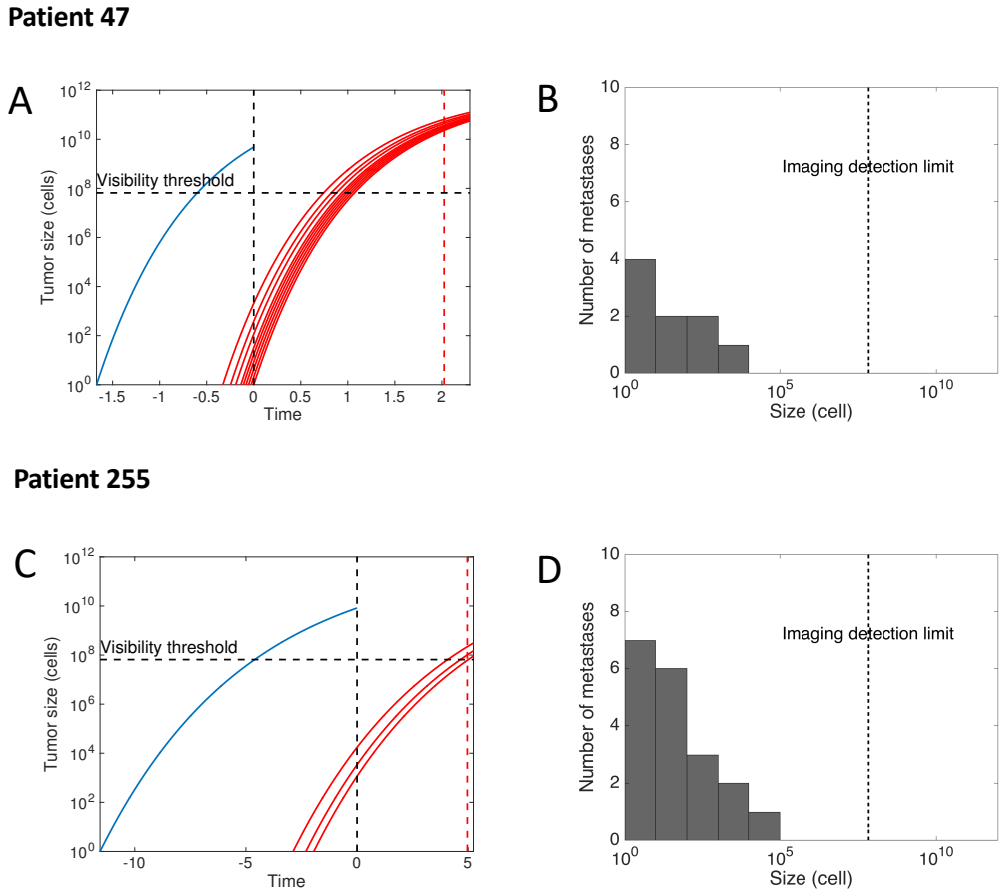

Patient ID	Tumor size (mm)	Ki67 (%)	HER2 (%)	CD44 (%)	TRIO (%)	EGFR (%)
47	20	32	100	0	0	50
255	25	1	60	90	60	0

Figure 5.6 – Simulations of the cancer history for two patients with tumour size and covariates values given in the Table. Simulations were performed using the estimated values of α and μ from the fit of the mechanistic model to the time to relapse data. Left: Growth of the primary tumour and of visible metastases. The red dashed line indicates the recorded TTR. Right: size distribution of the metastases at the time of diagnosis.

Chapter 6

Conclusions

6.1 Summary of the thesis achievements

This thesis has extended an established mechanistic model of the metastatic process [19] to describe primary tumour and metastatic dynamics in response to neoadjuvant sunitinib therapy in clinically relevant orthosurgical mouse models of spontaneous metastatic breast and kidney cancers. Model development was guided by a large dataset comprising longitudinal measurements of primary tumour size and metastatic burden in a total of 230 mice (132 mice for the breast model and 98 mice for the kidney model), as well as survival data and pre-surgical biomarkers (circulating tumour cells and myeloid-derived suppressor cells counts, proliferation and endothelial immunohistochemical markers). Simulations of the model with parameter values estimated from a previous study on control groups [19] have been used to test possible hypothesis for the differential effects of sunitinib on primary tumour and metastases. Population distributions obtained under the assumption of effect of therapy on metastatic growth failed to described the data. On the contrary, simulations obtained under the hypothesis of no effect of therapy on metastatic growth could reproduce well the behaviour of the experimental data. This has been observed in all treated groups of the breast animal model and suggested limited effect of treatment on the growth of metastases. To account for differences between treatment schedules, a kinetics-pharmacodynamics (K-PD) model has been developed on

the breast dataset, based on these simulation results. Primary tumour and metastatic burden data have been fitted simultaneously for vehicle and sunitinib-treated animals using the Stochastic Approximation of Expectation-Maximization (SAEM) algorithm [32] implemented in the nlmefitsa Matlab function. The calibrated K-PD model was able to describe both the structural dynamics and inter-subject variability of the experimental data in both vehicle and treated animals. Confirming previous results [19], interanimal variability was mainly characterised by the model parameter expressing the metastatic potential of the tumour, μ, which was also found to be significant in survival analysis. Effects of covariates on this model parameter have been assessed using linear regression and a number of machine learning regression techniques (artificial neural networks, support vector machines, random forest models) [33]. However, the biomarkers included in all tested machine learning algorithms demonstrated only limited predictive power on the mathematical parameter ($R^2 = 0.13 - 0.2$, best relative error on $\log \mu$ $9.83 \pm 10.70\%$).

A K-PD model of sunitinib neoadjuvant treatment has also been built for the kidney animal model. In this case, it was found that a model with different pre- and post-treatment primary tumour growth rates provided a better fit of the data, suggesting a post-treatment rebound effect. The calibrated model has then be used to investigate the effect of treatment discontinuation on primary tumour and metastatic burden dynamics. This analysis has shown that rebound in primary tumour growth caused by treatment cessation may result in increased metastatic burden compared to control animals, suggesting that prolonged therapy may be needed to achieve therapeutic benefit on metastasis.

The second study presented in this thesis has dealt with the prediction of metastatic relapse in breast cancer patients. A mathematical model for the time-to-relapse has been developed based on the size-structure population dynamics framework proposed by Iwata *et al.* [14] and the corresponding survival function has been derived in order to account for censored data. The model has been validated using a dataset containing distant metastatic free survival and clinical/pathological characteristics of 642 women that were diagnosed with early operable breast cancer. Patients included in this dataset did not

receive any kind of therapy in addition to surgery and localised radiation of the primary tumour, thus allowing to assess the natural history of the course of metastasis. Model parameters were estimated using a mixed-effects approach, using the implementation of the SAEM algorithm of the R saemix package [39]. Selection of the most predictive covariates to test in the mechanistic model was performed using the random survival forests (RSF) algorithm [40]. Achieving a concordance index of 0.67 (0.63-0.70), the mechanistic model had similar predictive performance to the RSF (c-index 0.67-0.71), Cox regression model (c-index 0.67 - 0.72) and machine learning classification algorithms for prediction of 5-year metastatic free survival. The proposed model represents a first attempt of mechanistic model in the context of time-to-event models for prediction of metastatic relapse. It allows to individually estimate the extent of the clinically occult metastatic burden and the time to relapse from clinical and histological data available at diagnosis, and thus could be used as a personalised prediction tool to better evaluate the risk of relapse and personalise adjuvant therapy.

6.2 Future work

Treatment of cancer in the neoadjuvant setting has several potential benefits, including reducing tumour size to convert an inoperable tumour into one that can be resected or improve surgical outcomes by sparing critical tissue in patients with resectable primary tumours. Furthermore, the neoadjuvant setting allows to assess whether patients will respond to treatment in case of relapse with distant metastases after surgery. However, the clinical utility of tyrosine kinase inhibitors (TKIs) for the treatment of early-stage cancers is still controversial [27], thus highlighting the need for further preclinical in vivo/in silico studies. This study has shown that antiangiogenic therapy may have limited effect on the growth of metastases, despite inhibiting primary tumour growth. These findings could be explained by the fact that micrometastatic tumours would rely on mechanisms of vascularisation that might not involve the VEGF pathway, thus suggesting that antiangiogenic therapy may have limited utility also in the adjuvant setting. Consequently,

surgery should not be delayed and if used in the pre-operative setting, antiangiogenic agents should be combined with other drugs capable of effectively inhibiting the growth of metastases. In this context, the proposed model may serve as a basis and extended to guide the rational design of treatment schedules and modes of combination before preclinical or clinical testing.

This analysis has also shown the limited value of pre-surgical biomarkers (Ki67 and CD31 expression levels in the primary tumour, CTC and MDSC counts) as predictors of metastatic potential and survival. Although likely to depend on the animal model of cancer, these results highlight the need to investigate other molecular and cellular markers.

The mechanistic model for predicting the time to metastatic relapse in breast cancer patients has shown similar predictive performance to well established statistical and machine learning techniques for the analysis of time-to-event data. The next step to achieve concrete clinical transfer, should be the evaluation of the model predictive performance on external datasets. In addition, the model could be adapted and fitted to data of treated patients in order to build a model that could also help in evaluating the benefit of different treatment options. This approach could also be applied for other types of cancers, such as prostate and kidney cancers, for which the low rate of relapse raises the issue of selecting those patients requiring additional therapy.

The main limitation of the mechanistic model is that it uses a linear covariate model, which may not be appropriate when complex relationships exist between covariates and outcome. This might explain why some covariates identified as predictive in the RSF analysis were then lost when assessed for significance on the parameters of the mechanistic model. One possibility to deal with this issue would be to combine the RSF algorithm with the mechanistic model, by using the latter to estimate the survival function in the terminal nodes.

Appendix A

Supplementary figures to Chapter 3

Figure S1. Comparison of simulation of therapy (A) vs no therapy (B) on metastases

Surgery at day 34

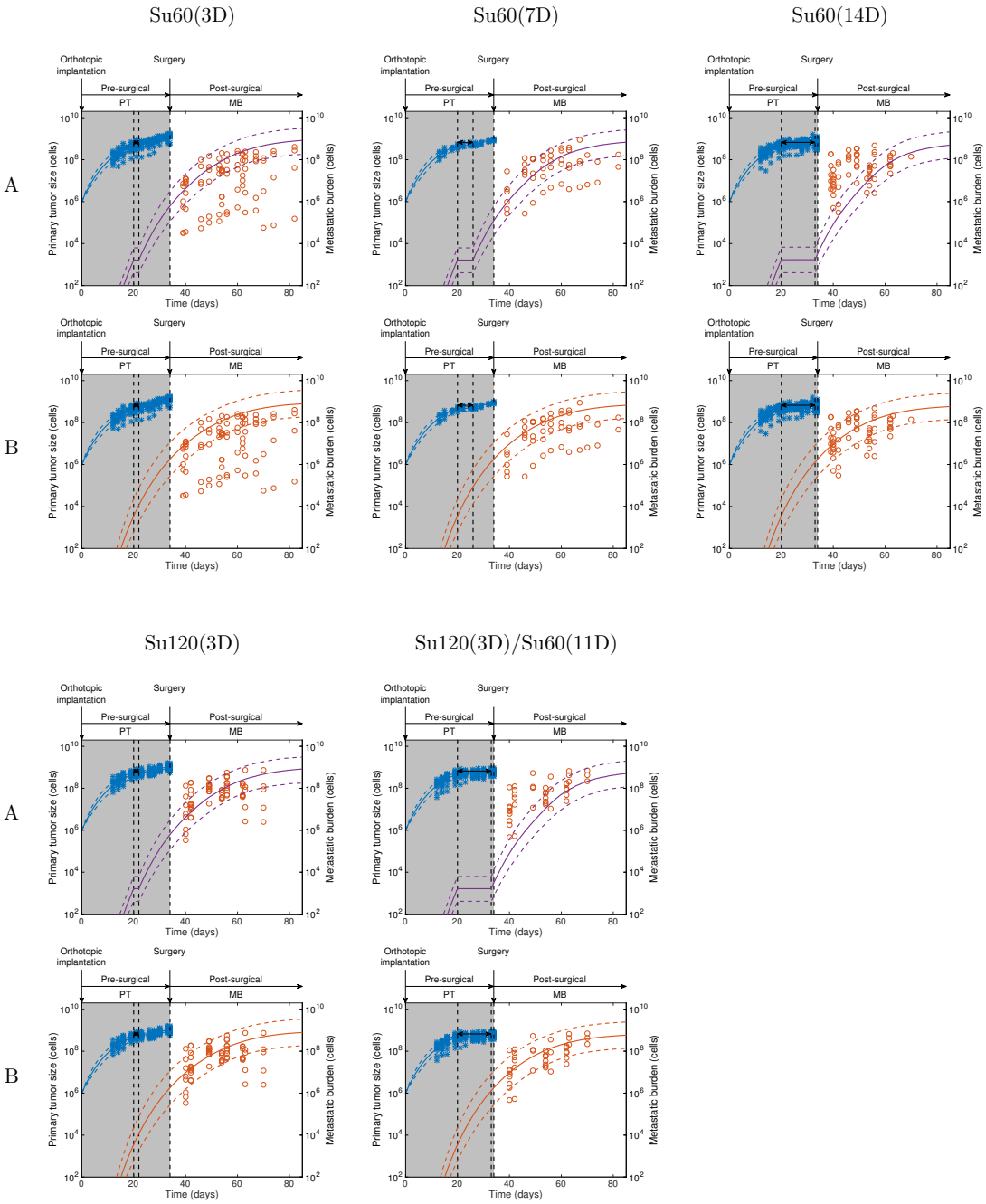

Surgery at day 38

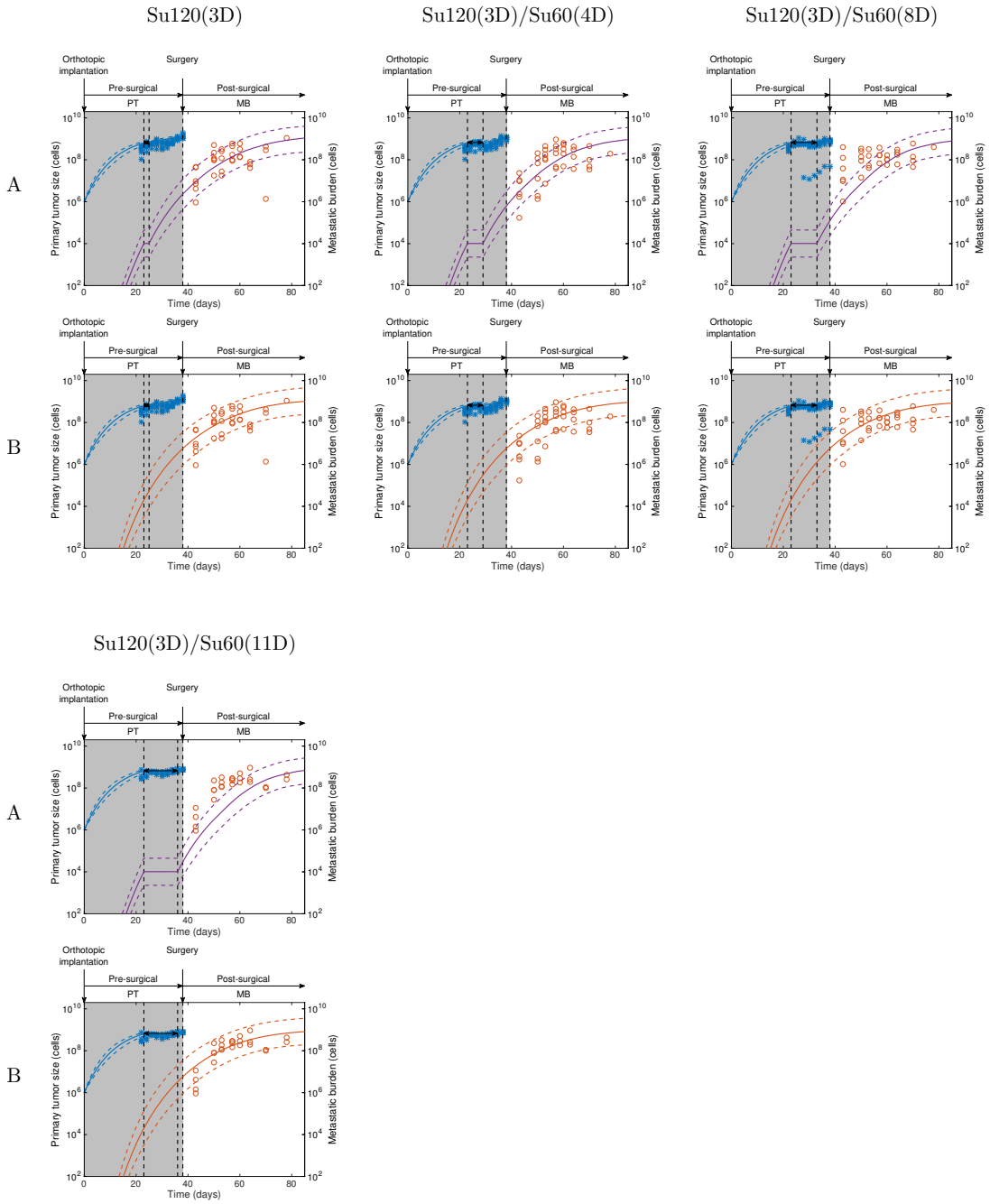

Figure S2. Population fits of all the groups used to calibrate the model parameters (surgery at day 34)

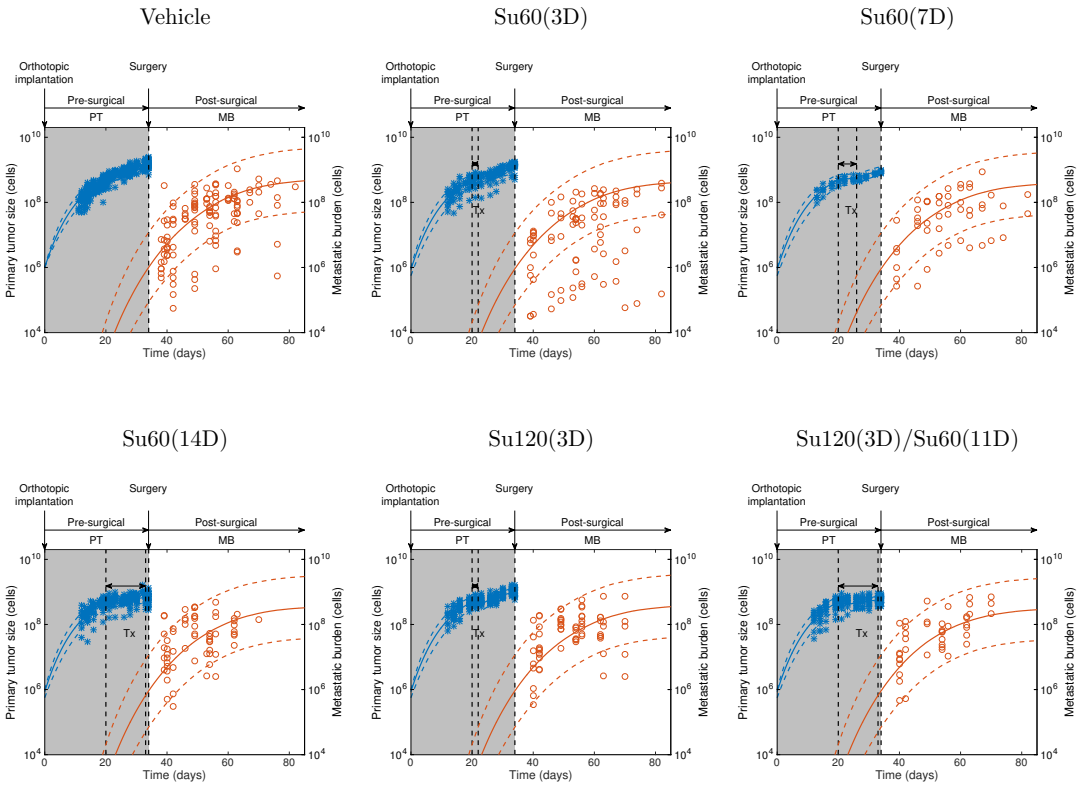

Figure S3. Representative individual fits of the model for Sunitinib-treated animals

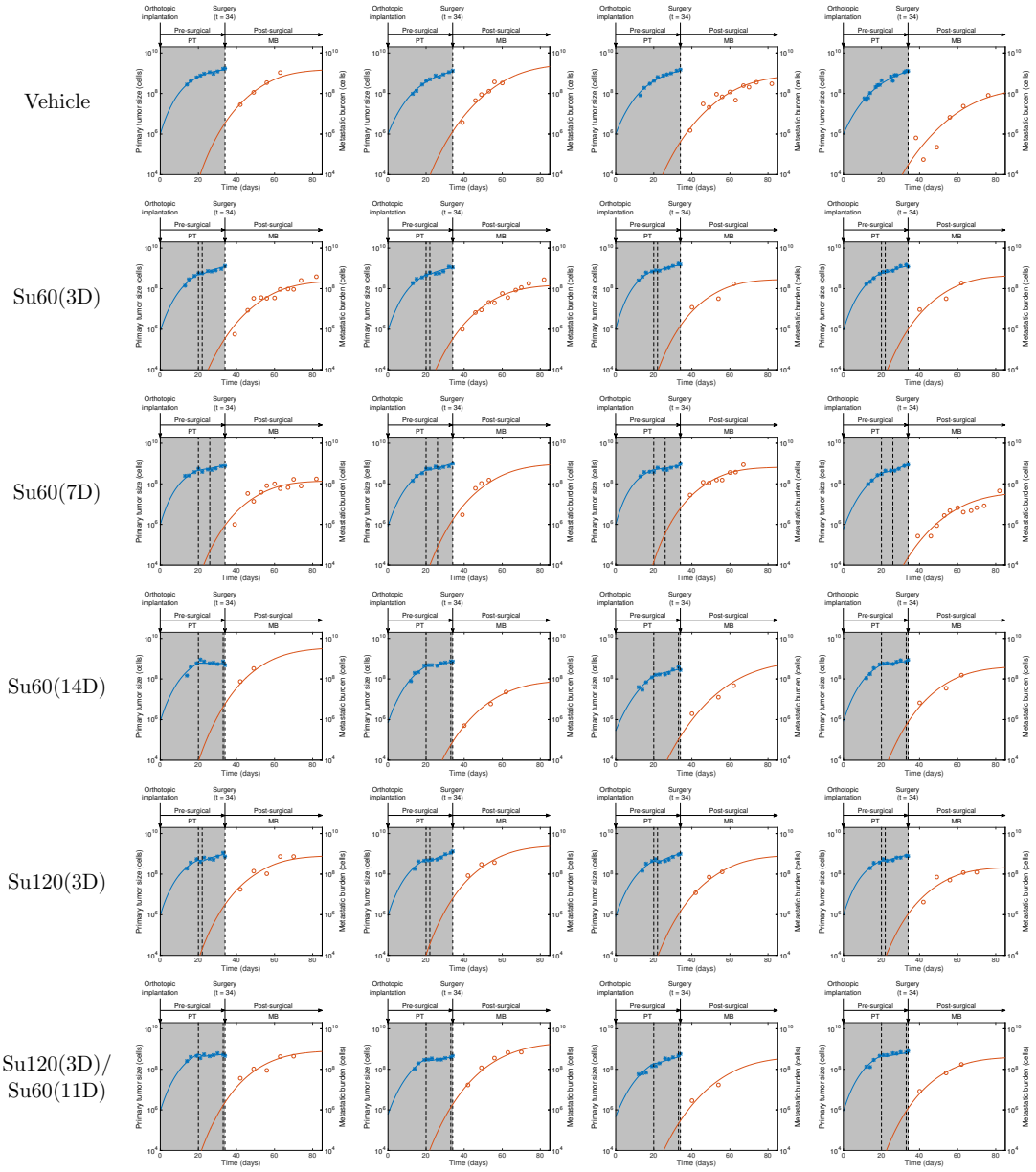

Figure S4. Individual parameters VS covariates

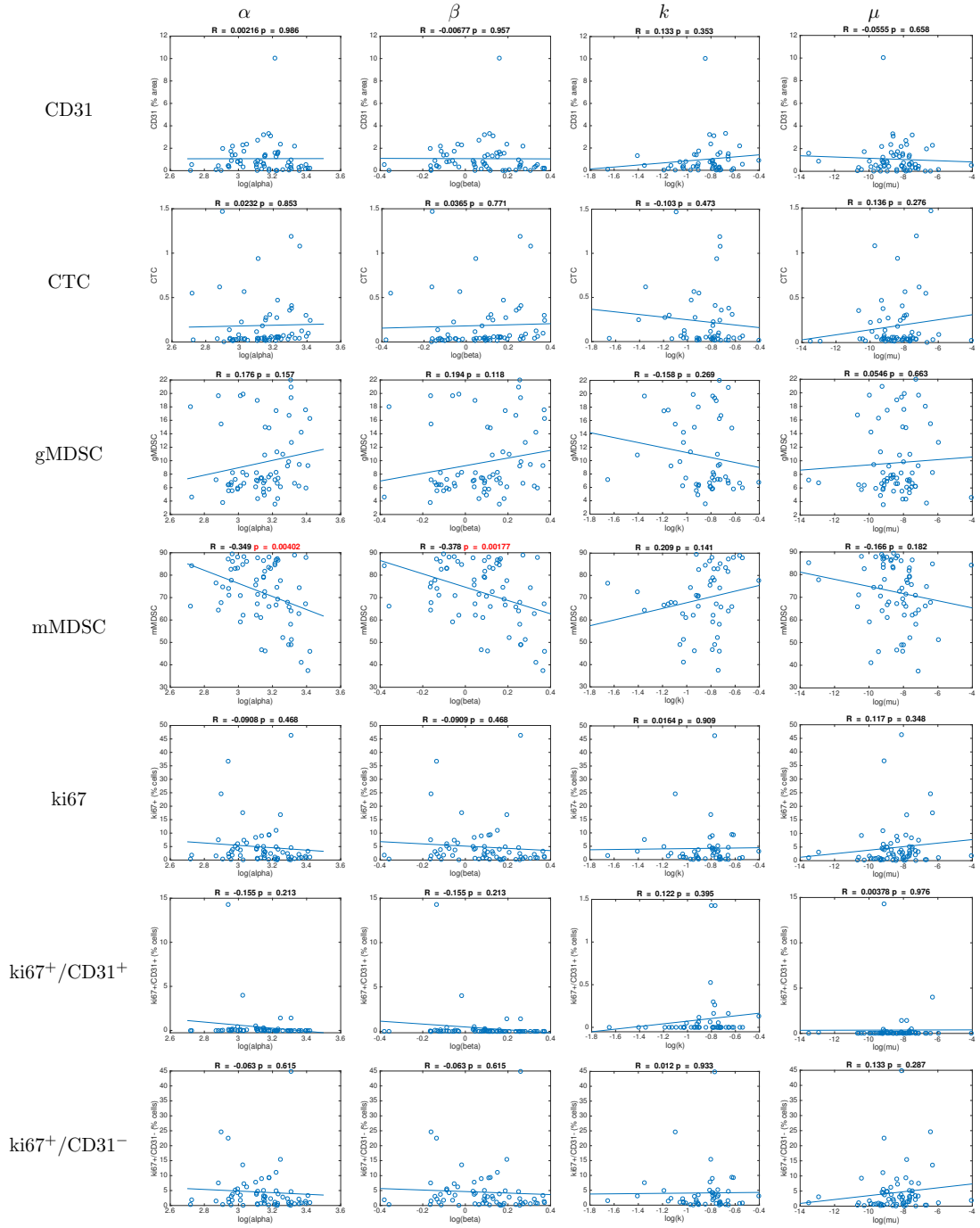

Figure S5. Observed vs Predicted values for the machine learning algorithms

Models for predicting μ.

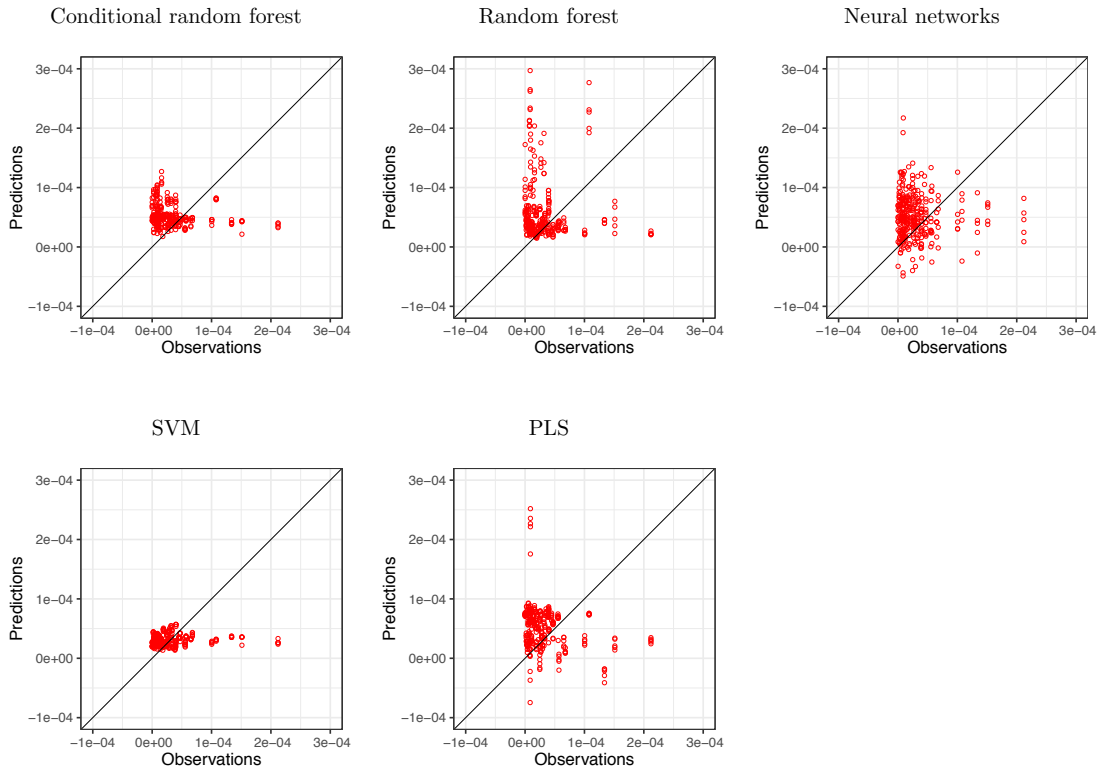

Models for predicting $\log \mu$.

Conditional random forest

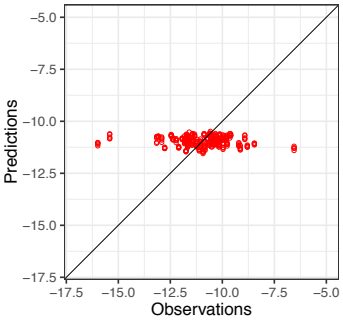

Random forest

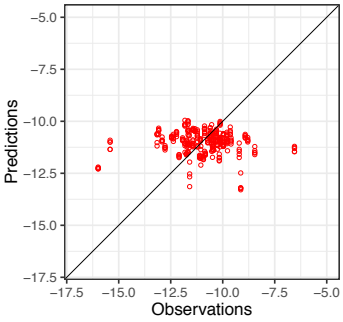

Neural networks

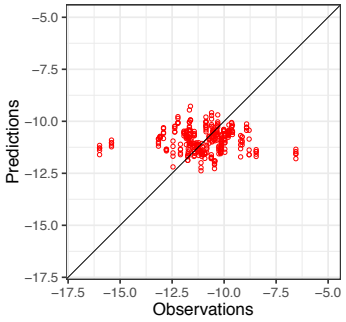

SVM

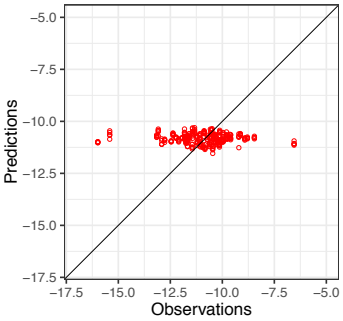

PLS

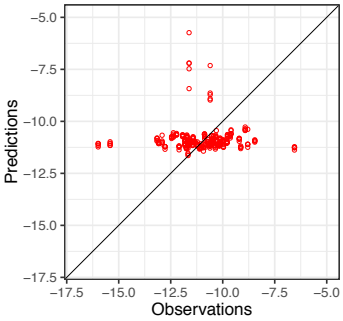

Appendix B

Supplementary figures to Chapter 4

Figure S1. Population fits of all the groups used to calibrate the model parameters

Surgery at day 30

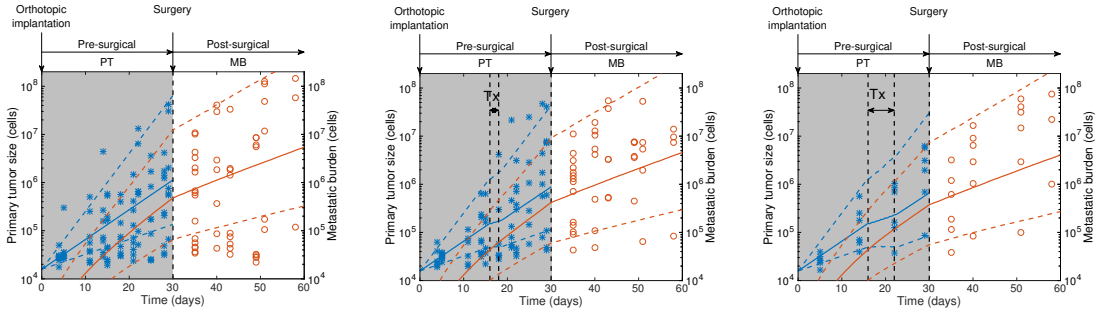

Vehicle | Su60(3D) | Su60(7D)

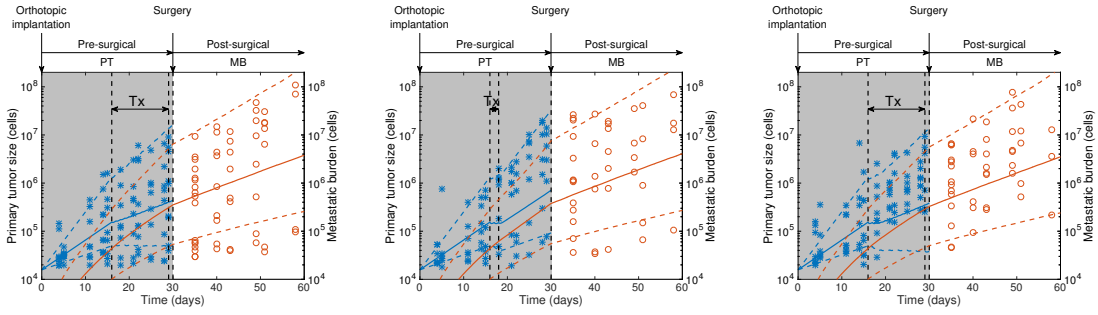

Su60(14D) | Su120(3D) | Su120(3D)/Su60(11D)

Surgery at day 26

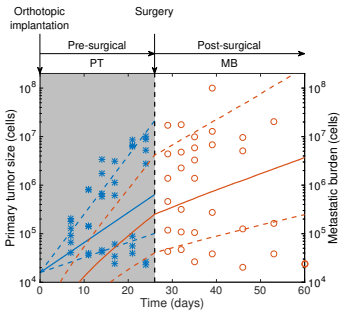

Vehicle

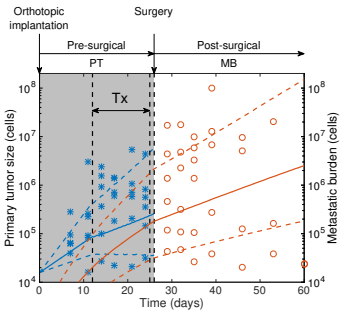

Su60(14D)

Surgery at day 23

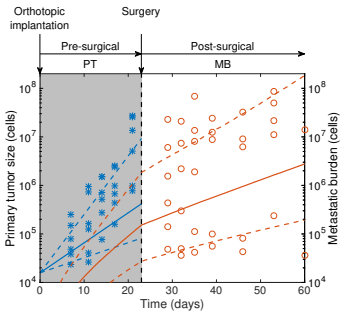

Vehicle

Figure S2. Representative individual fits of the model for Sunitinib-treated animals. (Surgery at day 30)

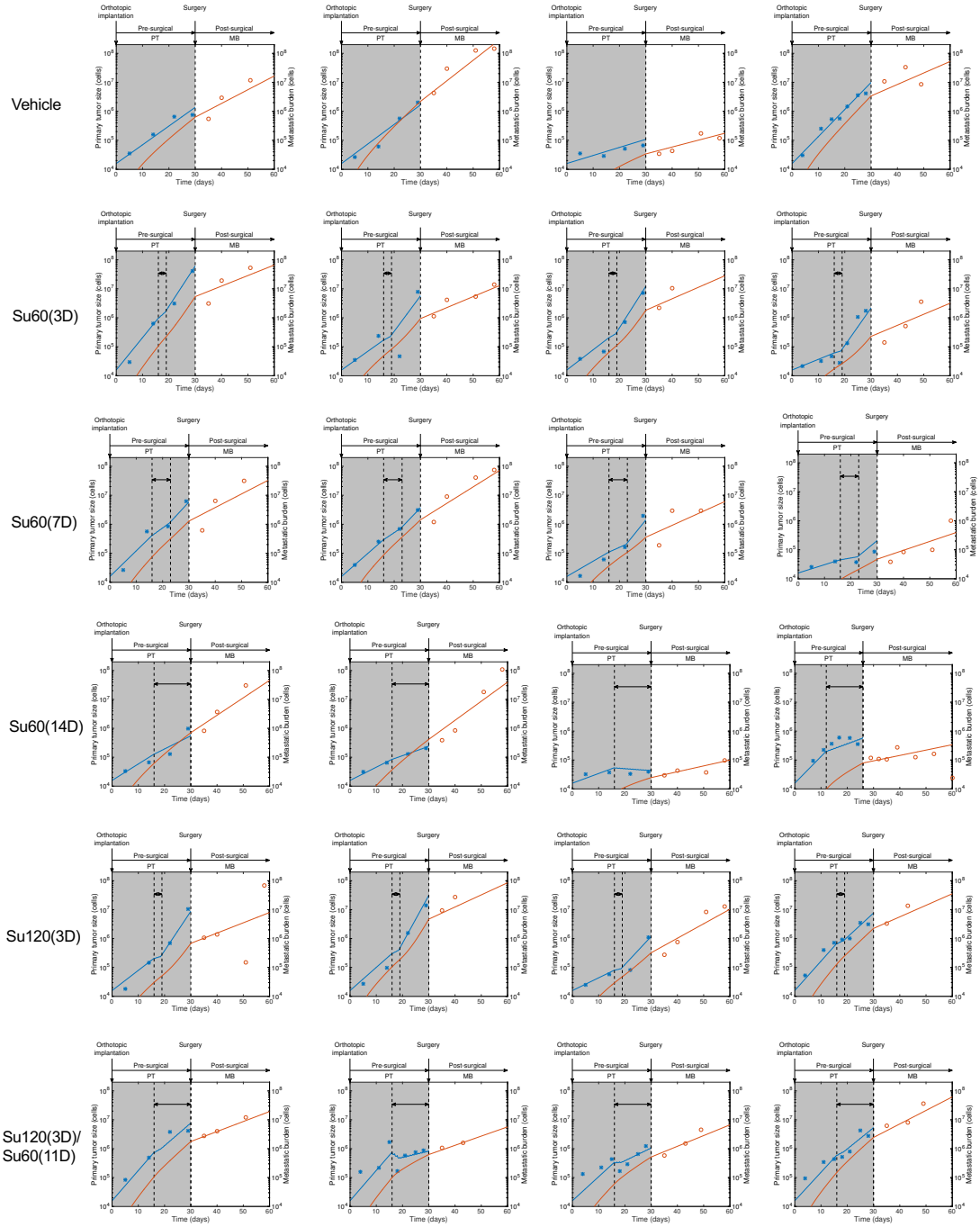

Appendix C

Supplementary figures to Chapter 5

Figure S1. Percentage of missing values in each variable

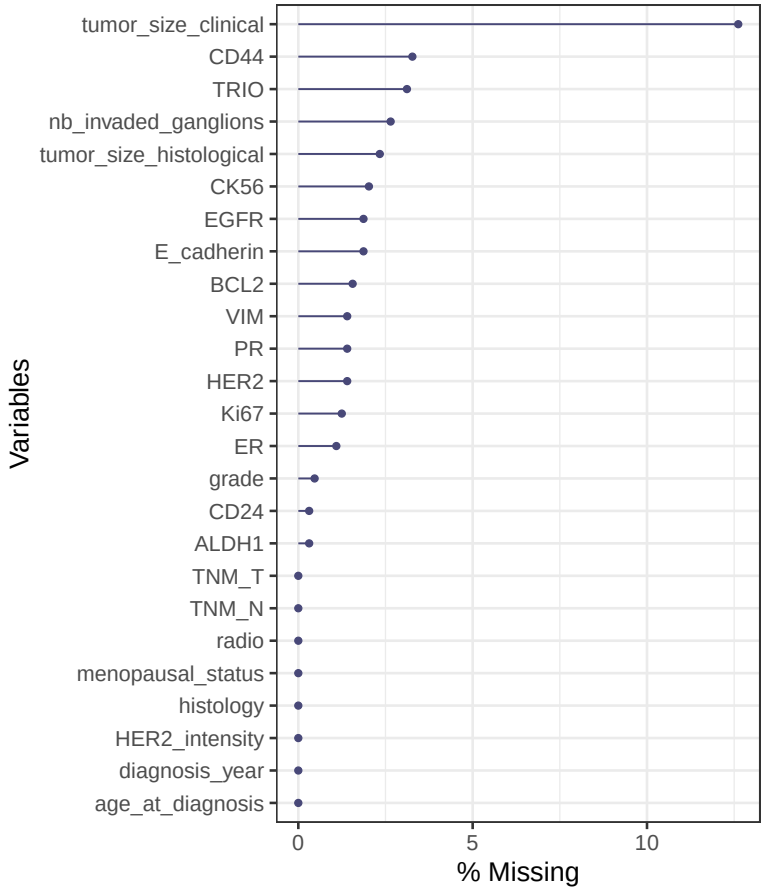

Figure S2. Predictions of the mechanistic model for individual patients

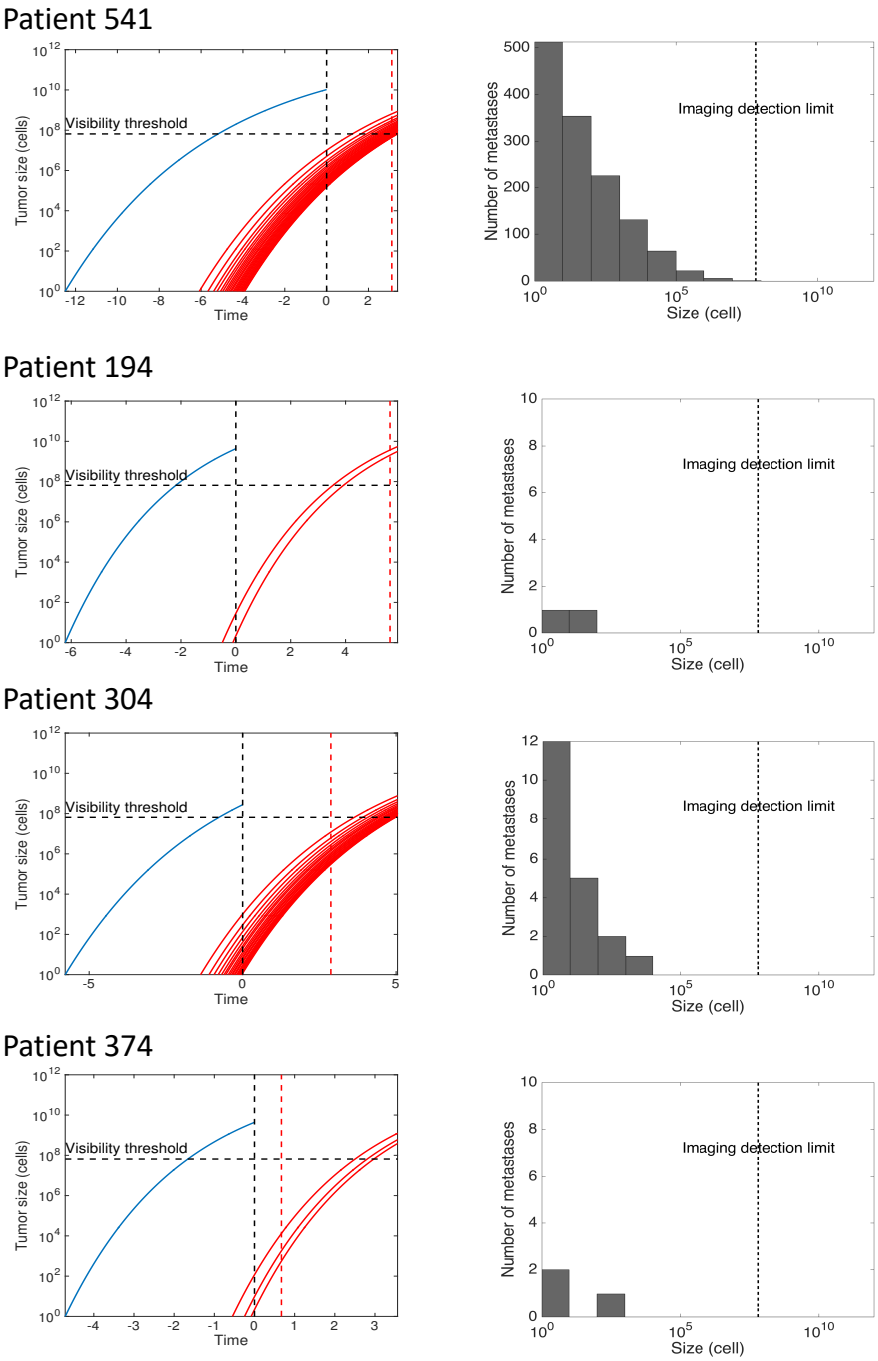

Patient 29

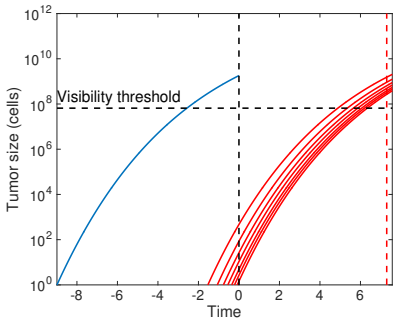

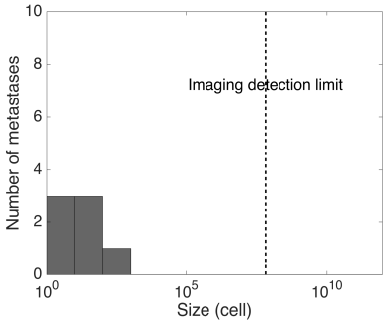

Patient 281

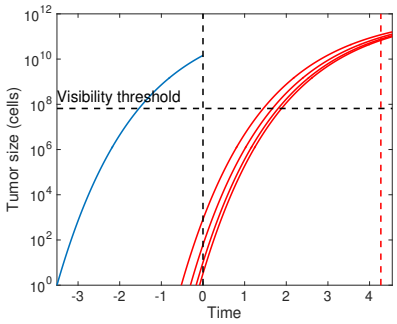

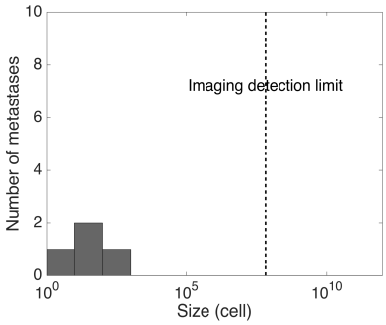

Patient 486

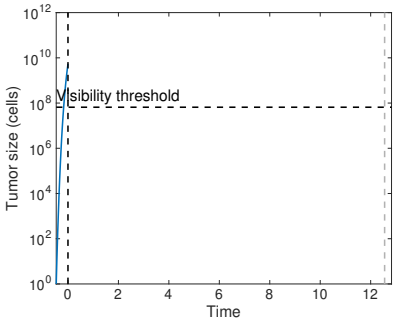

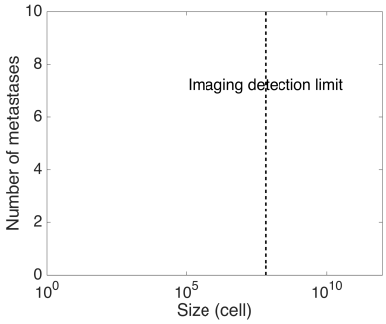

ID	V_{diag} (mm)	Ki67 (%)	HER2 (%)	CD44 (%)	TRIO (%)	EGFR (%)	Obs. TTR (cens)	Pred. TTR	Prediction error (days)
541	27	30	0	90	30	100	1137 (1)	523	614
194	20	15	100	40	12	0	2051(1)	1400	652
304	8	25	80	0	0	100	1049 (1)	1477	428
374	20	60	0	5	0	21	245 (1)	935	690
29	15	15	90	39	0	10	2663 (1)	1916	747
281	30	22	100	0	23	0	1559 (1)	538	1021
486	20	39	90	25	40	0	4582 (0)	$+\infty$	-

Figure S3. Calibration plots for the Cox model with the eight covariates selected through the RSF analysis.

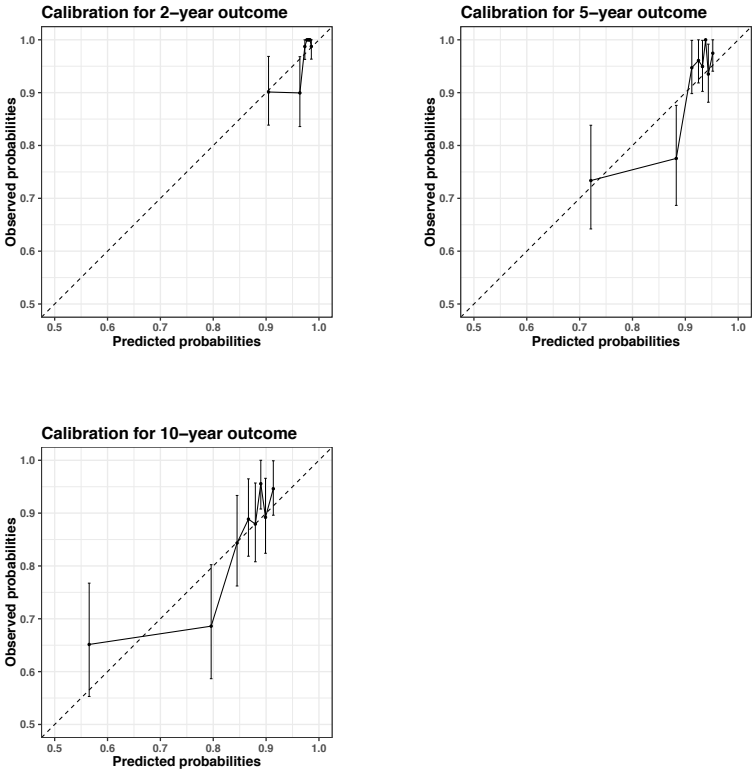

Bibliography

[1] World Health Organization, "Cancer." https://www.who.int/news-room/fact-sheets/detail/cancer.

[2] A. W. Lambert, D. R. Pattabiraman, and R. A. Weinberg, "Emerging Biological Principles of Metastasis," *Cell*, vol. 168, no. 4, pp. 670–691, 2017.

[3] P. S. Steeg, "Targeting metastasis," *Nat Rev Cancer*, vol. 16, no. 4, pp. 201–218, 2016.

[4] P. M. Altrock, L. L. Liu, and F. Michor, "The mathematics of cancer: Integrating quantitative models," *Nat Rev Cancer*, vol. 15, no. 12, pp. 730–745, 2015.

[5] F. Michor and K. Beal, "Improving Cancer Treatment via Mathematical Modeling: Surmounting the Challenges Is Worth the Effort," *Cell*, vol. 163, no. 5, pp. 1059–1063, 2015.

[6] D. Barbolosi, J. Ciccolini, B. Lacarelle, F. Barlési, and N. André, "Computational oncology–mathematical modelling of drug regimens for precision medicine," *Nat Rev Clin Oncol*, vol. 13, no. 4, pp. 242–254, 2016.

[7] S. Mollard, J. Ciccolini, D.-C. Imbs, R. El Cheikh, D. Barbolosi, and S. Benzekry, "Model driven optimization of antiangiogenics + cytotoxics combination: Application to breast cancer mice treated with bevacizumab + paclitaxel doublet leads to reduced tumor growth and fewer metastasis," *Oncotarget*, vol. 8, no. 14, pp. 23087–23098, 2017.

[8] J. Chmielecki, J. Foo, G. R. Oxnard, K. Hutchinson, K. Ohashi, R. Somwar, L. Wang, K. R. Amato, M. Arcila, M. L. Sos, N. D. Socci, A. Viale, E. de Stanchina, M. S. Ginsberg, R. K. Thomas, M. G. Kris, A. Inoue, M. Ladanyi, V. A. Miller, F. Michor, and W. Pao, "Optimization of dosing for EGFR-mutant non-small cell lung cancer with evolutionary cancer modeling," *Sci Transl Med*, vol. 3, no. 90, p. 90ra59, 2011.

[9] E. Baratchart, S. Benzekry, A. Bikfalvi, T. Colin, L. S. Cooley, R. Pineau, E. J. Ribot, O. Saut, and W. Souleyreau, "Computational Modelling of Metastasis Development in Renal Cell Carcinoma," *PLoS Comput Biol*, vol. 11, no. 11, p. e1004626, 2015.

[10] L. Norton and R. Simon, "Tumor size, sensitivity to therapy, and design of treatment schedules," *Cancer Treat Rep*, vol. 61, no. 7, pp. 1307–1317, 1977.

[11] P. Hahnfeldt, D. Panigrahy, J. Folkman, and L. Hlatky, "Tumor development under angiogenic signaling: A dynamical theory of tumor growth, treatment response, and postvascular dormancy," *Cancer Res*, vol. 59, no. 19, pp. 4770–4775, 1999.

[12] M. Simeoni, P. Magni, C. Cammia, G. De Nicolao, V. Croci, E. Pesenti, M. Germani, I. Poggesi, and M. Rocchetti, "Predictive pharmacokinetic-pharmacodynamic modeling of tumor growth kinetics in xenograft models after administration of anticancer agents," *Cancer Res*, vol. 64, no. 3, pp. 1094–1101, 2004.

[13] L. A. Liotta, J. Kleinerman, and G. M. Saidel, "Quantitative relationships of intravascular tumor cells, tumor vessels, and pulmonary metastases following tumor implantation," *Cancer Res*, vol. 34, no. 5, pp. 997–1004, 1974.

[14] K. Iwata, K. Kawasaki, and N. Shigesada, "A dynamical model for the growth and size distribution of multiple metastatic tumors," *J Theor Biol*, vol. 203, no. 2, pp. 177–186, 2000.

[15] L. Hanin and J. Rose, "Uncovering the natural history of cancer from post-mortem cross-sectional diameters of hepatic metastases," *Math Med Biol*, vol. 33, no. 4, pp. 397–416, 2016.

[16] H. Haeno, M. Gonen, M. B. Davis, J. M. Herman, C. A. Iacobuzio-Donahue, and F. Michor, "Computational Modeling of Pancreatic Cancer Reveals Kinetics of Metastasis Suggesting Optimum Treatment Strategies," *Cell*, vol. 148, no. 1, pp. 362–375, 2012.

[17] P. K. Newton, J. Mason, K. Bethel, L. A. Bazhenova, J. Nieva, and P. Kuhn, "A Stochastic Markov Chain Model to Describe Lung Cancer Growth and Metastasis," *PLoS One*, vol. 7, no. 4, p. e34637, 2012.

[18] N. Hartung, S. Mollard, D. Barbolosi, A. Benabdallah, G. Chapuisat, G. Henry, S. Giacometti, A. Iliadis, J. Ciccolini, C. Faivre, and F. Hubert, "Mathematical Modeling of Tumor Growth and Metastatic Spreading: Validation in Tumor-Bearing Mice," *Cancer Res*, vol. 74, no. 22, pp. 6397–6407, 2014.

[19] S. Benzekry, A. Tracz, M. Mastri, R. Corbelli, D. Barbolosi, and J. M. Ebos, "Modeling spontaneous metastasis following surgery: An in vivo-in silico approach," *Cancer Res*, vol. 76, no. 3, pp. 535–547, 2016.

[20] P. M. Ravdin, L. A. Siminoff, G. J. Davis, M. B. Mercer, J. Hewlett, N. Gerson, and H. L. Parker, "Computer Program to Assist in Making Decisions About Adjuvant Therapy for Women With Early Breast Cancer," *J Clin Oncol*, vol. 19, no. 4, pp. 980–991, 2001.

[21] X. Wu, Y. Ye, C. H. Barcenas, W.-H. Chow, Q. H. Meng, M. Chavez-MacGregor, M. A. T. Hildebrandt, H. Zhao, X. Gu, Y. Deng, E. Wagar, F. J. Esteva, D. Tripathy, and G. N. Hortobagyi, "Personalized Prognostic Prediction Models for Breast Cancer Recurrence and Survival Incorporating Multidimensional Data," *JNCI J Natl Cancer Inst*, vol. 109, no. 7, 2017.

[22] G. C. Wishart, E. M. Azzato, D. C. Greenberg, J. Rashbass, O. Kearins, G. Lawrence, C. Caldas, and P. D. Pharoah, "PREDICT: A new UK prognostic model that predicts survival following surgery for invasive breast cancer," *Breast Cancer Res*, vol. 12, no. 1, p. R1, 2010.

[23] X. Gong, M. Hu, and L. Zhao, "Big Data Toolsets to Pharmacometrics: Application of Machine Learning for Time-to-Event Analysis: Big Data Toolsets to Pharmacometrics," *Clin Transl Sci*, vol. 11, no. 3, pp. 305–311, 2018.

[24] G. C. Jayson, R. Kerbel, L. M. Ellis, and A. L. Harris, "Antiangiogenic therapy in oncology: Current status and future directions," *The Lancet*, vol. 388, no. 10043, pp. 518–529, 2016.

[25] M. Pàez-Ribes, E. Allen, J. Hudock, T. Takeda, H. Okuyama, F. Viñals, M. Inoue, G. Bergers, D. Hanahan, and O. Casanovas, "Antiangiogenic Therapy Elicits Malignant Progression of Tumors to Increased Local Invasion and Distant Metastasis," *Cancer Cell*, vol. 15, no. 3, pp. 220–231, 2009.

[26] J. M. L. Ebos, C. R. Lee, W. Cruz-Munoz, G. A. Bjarnason, J. G. Christensen, and R. S. Kerbel, "Accelerated metastasis after short-term treatment with a potent inhibitor of tumor angiogenesis," *Cancer Cell*, vol. 15, no. 3, pp. 232–239, 2009.

[27] J. M. L. Ebos, M. Mastri, C. R. Lee, A. Tracz, J. M. Hudson, K. Attwood, W. R. Cruz-Munoz, C. Jedeszko, P. Burns, and R. S. Kerbel, "Neoadjuvant antiangiogenic therapy reveals contrasts in primary and metastatic tumor efficacy," *EMBO Mol Med*, vol. 6, no. 12, pp. 1561–1576, 2014.

[28] J. M. L. Ebos and R. S. Kerbel, "Antiangiogenic therapy: Impact on invasion, disease progression, and metastasis," *Nat Rev Clin Oncol*, vol. 8, no. 4, pp. 210–221, 2011.

[29] P. Wolter, B. Beuselinck, S. Pans, and P. Schöffski, "Flare-up: An often unreported phenomenon nevertheless familiar to oncologists prescribing tyrosine kinase inhibitors," *Acta Oncol*, vol. 48, no. 4, pp. 621–624, 2009.

[30] I. M. E. Desar, S. F. Mulder, A. B. Stillebroer, D.-J. van Spronsen, W. T. A. van der Graaf, P. F. A. Mulders, and C. M. L. van Herpen, "The reverse side of the victory: Flare up of symptoms after discontinuation of sunitinib or sorafenib in renal cell cancer patients. A report of three cases," *Acta Oncol*, vol. 48, no. 6, pp. 927–931, 2009.

[31] W. Cacheux, T. Boisserie, L. Staudacher, O. Vignaux, B. Dousset, O. Soubrane, B. Terris, C. Mateus, S. Chaussade, and F. Goldwasser, "Reversible tumor growth acceleration following bevacizumab interruption in metastatic colorectal cancer patients scheduled for surgery," *Ann Oncol*, vol. 19, no. 9, pp. 1659–1661, 2008.

[32] M. Lavielle, *Mixed Effects Models for the Population Approach: Models, Tasks, Methods and Tools*. Chapman and Hall/CRC, 2014.

[33] M. Kuhn and K. Johnson, *Applied Predictive Modeling*, vol. 26. Springer, 2013.

[34] "American Cancer Society. Cancer Facts & Figures 2019," 2019.

[35] A. Noone, N. Howlader, M. Krapcho, D. Miller, A. Brest, M. Yu, J. Ruhl, Z. Tatalovich, A. Mariotto, and D. Lewis, "SEER cancer statistics review, 1975–2015," *Bethesda, MD: National Cancer Institute*, 2018.

[36] L. A. Liotta and E. C. Kohn, "Invasion and Metastases," *Holl.-Frei Cancer Med. 6th Ed.*, 2003.

[37] W. Kim, K. S. Kim, J. E. Lee, D.-Y. Noh, S.-W. Kim, Y. S. Jung, M. Y. Park, and R. W. Park, "Development of novel breast cancer recurrence prediction model using support vector machine," *J Breast Cancer*, vol. 15, no. 2, pp. 230–238, 2012.

[38] D. Delen, G. Walker, and A. Kadam, "Predicting breast cancer survivability: A comparison of three data mining methods," *Artif Intell Med*, vol. 34, no. 2, pp. 113–127, 2005.

[39] E. Comets, A. Lavenu, and M. Lavielle, "Parameter Estimation in Nonlinear Mixed Effect Models Using **saemix** , an *R* Implementation of the SAEM Algorithm," *J Stat Soft*, vol. 80, no. 3, 2017.

[40] H. Ishwaran and U. B. Kogalur, "randomForestSRC: Random Forests for Survival, Regression, and Classification (RF-SRC)," 2019.

[41] R. A. Weinberg, *The Biology of Cancer*. New York: Garland Science, 2 ed., 2013.

[42] I. J. Fidler, "The pathogenesis of cancer metastasis: The 'seed and soil' hypothesis revisited," *Nat Rev Cancer*, vol. 3, no. 6, pp. 453–458, 2003.

[43] J. Folkman, "Angiogenesis: An organizing principle for drug discovery?," *Nat Rev Drug Discov*, vol. 6, no. 4, pp. 273–286, 2007.

[44] S. Braun, K. Pantel, P. Müller, W. Janni, F. Hepp, C. R. Kentenich, S. Gastroph, A. Wischnik, T. Dimpfl, G. Kindermann, G. Riethmüller, and G. Schlimok, "Cytokeratin-positive cells in the bone marrow and survival of patients with stage I, II, or III breast cancer," *N Engl J Med*, vol. 342, no. 8, pp. 525–533, 2000.

[45] C. Sawyers, "Targeted cancer therapy," *Nature*, vol. 432, no. 7015, p. 294, 2004.

[46] R. D. Schreiber, L. J. Old, and M. J. Smyth, "Cancer immunoediting: Integrating immunity's roles in cancer suppression and promotion," *Science*, vol. 331, no. 6024, pp. 1565–1570, 2011.

[47] D. M. Pardoll, "The blockade of immune checkpoints in cancer immunotherapy," *Nat Rev Cancer*, vol. 12, no. 4, pp. 252–264, 2012.

[48] E. Saâda-Bouzid, C. Defaucheux, A. Karabajakian, V. P. Coloma, V. Servois, X. Paoletti, C. Even, J. Fayette, J. Guigay, D. Loirat, F. Peyrade, M. Alt, J. Gal, and C. Le Tourneau, "Hyperprogression during anti-PD-1/PD-L1 therapy in patients with recurrent and/or metastatic head and neck squamous cell carcinoma," *Ann Oncol*, vol. 28, no. 7, pp. 1605–1611, 2017.

[49] J. Folkman and M. Klagsbrun, "Angiogenic factors," *Science*, vol. 235, no. 4787, pp. 442–447, 1987.

[50] J. Folkman, "Tumor Angiogenesis: Therapeutic Implications," *N Engl J Med*, vol. 285, no. 21, pp. 1182–1186, 1971.

[51] N. Ferrara and R. S. Kerbel, "Angiogenesis as a therapeutic target," *Nature*, vol. 438, no. 7070, pp. 967–974, 2005.

[52] H. Hurwitz, L. Fehrenbacher, W. Novotny, T. Cartwright, J. Hainsworth, W. Heim, J. Berlin, A. Baron, S. Griffing, E. Holmgren, N. Ferrara, G. Fyfe, B. Rogers, R. Ross, and F. Kabbinavar, "Bevacizumab plus Irinotecan, Fluorouracil, and Leucovorin for Metastatic Colorectal Cancer," *N Engl J Med*, vol. 350, no. 23, pp. 2335–2342, 2004.

[53] R. J. Motzer, T. E. Hutson, P. Tomczak, M. D. Michaelson, R. M. Bukowski, O. Rixe, S. Oudard, S. Negrier, C. Szczylik, S. T. Kim, I. Chen, P. W. Bycott, C. M. Baum, and R. A. Figlin, "Sunitinib versus interferon alfa in metastatic renal-cell carcinoma," *N Engl J Med*, vol. 356, no. 2, pp. 115–124, 2007.

[54] R. J. Motzer, T. E. Hutson, P. Tomczak, M. D. Michaelson, R. M. Bukowski, S. Oudard, S. Negrier, C. Szczylik, R. Pili, G. A. Bjarnason, X. Garcia-del-Muro, J. A. Sosman, E. Solska, G. Wilding, J. A. Thompson, S. T. Kim, I. Chen, X. Huang, and R. A. Figlin, "Overall survival and updated results for sunitinib compared with interferon alfa in patients with metastatic renal cell carcinoma," *J Clin Oncol*, vol. 27, no. 22, pp. 3584–3590, 2009.

[55] B. Escudier, T. Eisen, W. M. Stadler, C. Szczylik, S. Oudard, M. Siebels, S. Negrier, C. Chevreau, E. Solska, A. A. Desai, F. Rolland, T. Demkow, T. E. Hutson, M. Gore, S. Freeman, B. Schwartz, M. Shan, R. Simantov, R. M. Bukowski, and TARGET Study Group, "Sorafenib in advanced clear-cell renal-cell carcinoma," *N Engl J Med*, vol. 356, no. 2, pp. 125–134, 2007.

[56] B. Escudier, T. Eisen, W. M. Stadler, C. Szczylik, S. Oudard, M. Staehler, S. Negrier, C. Chevreau, A. A. Desai, F. Rolland, T. Demkow, T. E. Hutson, M. Gore, S. Anderson, G. Hofilena, M. Shan, C. Pena, C. Lathia, and R. M. Bukowski, "Sorafenib for treatment of renal cell carcinoma: Final efficacy and safety results of the phase III treatment approaches in renal cancer global evaluation trial," *J Clin Oncol*, vol. 27, no. 20, pp. 3312–3318, 2009.

[57] J. M. Llovet, S. Ricci, V. Mazzaferro, P. Hilgard, E. Gane, J.-F. Blanc, A. C. de Oliveira, A. Santoro, J.-L. Raoul, A. Forner, M. Schwartz, C. Porta, S. Zeuzem, L. Bolondi, T. F. Greten, P. R. Galle, J.-F. Seitz, I. Borbath, D. Häussinger, T. Giannaris, M. Shan, M. Moscovici, D. Voliotis, J. Bruix, and SHARP Investigators Study Group, "Sorafenib in advanced hepatocellular carcinoma," *N Engl J Med*, vol. 359, no. 4, pp. 378–390, 2008.

[58] E. Raymond, L. Dahan, J.-L. Raoul, Y.-J. Bang, I. Borbath, C. Lombard-Bohas, J. Valle, P. Metrakos, D. Smith, A. Vinik, J.-S. Chen, D. Hörsch, P. Hammel, B. Wiedenmann, E. Van Cutsem, S. Patyna, D. R. Lu, C. Blanckmeister, R. Chao, and P. Ruszniewski, "Sunitinib malate for the treatment of pancreatic neuroendocrine tumors," *N Engl J Med*, vol. 364, no. 6, pp. 501–513, 2011.

[59] N. S. Vasudev and A. R. Reynolds, "Anti-angiogenic therapy for cancer: Current progress, unresolved questions and future directions," *Angiogenesis*, vol. 17, no. 3, pp. 471–494, 2014.

[60] M. Staehler, R. J. Motzer, D. J. George, H. S. Pandha, F. Donskov, B. Escudier, A. J. Pantuck, A. Patel, L. DeAnnuntis, H. Bhattacharyya, K. Ramaswamy, G. Zanotti, X. Lin, M. Lechuga, L. Serfass, J. Paty, and A. Ravaud, "Adjuvant sunitinib in patients with high-risk renal cell carcinoma: Safety, therapy management, and patient-reported outcomes in the S-TRAC trial," *Ann Oncol*, vol. 29, no. 10, pp. 2098–2104, 2018.

[61] A. de Gramont, E. Van Cutsem, H.-J. Schmoll, J. Tabernero, S. Clarke, M. J. Moore, D. Cunningham, T. H. Cartwright, J. R. Hecht, F. Rivera, S.-A. Im, G. Bodoky, R. Salazar, F. Maindrault-Goebel, E. Shacham-Shmueli, E. Bajetta, M. Makrutzki, A. Shang, T. André, and P. M. Hoff, "Bevacizumab plus oxaliplatin-based chemotherapy as adjuvant treatment for colon cancer (AVANT): A phase 3 randomised controlled trial," *Lancet Oncol*, vol. 13, no. 12, pp. 1225–1233, 2012.

[62] D. Cameron, J. Brown, R. Dent, C. Jackisch, J. Mackey, X. Pivot, G. G. Steger, T. M. Suter, M. Toi, M. Parmar, R. Laeufle, Y.-H. Im, G. Romieu, V. Harvey, O. Lipatov, T. Pienkowski, P. Cottu, A. Chan, S.-A. Im, P. S. Hall, L. Bubuteishvili-Pacaud, V. Henschel, R. J. Deurloo, C. Pallaud, and R. Bell, "Adjuvant bevacizumab-containing therapy in triple-negative breast cancer (BEATRICE): Primary results of a randomised, phase 3 trial," *Lancet Oncol*, vol. 14, no. 10, pp. 933–942, 2013.

[63] J. Bruix, T. Takayama, V. Mazzaferro, G.-Y. Chau, J. Yang, M. Kudo, J. Cai, R. T.-P. Poon, K.-H. Han, W.-Y. Tak, H. C. Lee, T. Song, S. Roayaie, L. Bolondi, K. S. Lee, M. Makuuchi, F. Souza, M.-A. Le Berre, G. Meinhardt, and J. M. Llovet, "STORM: A phase III randomized, double-blind, placebo-controlled trial of adjuvant sorafenib after resection or ablation to prevent recurrence of hepatocellular carcinoma (HCC)," *J Clin Oncol*, vol. 32, no. 15_suppl, pp. 4006–4006, 2014.

[64] R. S. Kerbel, "Inhibition of tumor angiogenesis as a strategy to circumvent acquired resistance to anti-cancer therapeutic agents," *Bioessays*, vol. 13, no. 1, pp. 31–36, 1991.

[65] V. L. Bridgeman, P. B. Vermeulen, S. Foo, A. Bilecz, F. Daley, E. Kostaras, M. R. Nathan, E. Wan, S. Frentzas, T. Schweiger, B. Hegedus, K. Hoetzenecker, F. Renyi-Vamos, E. A. Kuczynski, N. S. Vasudev, J. Larkin, M. Gore, H. F. Dvorak, S. Paku, R. S. Kerbel, B. Dome, and A. R. Reynolds, "Vessel co-option is common in human lung metastases and mediates resistance to anti-angiogenic therapy in preclinical lung metastasis models," *J Pathol*, vol. 241, no. 3, pp. 362–374, 2017.

[66] S. Frentzas, E. Simoneau, V. L. Bridgeman, P. B. Vermeulen, S. Foo, E. Kostaras, M. Nathan, A. Wotherspoon, Z.-H. Gao, Y. Shi, G. Van den Eynden, F. Daley, C. Peckitt, X. Tan, A. Salman, A. Lazaris, P. Gazinska, T. J. Berg, Z. Eltahir, L. Ritsma, J. Van Rheenen, A. Khashper, G. Brown, H. Nystrom, M. Sund, S. Van Laere, E. Loyer, L. Dirix, D. Cunningham, P. Metrakos, and A. R. Reynolds, "Vessel co-option mediates resistance to anti-angiogenic therapy in liver metastases," *Nat Med*, vol. 22, no. 11, pp. 1294–1302, 2016.

[67] W. P. J. Leenders, B. Küsters, K. Verrijp, C. Maass, P. Wesseling, A. Heerschap, D. Ruiter, A. Ryan, and R. de Waal, "Antiangiogenic therapy of cerebral melanoma metastases results in sustained tumor progression via vessel co-option," *Clin Cancer Res*, vol. 10, no. 18 Pt 1, pp. 6222–6230, 2004.

[68] T. E. Wheldon, *Mathematical Models in Cancer Research,*. Bristol: CRC Press, 1 edition ed., 1988.

[69] S. Benzekry, C. Lamont, A. Beheshti, A. Tracz, J. M. L. Ebos, L. Hlatky, and P. Hahnfeldt, "Classical Mathematical Models for Description and Prediction of Experimental Tumor Growth," *PLoS Comput Biol*, vol. 10, no. 8, p. e1003800, 2014.

[70] L. Simpson-Herren and H. H. Lloyd, "Kinetic parameters and growth curves for experimental tumor systems," *Cancer Chemother Rep*, vol. 54, no. 3, pp. 143–174, 1970.

[71] H. E. Skipper, F. M. Schabel, and W. S. Wilcox, "Experimental evaluation of potential anticancer agents. XIII. On the criteria and kinetics associated with "curability" of experimental leukemia," *Cancer Chemother Rep*, vol. 35, pp. 1–111, 1964.

[72] P. W. Sullivan and S. E. Salmon, "Kinetics of tumor growth and regression in IgG multiple myeloma," *J Clin Invest*, vol. 51, no. 7, pp. 1697–1708, 1972.

[73] J. S. Spratt, R. A. Greenberg, and L. S. Heuser, "Geometry, growth rates, and duration of cancer and carcinoma in situ of the breast before detection by screening," *Cancer Res*, vol. 46, no. 2, pp. 970–974, 1986.

[74] C. Vaghi, A. Rodallec, R. Fanciullino, J. Ciccolini, J. Mochel, M. Mastri, C. Poignard, J. M. Ebos, and S. Benzekry, "A reduced Gompertz model for predicting tumor age using a population approach," *bioRxiv*, p. 670869, 2019.

[75] A. K. Laird, "Dynamics of Tumor Growth," *Br J Cancer*, vol. 18, no. 3, pp. 490–502, 1964.

[76] A. K. Laird, "Dynamics of tumour growth: Comparison of growth rates and extrapolation of growth curve to one cell," *Br J Cancer*, vol. 19, pp. 278–291, 1965.

[77] Early Breast Cancer Trialists' Collaborative Group, "Systemic treatment of early breast cancer by hormonal, cytotoxic, or immune therapy. 133 randomised trials involving 31,000 recurrences and 24,000 deaths among 75,000 women," 1992.

[78] S. Benzekry, E. Pasquier, D. Barbolosi, B. Lacarelle, F. Barlési, N. André, and J. Ciccolini, "Metronomic reloaded: Theoretical models bringing chemotherapy into the era of precision medicine," *Semin Cancer Biol*, vol. 35, pp. 53–61, 2015.

[79] L. Norton and R. Simon, "The Norton-Simon hypothesis revisited," *Cancer Treat Rep*, vol. 70, no. 1, pp. 163–169, 1986.

[80] M. L. Citron, D. A. Berry, C. Cirrincione, C. Hudis, E. P. Winer, W. J. Gradishar, N. E. Davidson, S. Martino, R. Livingston, J. N. Ingle, E. A. Perez, J. Carpenter, D. Hurd, J. F. Holland, B. L. Smith, C. I. Sartor, E. H. Leung, J. Abrams, R. L. Schilsky, H. B. Muss, and L. Norton, "Randomized trial of dose-dense versus conventionally scheduled and sequential versus concurrent combination chemotherapy as postoperative adjuvant treatment of node-positive primary breast cancer: First report of Intergroup Trial C9741/Cancer and Leukemia Group B Trial 9741," *J Clin Oncol*, vol. 21, no. 8, pp. 1431–1439, 2003.

[81] S. Wilson, M. Tod, A. Ouerdani, A. Emde, Y. Yarden, A. Adda Berkane, S. Kassour, M. X. Wei, G. Freyer, B. You, E. Grenier, and B. Ribba, "Modeling and predicting optimal treatment scheduling between the antiangiogenic drug sunitinib and irinotecan in preclinical settings," *CPT Pharmacometrics Syst Pharmacol*, vol. 4, no. 12, pp. 720–727, 2015.

[82] D.-C. Imbs, R. E. Cheikh, A. Boyer, J. Ciccolini, C. Mascaux, B. Lacarelle, F. Barlesi, D. Barbolosi, and S. Benzekry, "Revisiting Bevacizumab + Cytotoxics Scheduling Using Mathematical Modeling: Proof of Concept Study in Experimental Non-Small Cell Lung Carcinoma," *CPT Pharmacomet Syst Pharmacol*, vol. 7, no. 1, pp. 42–50, 2018.

[83] R. K. Jain, "Normalizing tumor vasculature with anti-angiogenic therapy: A new paradigm for combination therapy," *Nat Med*, vol. 7, no. 9, pp. 987–989, 2001.

[84] R. K. Jain, "Normalization of tumor vasculature: An emerging concept in antiangiogenic therapy," *Science*, vol. 307, no. 5706, pp. 58–62, 2005.

[85] J. H. Goldie and A. J. Coldman, "A mathematic model for relating the drug sensitivity of tumors to their spontaneous mutation rate," *Cancer Treat Rep*, vol. 63, no. 11-12, pp. 1727–1733, 1979.

[86] C. Dang, T. A. Gilewski, A. Surbone, and L. Norton, "Growth Curve Analysis," *Holl-Frei Cancer Med*, 2003.

[87] J. Foo and F. Michor, "Evolution of Resistance to Targeted Anti-Cancer Therapies during Continuous and Pulsed Administration Strategies," *PLoS Comput Biol*, vol. 5, no. 11, p. e1000557, 2009.

[88] G. M. Saidel, L. A. Liotta, and J. Kleinerman, "System dynamics of metastatic process from an implanted tumor," *J Theor Biol*, vol. 56, no. 2, pp. 417–434, 1976.

[89] L. Hanin and S. Bunimovich-Mendrazitsky, "Reconstruction of the natural history of metastatic cancer and assessment of the effects of surgery: Gompertzian growth of the primary tumor," *Math Biosci*, vol. 247, pp. 47–58, 2014.

[90] M. Kuhn, J. Wing, S. Weston, A. Williams, C. Keefer, A. Engelhardt, T. Cooper, Z. Mayer, B. Kenkel, t. R. C. Team, M. Benesty, R. Lescarbeau, A. Ziem, L. Scrucca, Y. Tang, C. Candan, and a. T. Hunt, "Caret: Classification and Regression Training," 2018.

[91] C. Nicolò, M. Mastri, A. Tracz, J. M. Ebos, and S. Benzekry, "Abstract 4264: Mathematical modeling of differential effects of sunitinib on primary tumor and metastatic growth," *Cancer Res*, vol. 78, no. 13 Supplement, pp. 4264–4264, 2018.

[92] C. Nicolò, M. Mastri, J. M. Ebos, and S. Benzekry, "Machine learning combined to mechanistic modeling of differential effects of neo-adjuvant Sunitinib on primary tumor and metastatic growth," *to be submitted to Cancer Res*, 2019.

[93] M. Mastri, C. Nicolò, S. Benzekry, and J. M. Ebos, "Impact of treatment breaks and burst in the neo-adjuvant setting for anti-angiogenic therapy of kidney cancer," *to be submitted to Cancer Res*, 2019.

[94] B. Karimi, "Collaborative development of saemix (SAEM algorithm): https://github.com/belhal/saemix," 2019.

[95] C. Nicolò, C. Perier, M. Prague, G. MacGrogan, C. Bellera, O. Saut, and S. Benzekry, "Machine learning versus mechanistic modeling for prediction of metastatic relapse in breast cancer," *submitted to JCO Clinical Cancer Informatics*, 2019.

[96] J. S. Spratt, J. S. Meyer, and J. A. Spratt, "Rates of growth of human solid neoplasms: Part I," *J Surg Oncol*, vol. 60, no. 2, pp. 137–146, 1995.

[97] N. Hartung, "Efficient resolution of metastatic tumor growth models by reformulation into integral equations," *Discrete Contin Dyn Syst Ser B*, vol. 20, no. 2, pp. 445–467, 2015.

[98] S. Benzekry, *Modélisation, Analyse Mathématique de Thérapies Anti-Cancéreuses Pour Les Cancers Métastatiques*. Thesis, Aix-Marseille 1, 2011.

[99] D. Barbolosi, A. Benabdallah, F. Hubert, and F. Verga, "Mathematical and numerical analysis for a model of growing metastatic tumors," *Math Biosci*, vol. 218, no. 1, pp. 1–14, 2009.

[100] S. Benzekry, N. André, A. Benabdallah, J. Ciccolini, C. Faivre, F. Hubert, and D. Barbolosi, "Modeling the Impact of Anticancer Agents on Metastatic Spreading," *Math Model Nat Phenom*, vol. 7, no. 1, pp. 306–336, 2012.

[101] S. Benzekry and P. Hahnfeldt, "Maximum tolerated dose versus metronomic scheduling in the treatment of metastatic cancers.," *J Theor Biol*, vol. 335, pp. 235–44, 2013.

[102] S. Benzekry, A. Gandolfi, and P. Hahnfeldt, "Global dormancy of metastases due to systemic inhibition of angiogenesis," *PLoS ONE*, vol. 9, no. 1, p. e84249, 2014.

[103] S. Benzekry, C. Lamont, D. Barbolosi, L. Hlatky, and P. Hahnfeldt, "Mathematical Modeling of Tumor-Tumor Distant Interactions Supports a Systemic Control of Tumor Growth," *Cancer Res*, vol. 77, no. 18, pp. 5183–5193, 2017.

[104] L. Wasserman, *All of Statistics: A Concise Course in Statistical Inference*. Springer Science & Business Media, 2004.

[105] G. A. F. Seber and C. J. Wild, *Nonlinear Regression*. John Wiley & Sons, 2003.

[106] M. Bilous, C. Serdjebi, A. Boyer, P. Tomasini, C. Pouypoudat, D. Barbolosi, F. Barlesi, F. Chomy, and S. Benzekry, "Computational modeling reveals dynamics of brain metastasis in non-small cell lung cancer and provides a tool for personalized therapy," *bioRxiv*, p. 448282, 2018.

[107] L. Breiman, J. Friedman, C. J. Stone, and R. A. Olshen, *Classification and Regression Trees*. Taylor & Francis, 1984.

[108] T. Hothorn, K. Hornik, and A. Zeileis, "Unbiased Recursive Partitioning: A Conditional Inference Framework," *J Comput Graph Stat*, vol. 15, no. 3, pp. 651–674, 2006.

[109] D. R. Mould and R. N. Upton, "Basic Concepts in Population Modeling, Simulation, and Model-Based Drug Development," *CPT Pharmacometrics Syst Pharmacol*, vol. 1, no. 9, p. e6, 2012.

[110] B. Delyon, M. Lavielle, and E. Moulines, "Convergence of a stochastic approximation version of the EM algorithm," *Ann Statist*, vol. 27, no. 1, pp. 94–128, 1999.

[111] E. Kuhn and M. Lavielle, "Coupling a stochastic approximation version of EM with an MCMC procedure," *ESAIM Probab. Stat.*, vol. 8, pp. 115–131, 2004.

[112] A. P. Dempster, N. M. Laird, and D. B. Rubin, "Maximum likelihood from incomplete data via the EM algorithm," *J R Stat Soc Series B*, vol. 39, no. 1, pp. 1–38, 1977.

[113] C. F. J. Wu, "On the Convergence Properties of the EM Algorithm," *Ann Statist*, vol. 11, no. 1, pp. 95–103, 1983.

[114] S. Chib and E. Greenberg, "Understanding the Metropolis-Hastings Algorithm," *Am Stat*, vol. 49, no. 4, pp. 327–335, 1995.

[115] T. H. T. Nguyen, M.-S. Mouksassi, N. Holford, N. Al-Huniti, I. Freedman, A. C. Hooker, J. John, M. O. Karlsson, D. R. Mould, J. J. P. Ruixo, E. L. Plan, R. Savic, J. G. C. van Hasselt, B. Weber, C. Zhou, E. Comets, and F. Mentré, "Model Evaluation of Continuous Data Pharmacometric Models: Metrics and Graphics," *CPT Pharmacomet Syst Pharmacol*, vol. 6, no. 2, pp. 87–109, 2017.

[116] D. R. Mould and R. N. Upton, "Basic Concepts in Population Modeling, Simulation, and Model-Based Drug Development—Part 2: Introduction to Pharmacokinetic Modeling Methods," *CPT Pharmacometrics Syst Pharmacol*, vol. 2, no. 4, p. e38, 2013.

[117] "Monolix version 2019R1. Antony, France: Lixoft SAS, 2019. http://lixoft.com/products/monolix/."

[118] E. L. Kaplan and P. Meier, "Nonparametric Estimation from Incomplete Observations," *J Am Stat Assoc*, vol. 53, no. 282, pp. 457–481, 1958.

[119] P. K. Andersen, O. Borgan, R. D. Gill, and N. Keiding, *Statistical Models Based on Counting Processes*. Springer Series in Statistics, New York: Springer-Verlag, 1993.

[120] J. D. Kalbfleisch and R. L. Prentice, *The Statistical Analysis of Failure Time Data*. Wiley Series in Probability and Statistics, Hoboken, N.J: J. Wiley, 2nd ed ed., 2002.

[121] D. R. Cox, "Regression Models and Life-Tables," *J R Stat Soc Ser B*, vol. 34, no. 2, pp. 187–220, 1972.

[122] D. R. Cox, "Partial Likelihood," *Biometrika*, vol. 62, no. 2, p. 269, 1975.

[123] B. Efron, "The Efficiency of Cox's Likelihood Function for Censored Data," *J Am Stat Assoc*, vol. 72, no. 359, pp. 557–565, 1977.

[124] P. K. Andersen and R. D. Gill, "Cox's Regression Model for Counting Processes: A Large Sample Study," *Ann Statist*, vol. 10, no. 4, pp. 1100–1120, 1982.

[125] H. Ishwaran and U. B. Kogalur, "Random Survival Forests for R," *Rnews*, vol. 7, no. 2, pp. 25–31, 2007.

[126] M. R. Segal, "Regression Trees for Censored Data," *Biometrics*, vol. 44, no. 1, p. 35, 1988.

[127] T. Hothorn and B. Lausen, "On the exact distribution of maximally selected rank statistics," *Comput Stat Data Anal*, vol. 43, no. 2, pp. 121–137, 2003.

[128] H. Ishwaran, U. B. Kogalur, E. Z. Gorodeski, A. J. Minn, and M. S. Lauer, "High-Dimensional Variable Selection for Survival Data," *J Am Stat Assoc*, vol. 105, no. 489, pp. 205–217, 2010.

[129] F. E. Harrell, K. L. Lee, and D. B. Mark, "Multivariable prognostic models: Issues in developing models, evaluating assumptions and adequacy, and measuring and reducing errors," *Stat Med*, vol. 15, no. 4, pp. 361–387, 1996.

[130] K. B. Blagoev, J. Wilkerson, W. D. Stein, R. J. Motzer, S. E. Bates, and A. T. Fojo, "Sunitinib Does Not Accelerate Tumor Growth in Patients with Metastatic Renal Cell Carcinoma," *Cell Reports*, vol. 3, no. 2, pp. 277–281, 2013.

[131] Q. Zhou and J. M. Gallo, "Quantification of sunitinib in mouse plasma, brain tumor and normal brain using liquid chromatography-electrospray ionization-tandem mass spectrometry and pharmacokinetic application," *J Pharm Biomed Anal*, vol. 51, no. 4, p. 958, 2010.

[132] "Matlab with statistics and optimization toolboxes. The Mathworks Inc.; 2015."

[133] R. C. Team, "R: A language and environment for statistical computing. R Foundation for Statistical Computing, Vienna, Austria. https://www.R-project.org/.," 2018.

[134] "Monolix version 2018R1. Antony, France: Lixoft SAS, 2018. http://lixoft.com/products/monolix/."

[135] M. Lavielle and J. Chauvin, "Rsmlx: R Speaks 'Monolix'. R package version 1.1.0. https://CRAN.R-project.org/package=Rsmlx," 2018.

[136] M. Lavielle, E. Ilinca, and R. Kuate, "mlxR: Simulation of Longitudinal Data," 2019.

[137] R. M. Savic and M. O. Karlsson, "Importance of Shrinkage in Empirical Bayes Estimates for Diagnostics: Problems and Solutions," *AAPS J*, vol. 11, no. 3, pp. 558–569, 2009.

[138] S. Braga, J. Cardoso, S. Andre, M. Brito, P. Sanchez, L. Orvalho, L. Salgado, S. Dias, J. B. Pereira-Leal, and J. L. Passos-Coelho, "Does Hypoxic Response Mediate Primary Resistance to Sunitinib in Untreated Locally Advanced Breast Cancer?," *Curr Cancer Drug Targets*, vol. 17, no. 1, pp. 62–73, 2017.

[139] J. Ciccolini, S. Benzekry, B. Lacarelle, D. Barbolosi, and F. Barlési, "Improving efficacy of the combination between antiangiogenic and chemotherapy: Time for mathematical modeling support," *Proc Natl Acad Sci U S A*, vol. 112, no. 27, p. E3453, 2015.

[140] E. Reguera-Nuñez, S. Man, P. Xu, and R. S. Kerbel, "Preclinical impact of high dose intermittent antiangiogenic tyrosine kinase inhibitor pazopanib in intrinsically resistant tumor models," *Angiogenesis*, vol. 21, no. 4, pp. 793–804, 2018.

[141] M. J. Ratain and D. A. Goldstein, "Time Is Money: Optimizing the Scheduling of Nivolumab," *J Clin Oncol*, p. JCO1800045, 2018.

[142] E. di Tomaso, M. Snuderl, W. S. Kamoun, D. G. Duda, P. K. Auluck, L. Fazlollahi, O. C. Andronesi, M. P. Frosch, P. Y. Wen, S. R. Plotkin, E. T. Hedley-Whyte, A. G. Sorensen, T. T. Batchelor, and R. K. Jain, "Glioblastoma recurrence after cediranib therapy in patients: Lack of "rebound" revascularization as mode of escape," *Cancer Res*, vol. 71, no. 1, pp. 19–28, 2011.

[143] E. Senkus, S. Kyriakides, S. Ohno, F. Penault-Llorca, P. Poortmans, E. Rutgers, S. Zackrisson, and F. Cardoso, "Primary breast cancer: ESMO Clinical Practice Guidelines for diagnosis, treatment and follow-up," *Ann Oncol*, vol. 26, no. suppl 5, pp. v8–v30, 2015.

[144] S. Mook, M. K. Schmidt, E. J. Rutgers, A. O. van de Velde, O. Visser, S. M. Rutgers, N. Armstrong, L. J. van't Veer, and P. M. Ravdin, "Calibration and discriminatory accuracy of prognosis calculation for breast cancer with the online Adjuvant! program: A hospital-based retrospective cohort study," *Lancet Oncol*, vol. 10, no. 11, pp. 1070–1076, 2009.

[145] M. J. Duffy, N. Harbeck, M. Nap, R. Molina, A. Nicolini, E. Senkus, and F. Cardoso, "Clinical use of biomarkers in breast cancer: Updated guidelines from the European Group on Tumor Markers (EGTM)," *Eur J Cancer*, vol. 75, pp. 284–298, 2017.

[146] S. Koscielny, M. Tubiana, M. G. Lê, A. J. Valleron, H. Mouriesse, G. Contesso, and D. Sarrazin, "Breast cancer: Relationship between the size of the primary tumour and the probability of metastatic dissemination.," *Br J Cancer*, vol. 49, no. 6, pp. 709–715, 1984.

[147] H. Ishwaran, U. B. Kogalur, E. H. Blackstone, and M. S. Lauer, "Random survival forests," *Ann Appl Stat*, vol. 2, no. 3, pp. 841–860, 2008.

[148] I. de Mascarel, M. Debled, V. Brouste, L. Mauriac, G. Sierankowski, V. Velasco, S. Croce, F. Chibon, J. Boudeau, A. Debant, and G. MacGrogan, "Comprehensive prognostic analysis in breast cancer integrating clinical, tumoral, microenvironmental and immunohistochemical criteria," *Springerplus*, vol. 4, p. 528, 2015.

[149] D. J. Stekhoven and P. Bühlmann, "MissForest—non-parametric missing value imputation for mixed-type data," *Bioinformatics*, vol. 28, no. 1, pp. 112–118, 2012.

[150] M. W. Retsky, R. Demicheli, D. E. Swartzendruber, P. D. Bame, R. H. Wardwell, G. Bonadonna, J. F. Speer, and P. Valagussa, "Computer simulation of a breast cancer metastasis model," *Breast Cancer Res Treat*, vol. 45, no. 2, pp. 193–202, 1997.

[151] D. Commenges and H. Jacqmin-Gadda, *Dynamical Biostatistical Models*. Chapman and Hall/CRC, 2015.

[152] M. J. van de Vijver, Y. D. He, L. J. van't Veer, H. Dai, A. A. M. Hart, D. W. Voskuil, G. J. Schreiber, J. L. Peterse, C. Roberts, M. J. Marton, M. Parrish, D. Atsma, A. Witteveen, A. Glas, L. Delahaye, T. van der Velde, H. Bartelink, S. Rodenhuis, E. T. Rutgers, S. H. Friend, and R. Bernards, "A gene-expression signature as a predictor of survival in breast cancer," *N Engl J Med*, vol. 347, no. 25, pp. 1999–2009, 2002.

[153] T. G. Karrison, D. J. Ferguson, and P. Meier, "Dormancy of Mammary Carcinoma After Mastectomy," *J Natl Cancer Inst*, vol. 91, no. 1, pp. 80–85, 1999.

[154] J. W. Uhr and K. Pantel, "Controversies in clinical cancer dormancy," *Proc Natl Acad Sci USA*, vol. 108, no. 30, pp. 12396–12400, 2011.